



**A University of Sussex DPhil thesis**

Available online via Sussex Research Online:

<http://sro.sussex.ac.uk/>

This thesis is protected by copyright which belongs to the author.

This thesis cannot be reproduced or quoted extensively from without first obtaining permission in writing from the Author

The content must not be changed in any way or sold commercially in any format or medium without the formal permission of the Author

When referring to this work, full bibliographic details including the author, title, awarding institution and date of the thesis must be given

Please visit Sussex Research Online for more information and further details



**Synergistic Innate Immune Recognition of**  
**Coxsackievirus B5 by RIG-I and MDA5**

*Edward John Albert Richer*

A Thesis Submitted for the Degree of Doctor of Philosophy in  
Immunology

Department of Biochemistry

School of Life Sciences

University of Sussex

September 2011

I hereby declare that this thesis has not been, and will not be, submitted in whole or in part to another University for the award of any other degree.

**Signature:**.....

**Supervisors: Dr. Martha Triantafilou**

**Dr. Kathy Triantafilou**

**Infection & Immunity Group**

*Onwards!*

# ACKNOWLEDGEMENTS

First and foremost, I would like to thank my supervisors, Dr. Martha Triantafilou and Prof. Kathy Triantafilou, for their help, their guidance, their inspiration, and for providing an excellent working atmosphere in the lab during my three years there. I shall take this opportunity to thank my fellow lab partners (Daniel, Fred, and Gareth) and staff within the department (especially Ray) as well, for their help and all the fun times we shared.

Throughout my DPhil, and especially in the past year, I have made many friends whom I would like to thank for their support and amazing times together. Sarah, Nora, Diana, Marie, Hetty, and Giuseppe deserve special mentions. Top of the bunch though is Kyle, who has always been there for me with advice and wisdom, during both the highs and the lows. I shall remember and cherish the many adventures we shared together, whether sport, geocaching, gigging, or just randomly wandering and wondering.

Having been a Residential Advisor these past few years, I would like to thank all the wonderful people I have lived with and met throughout my time at University. I now have contacts all over the globe, and fully intend to take advantage of them and travel the world.

Finally, I would like to thank my family for their continuing support and belief in me. Now, who's up for some tennis?

# ABSTRACT

Coxsackievirus B5 (CBV5) is a positive sense, single-stranded RNA virus belonging to the *Enterovirus* genus of the Picornaviridae family. It can cause many serious diseases, including viral myocarditis (which can lead on to dilated cardiomyopathy), aseptic meningitis, and pancreatitis. The structure and cell cycle of CBV5 is typical of a picornavirus.

Viral RNA is detected by Toll-like receptors (TLRs) and retinoic acid inducible gene-I (RIG-I)-like receptors (RLRs). The RLR family, consisting of RIG-I, MDA5 (melanoma differentiation-associated gene 5), and LGP2, are pattern recognition receptors that detect a range of different viruses. RIG-I and MDA5 are homologous cytoplasmic proteins containing an N-terminal region with two caspase activation and recruitment domains (CARDs), a central SF2 type DExD/H-box RNA helicase domain, and a C-terminal repressor domain (RD). Once a viral ligand has been detected and bound by RIG-I and MDA5, both signal downstream through their CARDs to activate IRF3/7 and NF- $\kappa$ B indirectly, via the protein intermediate IPS-1 (IFN- $\beta$  promoter stimulator 1), and initiate an immune response.

RIG-I and MDA5 contribute to antiviral signalling in different ways depending on the virus involved. MDA5 has been shown to be critical for Picornaviridae detection, whilst RIG-I can detect a wide variety of different viruses and pathogen associated molecular patterns.

Results presented here show the expression levels of both are upregulated in response to CBV5 infection in human cardiac cells, with MDA5 expression levels being slightly greater than RIG-I. However, in Huh cells, RIG-I expression levels are greater than those of MDA5, indicating that it plays a role in CBV5 sensing. The presence of both phospho-I $\kappa$ B (corresponding to NF- $\kappa$ B activation) and IRF3 is detected in both cardiac cells and Huh cells in response to CBV5, and IFN- $\beta$  production is also greatly upregulated. RIG-I and MDA5 colocalise with the adaptor protein IPS-1 in response to CBV5 infection, again indicating the synergistic response by the two RLRs, and both RLRs form homodimers in the cytoplasm. Overall, this suggest that both MDA5 and RIG-I act synergistically to detect CBV5 and initiate a downstream immune response, although MDA5 appears to be the marginally stronger sensor.



# CONTENTS

<b>LIST OF FIGURES</b>	<b>VIII</b>
<b>LIST OF TABLES</b>	<b>X</b>
<b>ABBREVIATIONS</b>	<b>XI</b>
<b>CHAPTER 1. INTRODUCTION</b>	<b>1</b>
1.1 Picornaviridae	2
1.2 Cocksackievirus B5 Structure	5
1.3 Picornavirus Replication Cycle	9
1.3.1 Attachment	11
1.3.2 Uncoating	14
1.3.3 Translation	16
1.3.4 Protein Processing	19
1.3.5 Negative (-) and Positive (+) Sense RNA Synthesis	21
1.3.6 Assembly and Release	23
1.4 Innate Immunity and Toll-like Receptors	25
1.4.1 Toll-like Receptors	27
1.4.2 Toll-like Receptor Structure	30
1.4.3 Toll-like Receptor Signalling Pathways	32
1.4.4 Virus Recognition by Toll-like Receptors	35
1.4.4.1 TLR2	36
1.4.4.2 TLR3	37
1.4.4.3 TLR4	38
1.4.4.4 TLR7 and TLR8	39
1.4.4.5 TLR9	39
1.4.5 Viral Modulation of Toll-like Receptor Signalling Pathways	40
1.5 Innate Immunity and RIG-I-like Receptors	41
1.5.1 RIG-I, MDA5, and LGP2 Structures	41
1.5.2 CARDs and RLR Dimerisation	42

1.5.3 IPS-1	44
1.5.4 Host Response to Viral Infection	45
1.5.5 Viral Evasion of Host Recognition	48
1.5.6 RLR Ligands	49
1.5.6.1 RIG-I Ligands	49
1.5.6.2 MDA5 Ligands	52
1.5.6.3 LGP2 Ligands	53
1.6 Project Aims	54
 <b>CHAPTER 2: MATERIALS AND METHODS</b>	 <b>55</b>
2.1 Materials	56
2.1.1 Antibodies	56
2.2 Tissue Culture	58
2.2.1 Cell Lines	58
2.2.1.1 Human Cardiac Cell Line	58
2.2.1.2 Huh 7.5 and Huh 7.5.1. Cell Lines	58
2.2.1.3 LLC Cell Line	59
2.2.2 Thawing Cells	59
2.2.3 Propagating Cells	59
2.2.3.1 Adherent Cell Lines	60
2.2.4 Freezing Cells	60
2.3 Cocksackievirus B5 (CBV5)	62
2.3.1 Propagating CBV5	62
2.3.2 Purifying CBV5 using a Sucrose Density Gradient	62
2.3.3 Isolating Single-Stranded RNA from Purified CBV5	62
2.3.4 Preparing UV-Inactivated CBV5	63
2.4 Immunofluorescence	64
2.4.1 Direct Immunofluorescence	64
2.4.2 Indirect Immunofluorescence	65
2.5 Flow Cytometry	66
2.5.1 Principles of Flow Cytometry	66
2.6 Determining RIG-I and MDA5 Expression Levels	68
2.7 Phospho-IkB and IRF3 Detection	70
2.7.1 SDS-PAGE	70

2.7.1.1 Continuous SDS-PAGE	70
2.7.1.2 Discontinuous SDS-PAGE	70
2.7.1.3 Discontinuous SDS-PAGE Preparation	71
2.7.1.4 Sample Preparation for SDS-PAGE	73
2.7.2 Western Blot	74
2.7.2.1 Blocking and Primary Antibody Incubation	74
2.7.2.2 Secondary Antibody Incubation	75
2.7.3 Enhanced Chemiluminescence	75
2.7.4 Stripping and Reprobing Membranes	76
2.8 Immunoprecipitation	78
2.8.1 Pre-Clearing	78
2.8.2 Primary Antibody Incubation and Washing	79
2.8.3 SDS-PAGE	80
2.9 Confocal Microscopy	81
2.9.1 Slide Preparation	82
2.9.2 Confocal Image Analysis	85
2.9.2.1 LSM Image Browser and AxioVision LE	85
2.9.2.2 ImageJ and JACoP	86
2.9.2.3 Pearson's Correlation Coefficient	88
2.9.2.4 Mander's Overlap Coefficient	88
2.9.2.5 Mander's Colocalisation Coefficients	88
2.9.2.6 Costes' Randomisation Method	89
2.9.2.7 Costes' Threshold	89
2.10 Plasmid DNA	90
2.10.1 Plasmid DNA Preparation	90
2.10.1.1 Transformation	90
2.10.1.2 DNA Isolation	91
2.10.1.3 Agarose Gel Electrophoresis	92
2.10.2 Silencing	92
2.10.2.1 Day 1 – Cell Preparation	93
2.10.2.2 Day 2 – Transfection Reagent Preparation	93
2.10.2.3 Day 3 – Switch to Selection Medium	93
2.10.2.4 Day 4 – Check Knockdowns	94
2.10.2.5 Day 5 – Stimulation of Cells	94

2.11 Cytometric Bead Array	95
2.11.1 Assay Procedure	95
 <b>CHAPTER 3: RNA HELICASE INVOLVEMENT IN CBV5 INFECTION OF CARDIAC CELLS</b>	 <b>96</b>
3.1 Introduction	97
3.2 Results	100
3.2.1 MDA5 and RIG-I Expression Levels	100
3.2.2 Signalling Detection Upon Infection With CBV5	102
3.2.3 IFN- $\beta$ Production	105
3.2.4 Silencing of RIG-I and MDA5	106
3.2.4.1 psiRNA Purification	106
3.2.4.2 RIG-I Silenced and MDA5 Silenced Cardiac Response to CBV5	107
3.3 Conclusion	109
 <b>CHAPTER 4: DETERMINING THE ROLE OF MDA5 AND RIG-I IN CBV5 SENSING USING HUH CELLS</b>	 <b>111</b>
4.1 Introduction	112
4.2 Results	113
4.2.1 Expression Levels in Huh 7.5 Cells	113
4.2.2 Expression Levels in Huh 7.5.1 Cells	115
4.2.3 Phospho-I $\kappa$ B and IRF3 Detection in Huh 7.5 Cells	117
4.2.4 Phospho-I $\kappa$ B and IRF3 Detection in Huh 7.5.1 Cells	119
4.2.5 IFN- $\beta$ Production	121
4.3 Conclusion	123
 <b>CHAPTER 5: RLR DIMERISATION</b>	 <b>124</b>
5.1 Introduction	125
5.2 Results	127
5.2.1 MDA5 Homodimerisation	128
5.2.2 RIG-I Homodimerisation	129
5.2.3 LGP2 Monomers	130
5.2.4 MDA5 – LGP2	131

5.2.5 LGP2 –MDA5	132
5.2.6 RIG-I – LGP2	133
5.2.7 LGP2 – RIG-I	134
5.3 Conclusion	135
<b>CHAPTER 6: IMAGING OF RLR INTERACTIONS</b>	<b>136</b>
6.1 Introduction	137
6.2 Results	138
6.2.1 Colocalisation between IPS-1 and MDA5	139
6.2.2 Colocalisation between IPS-1 and RIG-I	141
6.3 Conclusion	143
<b>CHAPTER 7: DISCUSSION</b>	<b>144</b>
7.1 RNA Helicase Involvement in CBV5 Infection of Cardiac Cells	148
7.2 Determining the Role of RLRs in CBV5 Sensing Using Huh Cells	151
7.3 RLR Dimerisation	153
7.4 Imaging of RLR Interactions	155
7.5 Conclusion	157
<b>REFERENCES</b>	<b>160</b>
<b>APPENDIX</b>	<b>204</b>

# LIST OF FIGURES

1.1	Capsid structure of a Picornaviridae virion	5
1.2	$\beta$ -barrel jelly roll structure of CBV3	6
1.3	Genome organisation of an enterovirus	7
1.4	Replication cycle of a picornavirus	10
1.5	General representation of CAR structure	13
1.6	Diagrammatic structure of decay accelerating factor	13
1.7	Uncoating of a picornavirus	15
1.8	Cap-dependent and cap-independent translation initiation	18
1.9	Picornavirus virion assembly	24
1.10	TLR localisation	31
1.11	TLR signalling pathway	34
1.12	Virus interactions with TLRs	35
1.13	Modulation of TLR pathways by virus infection	40
1.14	Representative structures of the RLRs	42
1.15	RIG-I dimerisation	43
1.16	Representative structure of IPS-1	45
1.17	The RLR signalling pathway	47
1.18	Putative RIG-I ligands	51
2.1	Direct immunofluorescence	64
2.2	Indirect immunofluorescence	65
2.3	BD FACSCalibur <sup>TM</sup> flow cytometer	66
2.4	Apparatus used for SDS-PAGE	72
2.5	Principle of western blotting	77
2.6	Principle of ECL western blotting	77
2.7	Principle light pathways in confocal microscopy	81
2.8	Layout of Lab-Tek 8-well chamber slides	82
2.9	Layout of a haemocytometer	83
2.10	Costes' randomisation method	89
2.11	The psiRNA-h7SK GFPzeo plasmid	90

3.1 Expression levels of MDA5 in human cardiac cells	<b>101</b>
3.2 Expression levels of RIG-I in human cardiac cells	<b>101</b>
3.3 Phospho-I $\kappa$ B detection in human cardiac cells	<b>103</b>
3.4 IRF3 detection in human cardiac cells	<b>104</b>
3.5 IFN- $\beta$ production in human cardiac cells	<b>105</b>
3.6 Agarose gel of purified psi-RNA-RIG-I and psiRNA-MDA5	<b>106</b>
3.7 RIG-I, MDA5, and TLR7 expression after use of psiRNA	<b>107</b>
3.8 IFN- $\beta$ expression in human cardiac cells (psiRNA-RIG-I)	<b>108</b>
3.9 IFN- $\beta$ expression in human cardiac cells (psiRNA-MDA5)	<b>108</b>
4.1 MDA5 expression in Huh 7.5 cells	<b>113</b>
4.2 RIG-I expression in Huh 7.5 cells	<b>114</b>
4.3 Expression levels of MDA5 in Huh 7.5.1 cells	<b>115</b>
4.4 Expression levels of RIG-I in Huh 7.5.1 cells	<b>116</b>
4.5 Phospho-I $\kappa$ B detection in Huh 7.5 cells	<b>117</b>
4.6 IRF3 detection in Huh 7.5 cells	<b>118</b>
4.7 Phospho-I $\kappa$ B detection in Huh 7.5.1 cells	<b>119</b>
4.8 IRF3 detection in Huh 7.5.1 cells	<b>120</b>
4.9 IFN- $\beta$ production in Huh 7.5 cells	<b>122</b>
4.10 IFN- $\beta$ production in Huh 7.5.1 cells	<b>122</b>
5.1 Homodimerisation of MDA5	<b>128</b>
5.2 Homodimerisation of RIG-I	<b>129</b>
5.3 Monomers of LGP2	<b>130</b>
5.4 Association between MDA5 and LGP2	<b>131</b>
5.5 Association between LGP2 and MDA5	<b>132</b>
5.6 Association between RIG-I and LGP2	<b>133</b>
5.7 Association between LGP2 and RIG-I	<b>134</b>
6.1 Colocalisation between IPS-1 and MDA5 in cardiac cells	<b>140</b>
6.2 Colocalisation between IPS-1 and RIG-I in cardiac cells	<b>142</b>

# LIST OF TABLES

1.1 Kinetics of the picornavirus replication cycle	<b>9</b>
1.2 TLR recognition of microbial components	<b>29</b>
1.3 Putative RIG-I ligands	<b>50</b>



# ABBREVIATIONS

Ab	Antibody
APS	Ammonium Persulphate
ATCC	American Type Culture Collection
ATF	Activation Transcription Factor
BD	Becton Dickinson
BSA	Bovine Serum Albumin
CAR	Coxsackie-Adenovirus Receptor
CARD	Caspase Activation and Recruitment Domain
Cardif	CARD Adaptor Inducing Interferon-beta
CAV	Coxsackievirus A
CBA	Cytometric Bead Array
CBP	CREB Binding Protein
CBV	Coxsackievirus B
CLD	CARD-Like Domain
CO <sub>2</sub>	Carbon Dioxide
CRE	Cis-acting Replication Element
CREB	cAMP-Response Element-Binding Protein
Da	Dalton
DAF	Decay Accelerating Factor
DC	Dendritic Cell
DCM	Dilated Cardiomyopathy
DMEM	Dulbecco's Modified Eagle Medium
DMSO	Dimethyl sulfoxide

ds	Double-Stranded
EBV	Epstein-Barr Virus
ECACC	European Collection of Animal Cell Cultures
ECL	Enhanced Chemiluminescence
Fab	Fragment Antigen-Binding Region
FACS	Fluorescence-Activated Cell Sorting
FADD	Fas-Associated Death Domain
Fc	Fragment Crystallisable Region
FCS	Foetal Calf Serum
FITC	Fluorescein Isothiocyanate
FSC	Forward Scatter
GPI	Glycosylphosphatidylinositol
HBV	Hepatitis B Virus
HCMV	Human Cytomegalovirus
HCV	Hepatitis C Virus
HEK	Human Embryonic Kidney
HIV	Human Immunodeficiency Virus
HRP	Horseradish Peroxidase
HSV	Herpes Simplex Virus
Huh	Human Hepatocellular
IFN	Interferon
Ig	Immunoglobulin
I $\kappa$ B	Inhibitor of NF-kappa B
IKK	I $\kappa$ B Kinase
IPS-1	Interferon-beta Promoter Stimulator 1

IRAK	IL-1 Receptor Associated Kinase
IRES	Internal Ribosome Entry Site
IRF	Interferon Regulatory Factor
ISG	Interferon Stimulated Gene
JACoP	Just Another Colocalisation Plugin
KD	Knockdown
KO	Knockout
LB	Luria Broth
LBP	LPS-Binding Protein
LGP2	Laboratory of Genetics and Physiology 2
LLC	Lewis Lung Carcinoma
LLR	Leucine Rich Repeat
LPS	Lipopolysaccharide
LSM	Laser Scanning Microscope
mAb	Monoclonal Antibody
Mal	MyD88-Adaptor Like
MAPK	Mitogen-Activated Protein Kinase
MAVS	Mitochondrial Antiviral Signalling protein
MCMV	Murine Cytomegalovirus
MDA5	Melanoma Differentiation-Associated Gene 5
MHC Class I	Major Histocompatibility Complex Class I
MW	Molecular Weight
MyD88	Myeloid Differentiation Primary Response Gene 88
NaN <sub>3</sub>	Sodium Azide
NEMO	NF-κB Essential Modulator

NF- $\kappa$ B	Nuclear Factor kappa B
NK	Natural Killer
NS	Non-Structural
ORF	Open Reading Frame
pAb	Polyclonal Antibody
PABP	Poly(A)-Binding Protein
PAGE	Polyacrylamide Gel Electrophoresis
PAMP	Pathogen-Associated Molecular Pattern
PAS	Protein A Sepharose
PBS	Phosphate Buffered Saline
pDC	Plasmacytoid Dendritic Cell
PE	Phycoerythrin
PFA	Paraformaldehyde
Poly I:C	Polyinosinic: Polycytidylic Acid
PRR	Pattern Recognition Receptor
RD	Repressor Domain
RIG-I	Retinoic Acid Inducible Gene I
RING	Really Interesting New Gene
RIP-1	Receptor Interacting Protein 1
RLR	RIG-I-like Receptor
r(obs)	Pearson's Correlation Coefficient
RSV	Respiratory Syncytial Virus
RT	Room Temperature
SSC	Side Scatter
SCR	Short Consensus Repeat

SD	Standard Deviation
SDS	Sodium Dodecyl Sulphate
SeV	Sendai Virus
SF	Superfamily
shRNA	Short Hairpin RNA
siRNA	Small Interfering RNA
ss	Single-Stranded
TAB	TAK1 Binding Protein
TAK1	TGF-beta-Activated Kinase 1
TANK	TRAF-Associated NF- $\kappa$ B Activator
TBK1	TANK-Binding Kinase-1
TC	Tissue Culture
TEMED	Tetramethylethylenediamine
TGF	Transforming Growth Factor
TIR	Toll/IL-1 Receptor
TIRAP	TIR-Containing Adaptor Protein
TLR	Toll-Like Receptor
TNF	Tumour Necrosis Factor
TRAF	TNF Receptor Associated Factor
TRAM	TRIF-Related Adaptor Molecule
TRIF	TIR-Domain-Containing Adapter-Inducing Interferon-beta
TRITC	Tetramethylrhodamine Isothiocyanate
UTR	Untranslated Region
UV	Ultraviolet
VISA	Virus-Induced Signalling Adaptor

VPg	Viral Protein (VP) genome-linked
VSV	Vesicular Stomatitis Virus
VZV	Varicella-Zoster Virus
WNV	West Nile Virus

**Chapter 1**  
**INTRODUCTION**

The immune system is a wonder of the human body. It constantly protects us against millions of invading pathogens, ranging from viruses to bacteria, from fungi to parasitic worms. It does this every moment of every day, ceaselessly defending the body from diseases. Viruses are responsible for some of the most serious and deadly diseases in the world. Found in almost every ecosystem on Earth, there are millions of different types of viruses [Breitbart *et al.*, 2008]. Due to their enormous diversity and potential infectivity, the field of virology is vitally important. The structure of the virus, the life cycle, the diseases caused, how they infect the body, and the innate and adaptive immune response, among other things, are all being studied by virologists, in the hope to combat these most successful of predators.

### **1.1 Picornaviridae**

The Picornaviridae family (picornaviruses) are important human and animal pathogens, which cause a wide range of illnesses. The name comes from *pico*, meaning small, and RNA, referring to their genome, so a picornavirus is literally a small RNA virus.

Picornaviruses are group IV viruses (they contain single-stranded, positive sense genomes between 7.2 - 9kb long), of the order ***Picornavirales***. Five families are within this order: Dicistroviridae, Iflaviridae, Marnaviridae, Picornaviridae, and Secoviridae [Le Gall *et al.*, 2008]. The Picornaviridae family can be further subdivided into 12 distinct genera: *Aphthovirus*, *Avihepatovirus*, *Cardiovirus*, *Enterovirus*, *Erbovirus*, *Hepatovirus*, *Kobuvirus*, *Parechovirus*, *Sapelovirus*, *Senecavirus*, *Teschovirus*, and *Tremovirus* [NCBI Taxonomy Browser, URL].



Type B Coxsackieviruses (CBVs) belong to the *Enterovirus* genus, and the *Human enterovirus B* species. The *Enterovirus* genus consists of 10 species: *Bovine enterovirus*, *Human enterovirus A*, *Human enterovirus B*, *Human enterovirus C*, *Human enterovirus D*, *Human rhinovirus A*, *Human rhinovirus B*, *Human rhinovirus C*, *Porcine enterovirus B*, and *Simian enterovirus A*, accounting for over 265 serotypes of virus [Picornaviridae, Enteroviruses, URL]. Within the *Human enterovirus B* species, there are 60 serotypically distinct viruses, including Type B enteroviruses, echoviruses, and CBVs.

There are six different serotypes of CBVs, B1 – B6 (and serotypes A1 to A24 for Type A Coxsackieviruses), which cause both acute and chronic diseases. The virus enters the body through the gastrointestinal tract, and is mainly transmitted via the faecal-oral route, respiratory aerosols, and direct contact with secretions from an infected person. Infants, young children, and immunocompromised individuals are the most susceptible to infection, with illnesses usually lasting between two days and two weeks, occurring during the summer months between June and October [Strikas *et al.*, 1986]. Symptoms usually include fever, headache, sore throat, malaise, gastrointestinal distress, and muscle and chest pain. Rashes and blisters can also occur. Bornholm disease is typical of CBV infection [Brown, 1973]. The most serious diseases caused by CBV5 include viral myocarditis (which can lead on to dilated cardiomyopathy, DCM), aseptic meningitis, and pancreatitis.

Viral myocarditis is an inflammatory disease of the myocardium characterised by leukocyte infiltrate and necrosis of the myocytes [Bohn and Benson, 2002]. Although it is a rare disease, the mortality rate in newborns is approximately 75%, decreasing in older infants and children to between 10-25% [Bengtsson and Lamberger, 1966; English *et al.*, 2004]. Some patients can develop chronic myocarditis, whilst myocardial destruction can lead on to DCM. DCM is characterised by dilation and impaired contraction of the left or both ventricles of the heart, and is the major reason for cardiac transplantation in Europe and the USA [Manolio *et al.*, 1992].

Aseptic meningitis is characterised by serious inflammation of the layers lining the brain (the meninges), and is not caused by pyogenic bacteria. Enteroviruses are the most common cause of aseptic meningitis, with CBV5 and echovirus 6, 9, and 30 more likely to cause meningitis outbreaks, whilst coxsackievirus A9, CBV3, and CBV4 are mostly endemic [Lee and Davies, 2007]. Pancreatitis is the inflammation of the pancreas. Gallstones and heavy alcohol use cause the majority of cases of pancreatitis, but CBV infection has been shown to play a role as well [Huber and Ramsingh, 2004].

## **1.2 Coxsackievirus B5 Structure**

CBV5 consists of a non-enveloped icosahedral capsid enclosing a naked single-stranded, positive sense, polyadenylated RNA genome, 7402 nucleotides long, encoding a 2185 amino acid long polyprotein [Zhang *et al.*, 1993].

The virus capsid of CBV5 is arranged the same as for all picornaviruses. It is composed of 60 icosahedral subunits (12 pentagon-shaped pentamers of five protomers), each of which is composed of one copy of viral protein (VP) 1, VP2, VP3, and VP4. Interactions between VP1, VP2, and VP3 form the shell, whilst the smaller VP4 lies on the inner surface of the protein shell. The structure of the capsid can be seen in *Figure 1.1*.

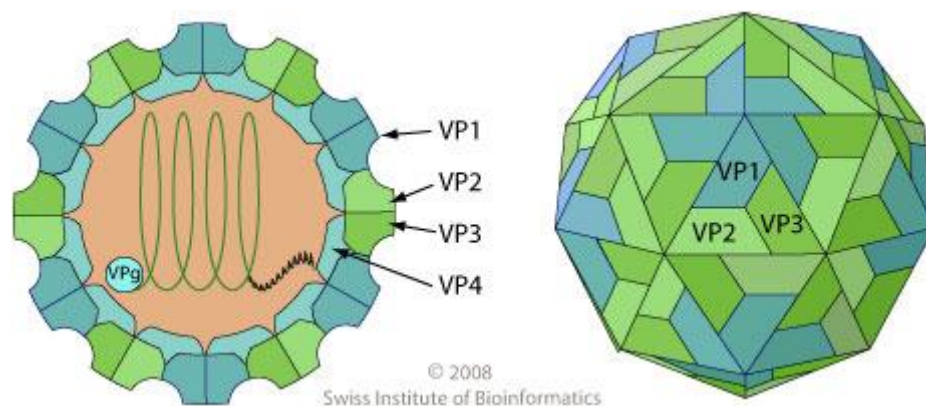


***Figure 1.1: Capsid structure of a Picornaviridae virion. VP1, VP2, and VP3 form the outer shell, with VP4 lying on the inner surface. Together, they make up a single protomer of the capsid [Viral Zone, Picornaviridae, URL].***

The 160S (sedimentary) spherical capsid (approximately 30nm in diameter) lacks a lipid envelope, making infectivity insensitive to solvents. It can also resist low pH, thereby enabling it to pass through the stomach and infect the intestine. Although VP1, VP2, and VP3 have no sequence homology, they do share a similar corrugated topology. The prominent star-shaped plateau (called the mesa) at the fivefold axis of symmetry is surrounded by a deep depression (called a canyon). The canyon is the receptor binding site of CBV5 virions. VP1, VP2, and VP3, approximately 35 kDa each, are folded into eight-stranded antiparallel  $\beta$ -sheet structures, termed a  $\beta$ -barrel jelly roll [Rossmann *et al.*, 1985]. VP1 is located at the 12 fivefold axes, whereas VP2 and VP3 are located at the quasi-sixfold axes [UniProtKB, Q03053, URL]. Although as yet unsolved for CBV5, the  $\beta$ -barrel jelly roll structure of CBV3 has been determined to a resolution of 3.5 Ångstroms [Muckelbauer *et al.*, 1995], as can be seen in *Figure 1.2*.

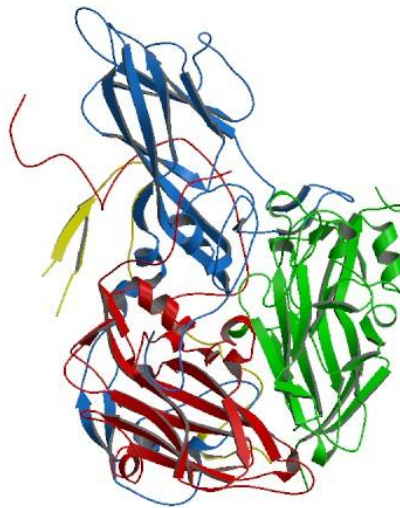


**Figure 1.2:**  $\beta$ -barrel jelly roll structure of CBV3. VP1 is shown in blue, VP2 in red, VP3 in green, and VP4 in yellow. VP1, VP2, and VP3 are each folded into eight-stranded antiparallel  $\beta$ -sheets with a jelly-roll topology [ViperDB, URL].

Underneath the canyon floor, within the core of the VP1  $\beta$ -barrel, is a hydrophobic pocket, occupied by a fatty acid ‘pocket factor’, which is thought to mediate the stability of the capsid and is released before uncoating [Airaksinen, 2000; Smyth and Martin, 2002]. The CBV5 genome exhibits the same gene organisation as other enterovirus genomes, and can be seen in *Figure 1.3*.

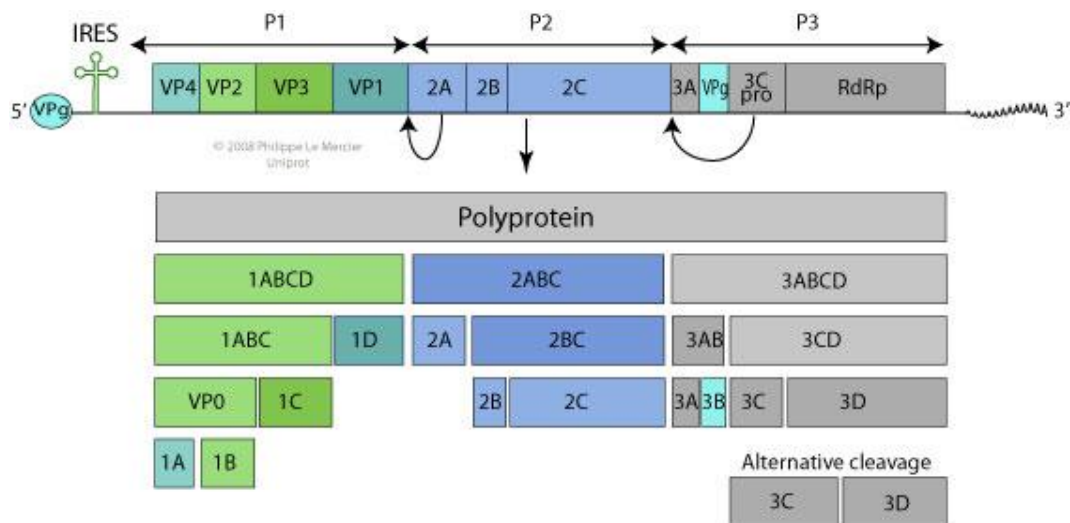


**Figure 1.3: Genome organisation of an enterovirus.** A 5' UTR containing an IRES is followed by a single open reading frame (ORF) divided into three regions, and ends with a short 3' UTR with a poly(A) tract. P1, P2, and P3 are the products of the initial proteolytic cleavages of the viral polyprotein. Abbreviations: VP, viral protein; UTR, untranslated region; IRES, internal ribosome entry site; VPg, viral protein genome-linked [Viral Zone, Enterovirus, URL].

The enterovirus genome consists of a single open reading frame (ORF) encoding a polyprotein. At the 5' end is long (~600-1300 nucleotides) and highly structured untranslated region (UTR). This 5' UTR contains a cloverleaf secondary structure termed a Type I internal ribosome entry site (IRES), as well as a covalently linked 22 – 24 amino acid long VPg region (viral protein genome-linked) in place of a

methyated nucleotide cap structure. The shorter 3' UTR (~50-100 nucleotides) contains a pseudoknot secondary structure and a short poly(A) tract, which is essential for virus infectivity [Spector and Baltimore, 1974]. The 5' UTR is involved in the initiation of translation, with VPg acting as the protein primer of RNA synthesis [Pelletier and Sonenberg, 1988; Jang *et al.*, 1988], whilst the 3' UTR is important in initiating the synthesis of negative-strand RNA [Rohll *et al.*, 1995], and may have a role in increasing the efficiency of viral replication and determining tissue tropism [Brown *et al.*, 2004].

During translation, the ORF encoding the single viral polyprotein is proteolytically cleaved into the three precursor proteins P1, P2, and P3. These are further cleaved into the structural proteins VP1 to VP4 (from P1), and seven non-structural proteins (2A to 2C and 3A to 3D), involved in protein processing and genome replication. Each protein has a specific function in viral replication, and many of the intermediate cleavage products are also functional, as detailed later.

### **1.3 Picornavirus Replication Cycle**

The picornavirus replication cycle takes place entirely within the cytoplasm of the cell, and can even occur in enucleated cells [Pollack and Goldman, 1973; Bossart and Bienz, 1979]. The replication cycle can be divided into eight main stages: attachment, uncoating, translation, protein processing, negative (-) sense RNA synthesis, positive (+) sense RNA synthesis, assembly, and release. *Figure 1.4* provides an overview of the picornavirus replication cycle, with the eight most significant stages highlighted.

The picornavirus replication cycle occurs rapidly, with the cycle generally being completed within 5-10 hours of infection. *Table 1.1* outlines the kinetics of the picornavirus replication cycle.

***Table 1.1: Kinetics of the picornavirus replication cycle.***

<b>Time after infection</b>	<b>Event</b>
~1-2 hours	Sharp decrease in host cell macromolecular synthesis
~2-3 hours	Start of viral protein synthesis, vacuolation of cytoplasm
~3-4 hours	Permeabilisation of plasma membrane
~4-6 hours	Virus assembly in cytoplasm
~6-10 hours	Cell lysis and release of virions

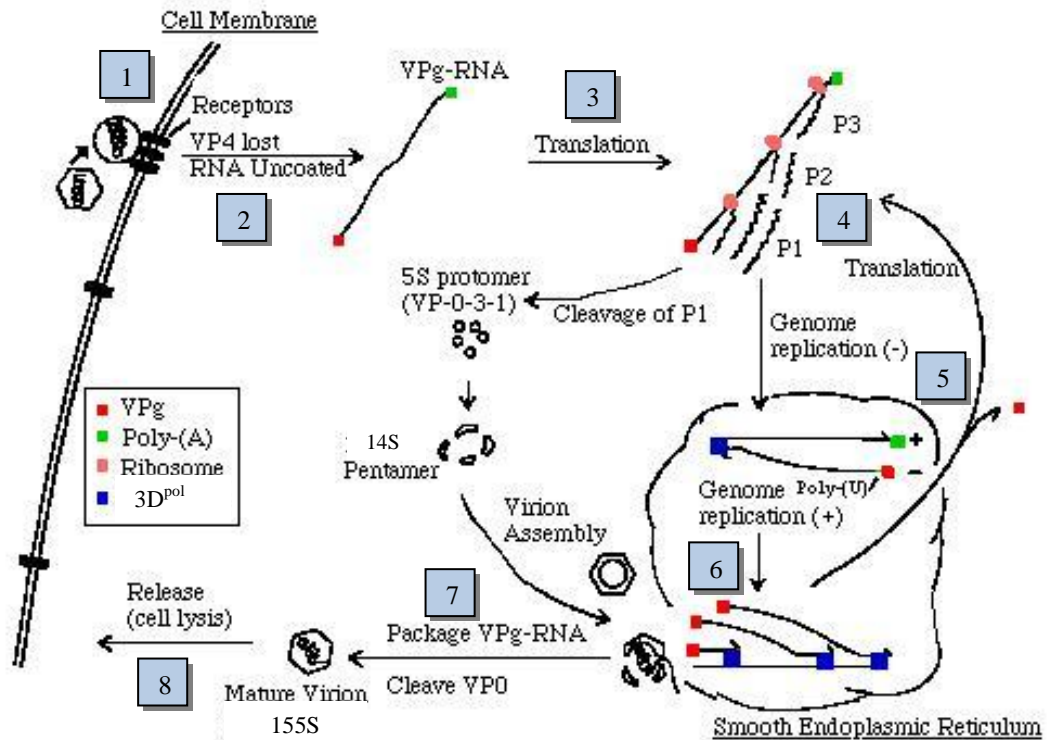


**Figure 1.4: Replication cycle of a picornavirus.** The virion attaches to its specific receptor (1) and uncoats, releasing its viral RNA into the cytoplasm (2). The viral RNA is then translated into a polyprotein using the host machinery (3). Cleavage of the polyprotein into structural (P1) and non-structural (P2 and P3) regions then occurs (4). The positive (+) sense viral RNA is used as a template to synthesise complementary negative (-) sense RNA (5), from which large amounts of (+) sense RNA can then be synthesised (6). Cleavage of P1 into VP0, VP1, and VP3 occurs simultaneously, resulting in a procapsid, which is packaged with the viral (+) sense RNA (7). VP0 is cleaved, and the mature virion is released from the cell (8) [modified from MicrobiologyBytes, URL].



### 1.3.1 Attachment

The first step in the picornavirus replication cycle is the attachment of the virion to specific host cell receptors. The attachment phase is the determinant of tissue tropism, as viruses can only infect cells that have particular cell surface receptors. Picornaviruses use a wide range of cell surface molecules for cellular receptors, and certain viruses can bind to several different receptors. CBV5 has been shown to have many cell surface binding receptors, with the two most common being coxsackievirus-adenovirus receptor (CAR), a member of the immunoglobulin (Ig) superfamily [Bergelson *et al.*, 1997a], and decay accelerating factor (DAF / CD55) [Bergelson *et al.*, 1995; Shafren *et al.*, 1995]. A further five cell surface receptors, found on the surface of human cardiac cells, have also been shown to interact with CBV5 [Orthopoulos *et al.*, 2004].

CAR is a 46 kDa transmembrane protein, consisting of 365 amino acids with a short leader, a 222 amino acid extracellular domain, a membrane-spanning helical domain, and a 107 amino acid intracellular domain [Bergelson *et al.*, 1997b]. Analysis of the CAR amino acid sequence suggests that the extracellular domain consists of two Ig-like domains (Ig V-like and Ig C2-like), as can be seen in *Figure 1.5*.

DAF is a 70 kDa glycosylphosphatidylinositol (GPI)-anchored protein found on most cell surfaces that regulates the complement system on the cell surface. It prevents the assembly or promotes the disassembly of the C3-convertase of the alternative complement pathway, thereby blocking the formation of the membrane attack complex. It consists of four short consensus repeat (SCR) domains

followed by a heavily *O*-glycosylated serine and threonine-rich domain, attached to the cell membrane by a GPI anchor [Nicholson-Weller and Wang, 1994], as seen in *Figure 1.6*.

The precise mechanism of CBV5 attachment is yet to be elucidated, with the most likely theory currently being the “canyon hypothesis” [Rossmann *et al.*, 2002]. The canyon, which surrounds the fivefold axis of symmetry, contains deeply buried, conserved amino acid residues that bind the amino terminal domains of CAR and DAF. The residues outside the canyon are hyper-variable and vulnerable to attack by antibodies [Petrella *et al.*, 2002; Rossmann *et al.*, 2002], which are too large to penetrate deep into the canyon, thereby allowing the virus to escape the host immune surveillance.

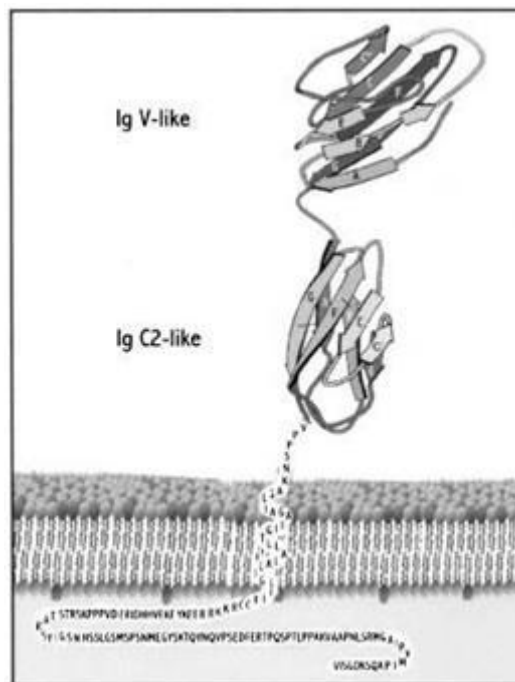


**Figure 1.5: General representation of CAR structure**, depicting the two Ig-like domains Ig V-like (starting at the amino terminus and ending near residue 120) and Ig C2-like (found approximately between residues 124 to 210) [Carson, 2001].

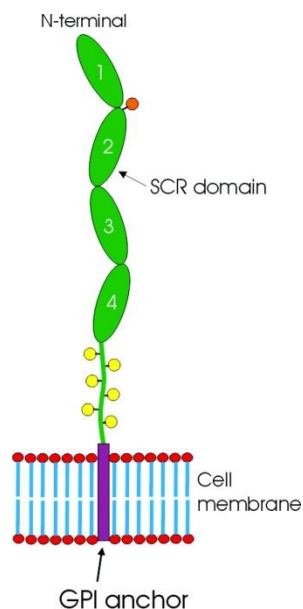


**Figure 1.6: Diagrammatic structure of decay accelerating factor (DAF).** The green ellipses represent the four short consensus repeat (SCR) domains. The yellow spheres are O-linked and the orange spheres are N-linked carbohydrate moieties. DAF is attached to the cell membrane via a glycosylphosphatidylinositol (GPI) anchor [He et al., 2002].

### 1.3.2 Uncoating

The uncoating stage of the picornavirus replication cycle is even less well understood than the attachment phase. For a virus to survive and infect new hosts, the viral capsid must be stable and strong enough to protect the viral genome during transmission between hosts, whilst at the same time, upon receiving the appropriate signal, it must be able to dissociate or alter its conformation sufficiently to allow the genome to be released into the host cell's cytoplasm.

After binding to the receptor, the picornavirus capsid undergoes a permanent structural rearrangement inside a clathrin-coated pit. The main characterisation of this is the loss of VP4 [Crowell and Philipson, 1971] and the shift from a 160S particle to a 135S particle. The 135S particles, also known as *altered*, or *A particles*, contain the viral RNA, but have lost VP4. These *A particles* also have the hydrophobic N-terminus of VP1 exposed externally, which has an increased affinity for the cellular membrane [Fricks and Hogle, 1990]. This exposed N-terminus of VP1 inserts into the cell membrane, forming a channel in the fivefold axis mesa, through which the viral RNA can travel into the cytoplasm [Smyth and Martin, 2002; Tosteson and Chow, 1997], as shown in *Figure 1.7*.

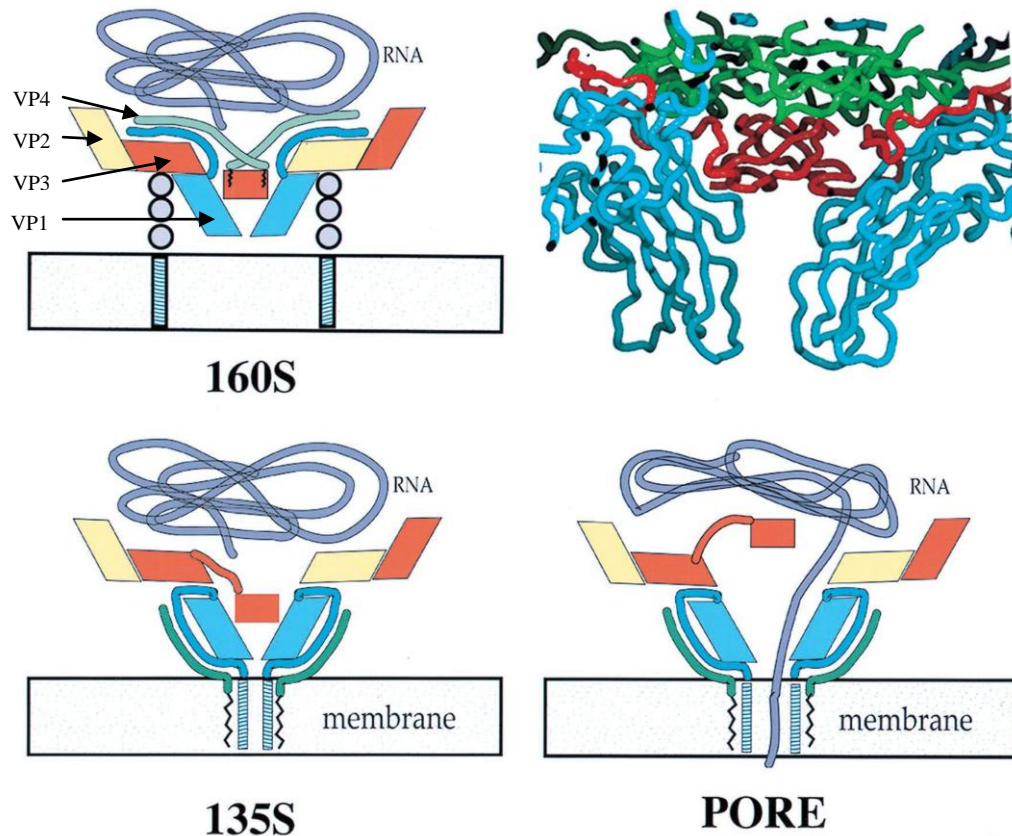


**Figure 1.7: Uncoating of a picornavirus.** A potential mechanism for transferring viral RNA across the cell membrane. VP1, VP2, VP3, and VP4 are coloured cyan, yellow, red, and green, respectively. In the crystal structure of the virion (upper right), the beta-tube of VP3 (red) forms a plug at the fivefold axis that separates the virus interior from the outer surface. Attachment of the 160S particle (upper left) to the virus receptor (three gray circles) triggers conversion to the 135S form (lower left). Upon conversion, cell attachment is mediated by externalised VP4 (green tubes) and the N-termini of VP1 (blue tubes). The N-termini emerge from the bottom of the canyon and extend along the sides of the fivefold axis mesa towards the apex. Once the N-terminal helices of VP1 have inserted into the membrane, they rearrange to form a pore (lower right). To permit the RNA (purple tube) to pass through the pore into the cytoplasm, it would be necessary for the VP3 beta-tube (red rectangle) to shift on its 40-residue tether (red tube) and for the VP1 barrels to splay farther apart [modified from Belnap et al., 2000].

### 1.3.3 Translation

Once in the cytoplasm, the viral RNA is translated into a polyprotein using the host cell's translational machinery, via a mechanism of cap-independent translation known as internal ribosome entry [Jang *et al.*, 1998; Pelletier *et al.*, 1988]. During viral infection, the host cell machinery is rapidly shut down, to allow the viral gene expression to initiate and persist. This is possible due to the two different translation initiation mechanisms involved: The host cell uses a cap-dependent mechanism; whilst picornaviruses use a cap-independent mechanism (*Figure 1.8*).

In cap-dependent translation initiation, the eIF4E component of the cap binding complex (eIF4F) interacts with the cap structure covalently linked to the 5' end of the mRNA. The 40S ribosomal subunit, complexed with eIF2-Met-tRNA-GTP, eIF3, and eIF1A, gets recruited to the mRNA and scans along it until the start codon is reached. The 60S ribosomal subunit then joins the complex, initiation factors are released, and translation begins [Bedard and Semler, 2004].

Picornavirus RNA genomes utilise the cap-independent translation initiation mechanism, as they do not have a 7-methyl G cap structure found at the 5' end of their genome. Instead, they contain a VPg region and a Type I IRES within a long, highly structured 5' UTR, which contains several, non-authentic start codons that potentially preclude a scanning ribosome [Racaniello and Baltimore, 1981], and is where viral translation initiates. To ensure the host cell machinery switches from cellular to viral processes, the viral proteinases 2A and 3C cleave several cellular proteins, including eIF4G, causing a rapid shut off of cap-dependent translation

[Kräusslich *et al.*, 1987]. Poly(A)-binding protein (PABP) cleavage by 2A has also been shown to inhibit host cell translation [Kerekatte *et al.*, 1999].

The IRES elements are divided into three groups, Type I, Type II, and Type III, based on sequence similarity and structure homology [Wimmer *et al.*, 1993; Borman *et al.*, 1997], with CBVs containing Type I IRESs. The 5' UTR of CBV RNA is predicted to contain six major stem-loop structures upstream of the translation start site, and the IRES is located within the region between stem-loops II and V (*Figure 1.8*) [Martinez-Salas and Fernandez-Miragall, 2004; Pelletier *et al.*, 1988]. The stem-loop IV structure has been shown to be important for translation [Trono *et al.*, 1988] and cellular protein binding [Gamarnik and Andino, 2000], such as by poly(rC) binding protein (PCBP2), which interacts with the IRES and is necessary for efficient translation [Blyn *et al.*, 1997; Walter *et al.*, 1999; Sean *et al.*, 2009].

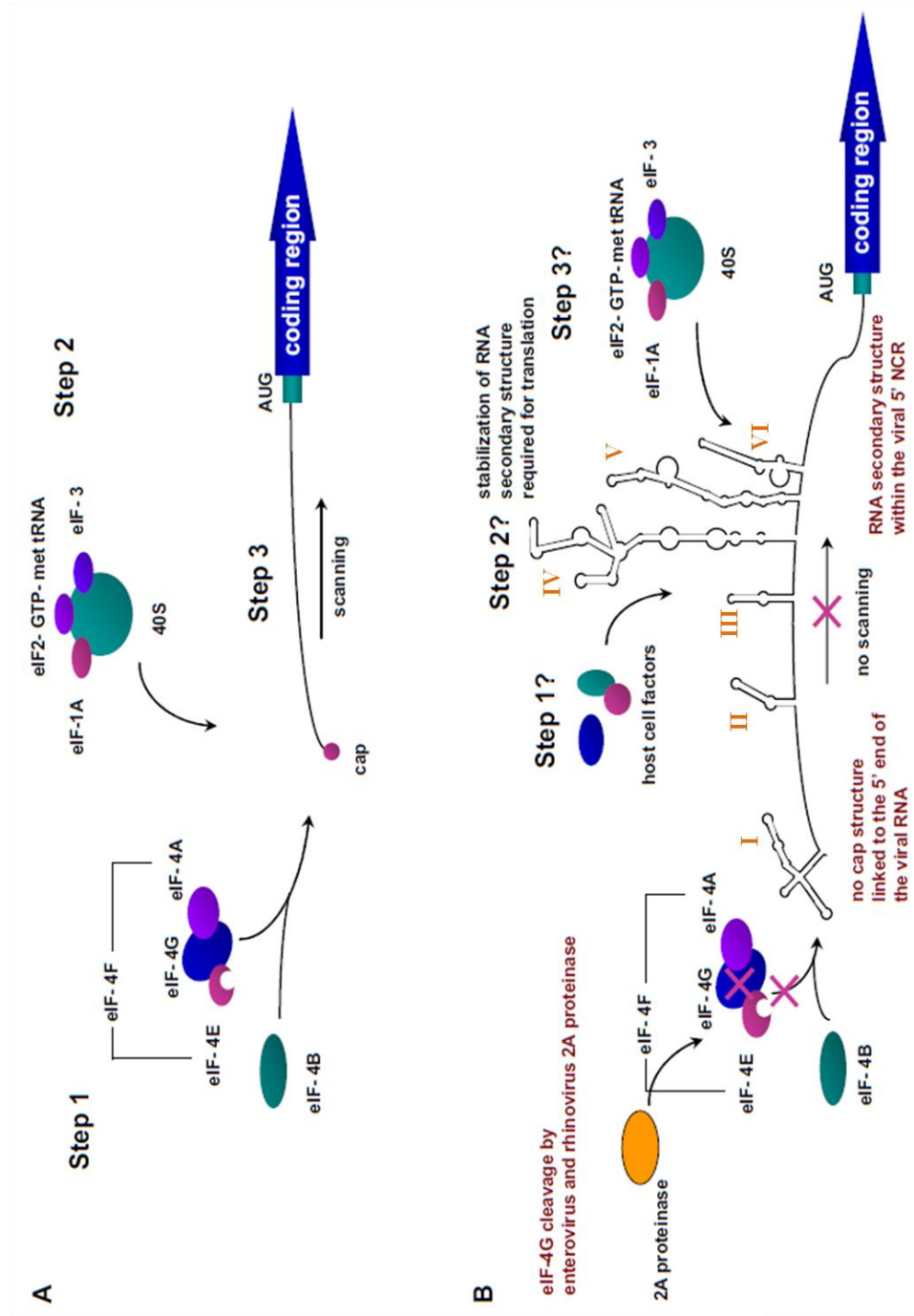


**Figure 1.8: The mechanisms of cap-dependent and cap-independent translation initiation.** Panel A shows the steps of translation initiation for canonical cap-dependent translation. The characteristics of picornavirus RNA and the cleavage events during an infection that prevent cap-dependent translation of viral RNA are highlighted in red in Panel B. Although the mechanism of cap-independent translation of picornaviruses is not fully understood, the predicted steps of picornavirus translation initiation are highlighted [modified from Bedard and Semler, 2004].



#### 1.3.4 Protein Processing

Once translated, the viral polyprotein gets proteolytically cleaved into precursor and mature viral proteins (*Figure 1.3*). The primary cleavage event is mediated by the viral cysteine proteinase 2A, which cleaves the polyprotein at the junction between P1 and P2. This self-cleavage occurs in *cis*, resulting in the structural P1 precursor and the nascent non-structural P2-P3 protein [Toyoda *et al.*, 1986]. Translation slows down markedly if P1 is not removed from the nascent chain, and further processing is unlikely to occur [Nicklin *et al.*, 1987]. The 2A proteinase also cleaves the eIF4G component of the cap binding complex, causing a rapid shutdown of host cell translation [Kräusslich *et al.*, 1987]. Secondary cleavage events are carried out in *trans* by the viral cysteine proteinase 3C, and its precursor 3CD, both of which process key replication proteins within the P2 and P3 regions.

Each of the viral proteins involved in RNA replication has a specific function, with some proteins having multiple roles to play. The P1 region encodes for the four structural capsid proteins, VP1 to VP4. It is initially cleaved into VP1, VP3, and VP0 [Jore *et al.*, 1988], then during maturation, VP0 is cleaved into VP2 and VP4 in a final processing step [Basavappa *et al.*, 1994].

The proteins from the P2 region of the polypeptide (2A, 2B, and 2C) are involved in protein processing, host cell membrane rearrangement, and RNA replication. The viral cysteine proteinase 2A plays a vital role in the initial processing events, as mentioned above, and has also been shown to function in RNA replication [Li *et al.*, 2001]. 2B affects membrane integrity, resulting in an increase in

permeability, which is important for virion release during the late stages of infection [van Kuppeveld *et al.*, 1997; Doedens and Kirkegaard, 1995], whilst 2C, and its precursor protein 2BC, induce structural rearrangements of intracellular membranes and are involved in the formation of viral-induced cytoplasmic vesicles [Cho *et al.*, 1994; Echeverri and Dasgupta, 1995].

The P3 proteins (3A, 3B, 3C, 3D, and their precursors) are crucial for immune response interference and viral RNA replication. 3A inhibits both transport between the endoplasmic reticulum and the Golgi apparatus [Doedens *et al.*, 1997], and major histocompatibility complex (MHC) Class I-dependent antigen presentation [Deitz *et al.*, 2000]. 3B (also called VPg), is the protein primer covalently linked to the 5' end of both positive- and negative-strand RNAs. 3AB is involved in RNA replication [Giachetti *et al.*, 1992] and membrane association of RNA replication complexes [Towner *et al.*, 1996], and it also stimulates the activity of 3D [Paul *et al.*, 1994] and the self-cleavage of 3CD [Molla *et al.*, 1994]. The viral cysteine proteinase 3C, as well as carrying out secondary cleavage events, binds to the cloverleaf RNA structure called stem-loop I (*Figure 1.8*) along with its precursor 3CD, influencing viral genome replication [Bell *et al.*, 1999; Zell *et al.*, 2002]. Protein 3D, known as the viral RNA-dependent RNA polymerase 3D<sup>pol</sup>, is responsible for VPg uridylation and RNA chain elongation during viral RNA synthesis [Kerkvliet *et al.*, 2010]. It is an error-prone polymerase, integrating 1-2 nucleotides per replication of each viral template, resulting in an increased mutation frequency and evolution rate, potentially enhancing the fitness of the picornavirus population.

### 1.3.5 Negative (-) and Positive (+) Sense RNA Synthesis

Picornaviruses contain single-stranded, positive sense RNA genomes, and use a unique mechanism to replicate themselves, involving several different RNA-protein and protein-protein interactions. The positive sense viral RNA strand, as well as serving as a template for protein synthesis, is used as a template to synthesise complementary negative sense RNA strands with poly(U) tails, which are in turn used to synthesise large amounts of positive sense RNA genomes. This occurs near the smooth endoplasmic reticulum in the host cell [Mosser *et al.*, 1972; Schlegel *et al.*, 1996]. These positive sense RNA strands can then be packaged into virions, or act as templates for subsequent rounds of cap-independent translation for the synthesis of more viral proteins.

3D<sup>pol</sup> is an essential protein involved in this synthesis process. As well as catalysing chain elongation during viral RNA synthesis, it also generates the protein primer, VPg-pU-pU, in a process called VPg uridylylation [Paul *et al.*, 1998]. 3D<sup>pol</sup> covalently couples uridine nucleotides to a conserved tyrosine residue in the VPg protein, located at the 5' end of both positive and negative sense viral RNA. The cis-acting replication element (CRE), a sequence within the coding region of the picornavirus genomic RNA, serves as a template for VPg uridylylation by 3D<sup>pol</sup>, and is stimulated by the binding of 3AB and 3CD [Molla *et al.*, 1994; Rieder *et al.*, 2000; Pathak *et al.*, 2008]. Following on from VPg uridylylation, the viral 3' poly(A) tract acts as the initiation site for negative sense RNA synthesis. A double-stranded RNA intermediate, termed the replicative form, is produced first, which brings the CRE in proximity of VPg uridylylation and initiation. The new negative sense RNA strands are then used as templates for

multiple initiation events to produce large quantities of positive sense viral RNA strands.

Positive sense RNA synthesis is dependent upon the uridylylation of VPg, which occurs at the CRE of the RNA [Murray and Barton, 2003], and thus, positive sense RNA initiation occurs at the 3' end of the negative sense replicative form. A single negative sense RNA strand can serve as a template for the production of several positive sense RNA genomes, with a ratio of positive to negative viral RNA strands being between 40:1 and 70:1 [Novak and Kirkegaard, 1991].

### 1.3.6 Assembly and Release

Virion assembly begins when the P1 precursor protein is cleaved by the proteinase 3CD into the capsid 5S protomer, consisting of one each of VP0, VP1, and VP3 (*Figures 1.3 and 1.4*). Five of these protomers then assemble to form the 14S pentamer [Palmenberg, 1982], followed by twelve pentamers associating together to form the 73S procapsid.

Newly synthesised positive sense RNA is encapsidated within the procapsid, forming a 155S provirion. This is a highly specific process, resulting in only positive sense RNA strands being packaged [Novak and Kirkegaard, 1991], and it has been suggested that glutathione, or a glutathione-dependent process, is required for efficient encapsidation of viral RNA to produce infectious virions [Smith and Dawson, 2006]. During RNA encapsidation, VP0 is cleaved into VP2 and VP4. This process is called the maturation cleavage, and it locks the assembled capsid into a stable, mature, 155S virion. Maturation cleavage does not involve the action of either of the proteinases 2A or 3C, since the VP0 scissile bond is located in the interior of empty and mature virions, and is therefore inaccessible to viral or host proteinases. When VP0 is cleaved, an ordered N-terminal network containing an interlocking seven-stranded  $\beta$ -sheet formed by capsid residues from adjacent pentamers is established, resulting in an increase in particle stability and the acquisition of infectivity [Basavappa *et al.*, 1994]. Once the virions have been assembled, they are released from the cell via cell lysis. The steps involved in picornavirus virion assembly can be seen in *Figure 1.9*.

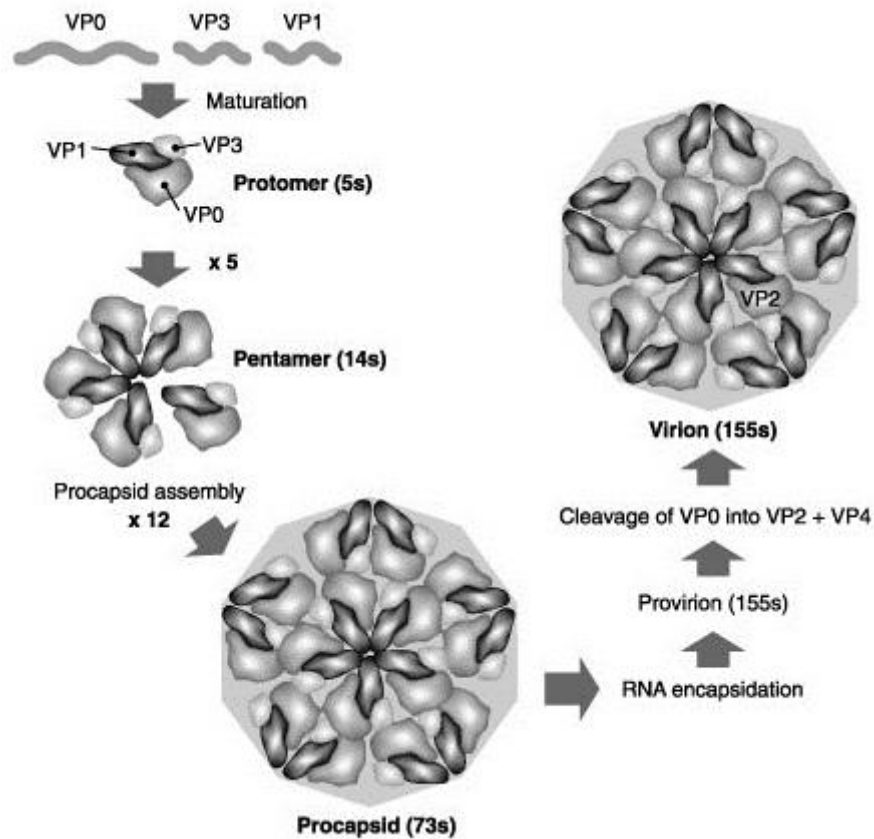


**Figure 1.9: Picornavirus virion assembly.** Precursor proteins (VP0, VP3, and VP1) associate to form 5S protomers, which then assemble to form 14S pentamers. Twelve of these assemble to form the 73S procapsid into which virion RNA is incorporated. Final cleavage of VP0 into VP2 and VP4 takes place to form the mature virus particle [modified from Wagner et al., 2008].

#### **1.4 Innate Immunity and Toll-like Receptors**

All living organisms are constantly exposed to invasive microorganisms present in the environment that need to be detected and dealt with effectively to ensure survival. Invading pathogens initiate an immune response in the host via two main branches of immunity: innate (non-specific) immunity and adaptive (antigen specific; also known as acquired) immunity. The adaptive immune response, present only in vertebrates, is mediated by B and T cells. This response is very specific, as both B cells (antibody producing) and T cells (killer and helper) express highly diverse antigen receptors, generated through DNA rearrangement, which enable them to detect and respond to a wide range of potential antigens. This provides life-long immunological memory, but can take weeks or months to establish sufficient levels of immunity. On the other hand, innate immunity, present in almost all multicellular organisms, is the first line of defence against pathogens, and responds rapidly to invading microbes.

Innate immune cells, such as macrophages and dendritic cells (DCs), express a class of immune-sensor molecules termed pattern recognition receptors (PRRs). Proposed over 20 years ago [Janeway, 1989], PRRs, which can distinguish self from non-self, recognise certain microbial components, termed pathogen-associated molecular patterns (PAMPs), and initiate an appropriate immune response. PAMPs are highly conserved structures that are usually essential for microbial survival or pathogenicity, and entire classes of pathogens share these invariant structures. Recognition of PAMPs by PRRs leads to the rapid activation of latent transcription factors to stimulate the expression of antimicrobial genes and the production of type I interferons (IFN). Type I IFNs (consisting of multiple

IFN- $\alpha$  isoforms, a single IFN-  $\beta$  one, and other members, including IFN- $\epsilon$ , - $\kappa$ , and - $\omega$ ) are pleiotropic cytokines that mediate induction of the innate immune response, as well as the subsequent development of the adaptive immune response [Akira and Takeuchi, 2007]. They induce maturation of DCs by increasing the expression of costimulatory molecules (such as CD80, CD86, and CD40), and they also increase antigen presentation via MHC class I, which facilitates cross-presentation of the viral antigens. As well as this, type I IFNs also mediate induction of antigen-specific CD8<sup>+</sup> T cell responses and chemokines, which results in stimulation and recruitment of lymphocytes and monocytes to inflamed sites. To fully induce an antimicrobial state, type I IFNs also upregulate hundreds of effector molecules that directly influence protein synthesis, cell growth, and survival [Kawai and Akira, 2006]. Type I IFNs are transcriptionally upregulated through the coordinated activation of latent transcription factors, including nuclear factor- $\kappa$ B (NF- $\kappa$ B), activating transcription factor 2-c-Jun (ATF2-c-Jun), mitogen-activated protein kinases (MAPKs), IFN Regulatory Factor 3 (IRF3), and IRF7.



### 1.4.1 Toll-like Receptors

The Toll-like receptors (TLRs) are an important class of PPRs that have been shown to recognise an increasingly diverse set of pathogens, leading to the activation of the innate and adaptive immune response. TLRs were originally identified based on their sequence homology with the Toll receptor in *Drosophila*, which is essential in controlling dorsoventral polarity during embryogenesis, and also plays a critical role in the fly's innate immune response to fungal pathogens [Lemaitre *et al.*, 1996; Medzhitov *et al.*, 1997; Rock *et al.*, 1998]. The amino acid sequence of the Toll receptor in *Drosophila* and the cytoplasmic portion of the mammalian interleukin-1 receptor (IL-1R) is highly conserved [Gay and Keith, 1991], and is termed the Toll/IL-1R (TIR) domain, with activation of IL-1R signalling pathways activating NF- $\kappa$ B, a transcription factor homologous to *Drosophila* Dorsal [Belvin and Anderson, 1996].

Upon the discovery of *Drosophila* Toll homologues, a whole family of TLRs has since been identified. Currently, there are 13 members within the TLR family: TLR1 – TLR9 are conserved in both human and mice; TLR10 is functional only in humans; whilst TLR11 – TLR13 are present only in mice [Medzhitov *et al.*, 1997; Rock *et al.*, 1998; Takeuchi *et al.*, 1999; Chuang and Ulevitch, 2000; Du *et al.*, 2000; Tabeta *et al.*, 2004; Zhang *et al.*, 2004]. Each TLR recognises a particular PAMP, and initiates the appropriate downstream signalling to activate the innate and adaptive immune response. The ligand for TLR4 was the first identified, and found to be lipopolysaccharide (LPS), a cell-wall component mainly found in Gram-negative bacteria [Hoshino *et al.*, 1999]. Other bacterial lipoprotein moieties are recognised by TLR1, TLR2, and TLR6. TLR1 and TLR2

form a heterodimer and recognise several triacyl lipopeptides (including Pam3CSK4) [Takeuchi *et al.*, 2002], whilst TLR2 and TLR6 can form another heterodimer and recognise diacyl lipopeptides (such as MALP-2) [Takeuchi *et al.*, 2001]. TLR2 is essential for the recognition of lipoteichoic acid (LTA) from Gram-positive bacteria, and peptidoglycan, lipoarabinomannan, porins, GPI-anchored proteins and Hemagglutinin proteins from bacteria, viruses, and parasites [Akira *et al.*, 2006]. TLR9 is responsible for the recognition of unmethylated CpG DNA [Wagner, 2002], DNA from DNA viruses, and hemozoin [Coban *et al.*, 2005]. TLR3 recognises polyinosinic: polycytidylic acid (Poly I:C), a synthetic double-stranded RNA (dsRNA) analogue, and dsRNA from Reovirus and rotaviruses [Akira *et al.*, 2006]. Single-stranded RNA (ssRNA), on the other hand, is recognised by TLR7/8 [Diebold *et al.*, 2004]. Finally, TLR5 recognises flagellin, a component of bacterial flagella [Hayashi *et al.*, 2001], and TLR11 recognises a parasite-derived profilin-like protein [Yarovinsky *et al.*, 2005]. *Table 1.2* shows which microbial component from which species is detected by which TLR(s).

**Table 1.2: TLR recognition of microbial components** [modified from Akira et al., 2006].

Microbial Components	Species	TLR Usage
<b>Bacteria</b>		
LPS	Gram-negative bacteria	TLR4
Diacyl lipopeptides	<i>Mycoplasma</i>	TLR6/ TLR2
Triacyl lipopeptides	Bacteria and mycobacteria	TLR1/ TLR2
LTA	Group B <i>Streptococcus</i>	TLR6/ TLR2
PG	Gram-positive bacteria	TLR2
Porins	<i>Neisseria</i>	TLR2
Lipoarabinomannan	Mycobacteria	TLR2
Flagellin	Flagellated bacteria	TLR5
CpG DNA	Bacteria and mycobacteria	TLR9
ND	Uropathogenic bacteria	TLR11
<b>Fungus</b>		
Zymosan	<i>Saccharomyces cerevisiae</i>	TLR6/ TLR2
Phospholipomannan	<i>Candida albicans</i>	TLR2
Mannan	<i>Candida albicans</i>	TLR4
Glucuronoxylomannan	<i>Cryptococcus neoformans</i>	TLR2 and TLR4
<b>Parasites</b>		
tGPI-mutin	<i>Trypanosoma</i>	TLR2
Glycoinositolphospholipids	<i>Trypanosoma</i>	TLR4
Hemozoin	<i>Plasmodium</i>	TLR9
Profilin-like molecule	<i>Toxoplasma gondii</i>	TLR11
<b>Viruses</b>		
DNA	Viruses	TLR9
dsRNA	Viruses	TLR3
ssRNA	RNA viruses	TLR7 and TLR8
Envelope proteins	RSV, MMTV	TLR4
Hemagglutinin protein	Measles virus	TLR2
ND	HCMV, HSV1	TLR2
<b>Host</b>		
Heat-shock protein 60, 70		TLR4
Fibrinogen		TLR4
ND = Not Determined		

### 1.4.2 Toll-like Receptor Structure

The members of the TLR family are Type I transmembrane proteins consisting of three major domains: a leucine rich extracellular domain; a transmembrane domain; and a cytoplasmic TIR domain (*Figure 1.10*). The extracellular domain contains a leucine rich repeat (LRR), composed of 19-25 tandem copies of the “xLxxLxLxx” motif, 24-29 amino acids in length, in a horseshoe-like structure [Akira *et al.*, 2006; Jin and Lee, 2008]. All TLRs form hetero- and homodimers, facilitating dimerisation of the TIR domain to activate intracellular signalling. Some TLRs require additional proteins to be bound to them to be fully functional. TLR4 is tightly bound to MD-2 on the cell surface, a molecule that confers responsiveness to LPS [Shimazu *et al.*, 1999]. CD14 and LPS-binding protein (LBP) are also involved in LPS recognition by TLR4, as CD14 transfers the LBP-LPS complex to TLR4/MD-2 to induce cellular activation [Kitchens, 2000]. TLR2 heterodimerises with TLR1 and TLR6, as well as non-TLR receptors such as CD36 or Dectin-1, to enable recognition of various TLR2 ligands [Gantner *et al.*, 2003; Hoebe *et al.*, 2005]. The crystal structures of TLR3 [Choe *et al.*, 2005], TLR4 [Kim *et al.*, 2007], and TLR1, TLR2, and TLR6 [Jin *et al.*, 2007; Kang *et al.*, 2009], with or without their ligands, have been elucidated. The TLRs can be separated into intracellular and extracellular members, as shown in *Figure 1.10*.

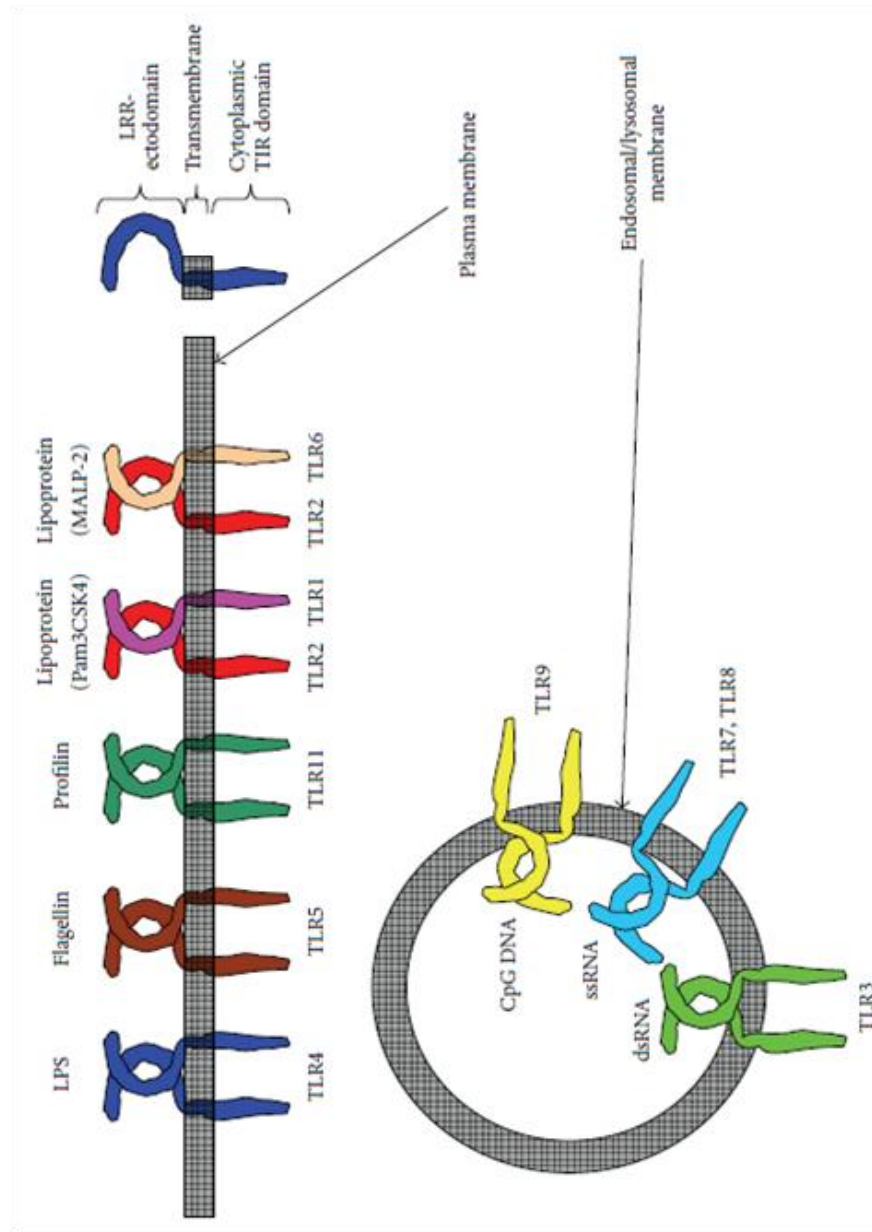


**Figure 1.10: TLR localisation.** *TLR1, TLR2, TLR4, TLR5, TLR6, and TLR11 recognise their ligands on the cell surface, whilst TLR3, TLR7, TLR8, and TLR9 are located intracellularly, in endosomes and lysosomes [Yamamoto and Takeda, 2010].*

### 1.4.3 Toll-like Receptor Signalling Pathways

Once TLRs have recognised their PAMP, they signal downstream, through their TIR domains, via two different pathways: the MyD88-dependent pathway (all TLRs except TLR3); and the MyD88-independent (TRIF-dependent) pathway (TLR3 and TLR4) (*Figure 1.11*). MyD88 (Myeloid differentiation primary response gene 88) is a member of the family of cytoplasmic TIR domain-containing adaptor molecules, which also includes TIRAP (TIR-containing adaptor protein, also known as Mal; MyD88-adaptor like), TRIF (TIR-domain-containing adapter-inducing IFN- $\beta$ ), and TRAM (TRIF-related adaptor molecule). The TIR domain of TLRs selectively recruits specific TIR domain-containing adaptors, thereby generating signalling specificity for each TLR [Yamamoto *et al.*, 2004].

MyD88, a master adaptor molecule, is used by all TLRs except TLR3, and is also utilised by all IL-1R family members [Akira *et al.*, 2006]. Mal/TIRAP interacts with MyD88 through the TIR domain, and selectively participates in TLR2- and TLR4-mediated MyD88-dependent signalling pathways [Yamamoto *et al.*, 2002]. In the MyD88-dependent pathway, MyD88, through a homophilic interaction of the death domain, interacts with IL-1R-associated kinase (IRAK) 4 [Li *et al.*, 2002]. IRAK4, via IRAK1, regulates the activity of tumour necrosis factor (TNF) receptor-associated factor (TRAF) 6, a RING finger-containing E3 ligase, which is involved in lysine 63 (K63)-linked ubiquitination-mediated signalling. TRAF6, catalysed by the E2 ubiquitin conjugating enzyme complex Ubc13 and UEV1A, activates the TAK1 – TABs complex [Adhikari *et al.*, 2007]. This complex activates the IKK (IkB kinase) complex of NEMO (NF- $\kappa$ B essential modulator),

IKK- $\alpha$ , and IKK- $\beta$ , which in turn phosphorylates I $\kappa$ B, tabbing it for ubiquitination and targeting it to the proteosome for degradation, thereby releasing NF- $\kappa$ B and allowing it to translocate to the nucleus [Karin and Ben-Neriah, 2000].

The TRIF-dependent pathway induces the expression of Type I IFN, and is only utilised by TLR3 and TLR4. TRIF is bound to TLR3 through the TIR domain, but TLR4 requires TRAM to activate TRIF-dependent signalling [Yamamoto *et al.*, 2003a; Yamamoto *et al.*, 2003b]. TRIF signals to TRAF3, which activates the IKK complex of TRAF-associated NF- $\kappa$ B activator (TANK)-binding kinase 1 (TBK1) and IKK $\epsilon$ . This complex activates the signal-dependent phosphorylation of IRF3 and IRF7, causing homo- or heterodimerisation, nuclear translocation, and assembly onto the IFN- $\beta$  enhancer, assisted by CBP/p300 (CREB binding protein) [Fitzgerald *et al.*, 2003; Sharma *et al.*, 2003].

Depending on which pathway is used, the latent transcription factors NF- $\kappa$ B, ATF2-c-Jun, MAPKs, IRF3, or IRF7 are activated, resulting in the upregulation of Type I IFNs, leading on to inflammation, immune regulation, survival, and proliferation [Yamamoto and Takeda, 2010]. The two different signalling pathways can be seen in *Figure 1.11*.

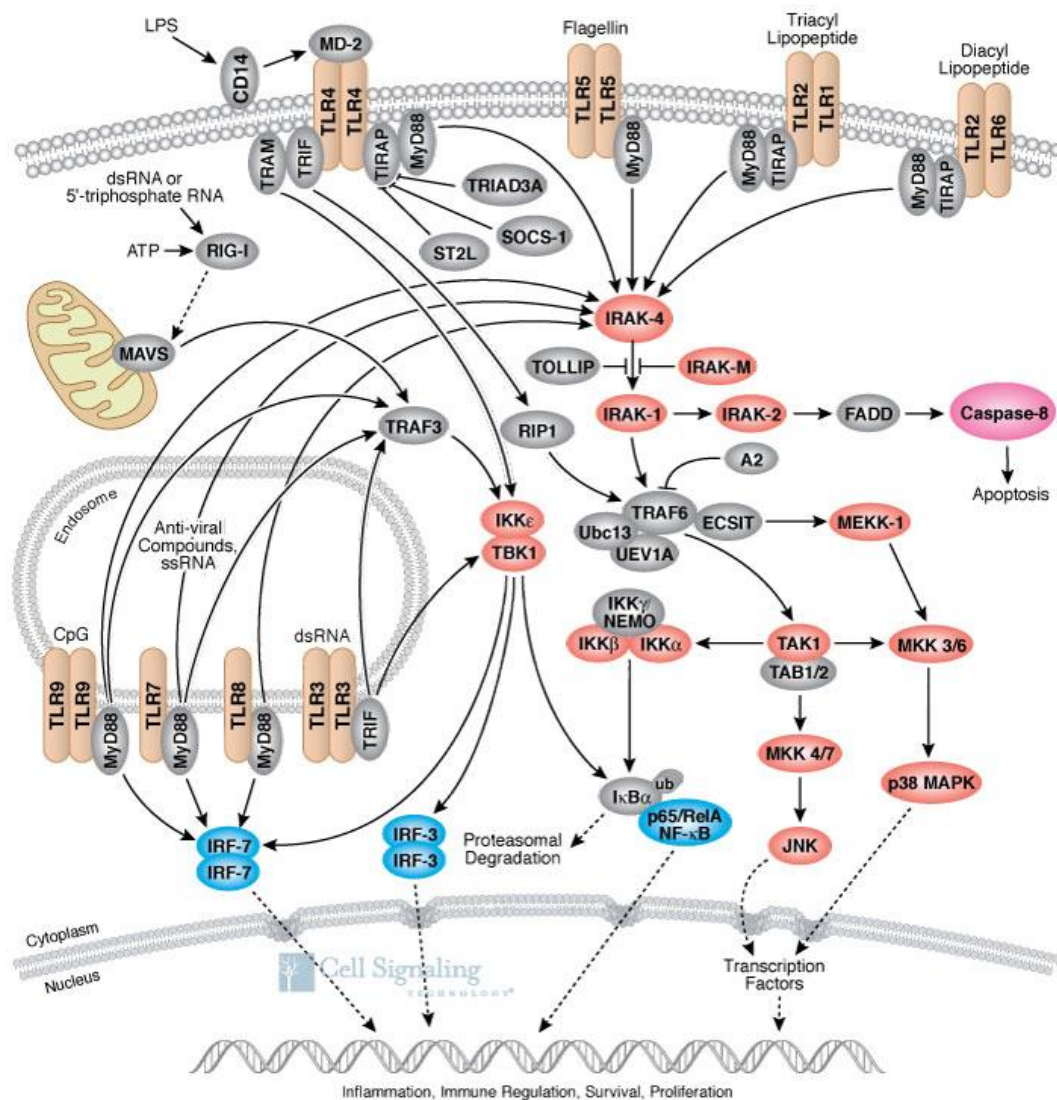


**Figure 1.11: TLR signalling pathway.** Each TLR recognises its specific PAMP, then signals via the MyD88- or TRIF-dependent pathway, leading to the activation of the latent transcription factors NF-κB, ATF2-c-Jun, MAPKs, IRF3, and IRF7, resulting in the upregulation of Type I IFNs [Cell Signaling Technology, URL].



#### 1.4.4 Virus Recognition by Toll-like Receptors

Although a lot of study has gone into how TLRs detect bacteria, several TLRs are also important for the recognition of different viruses. TLR2 and TLR4, located on the cell surface, recognise viral envelope glycoproteins on virions, whilst the intracellular TLRs (TLR3, TLR7, TLR8, and TLR9), recognise viral nucleic acids. A wide range of viruses are detected by these TLRs, and *Figure 1.12* shows which TLRs interact with which viruses [Takeda and Akira, 2005; Akira *et al.*, 2006; Finberg *et al.*, 2007; Xagorari and Chlichlia, 2008].

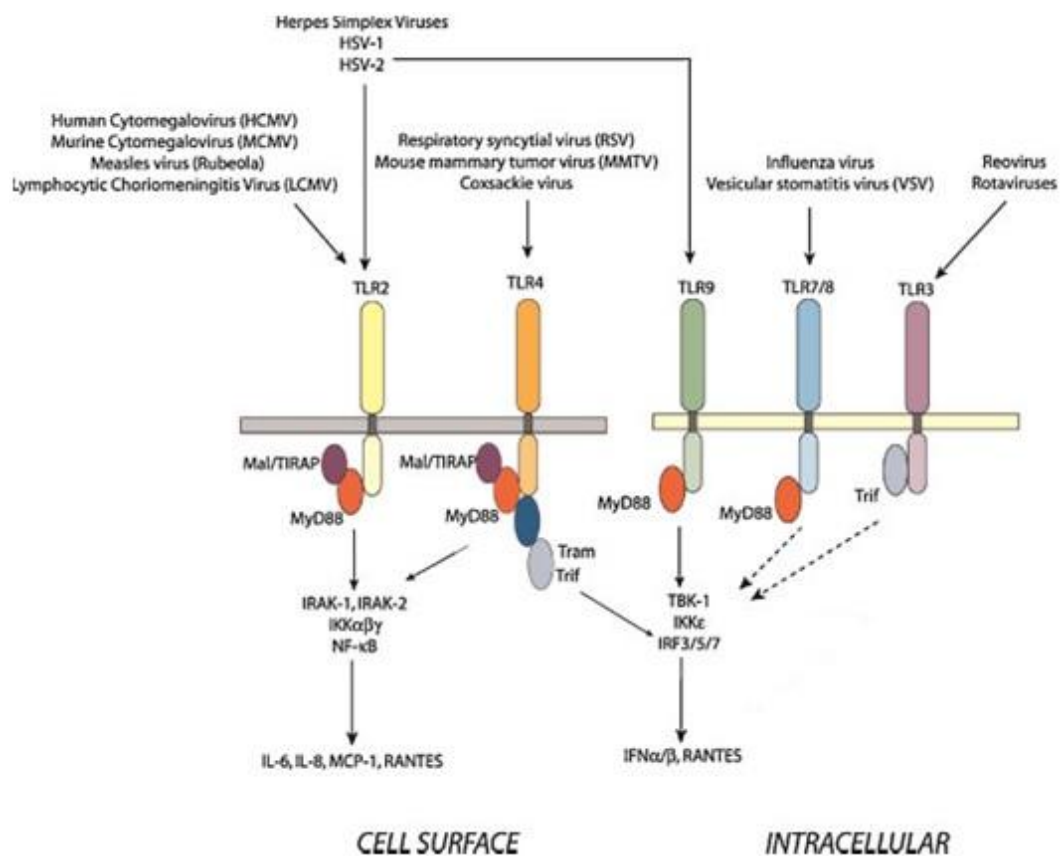


**Figure 1.12: Virus interactions with TLRs.** Innate immune activation by viruses is triggered by transmembrane TLRs both on the cell surface (TLR2 and TLR4) and within endosomal/ER intracellular compartments (TLR9, TLR7/8 and TLR3). TLRs activate type I IFN and inflammatory cytokine production via IRF and NF- $\kappa$ B. The TLRs have a cytoplasmic signalling motif, the TIR domain, which is essential for activation of shared downstream adapters (MyD88, Mal/TIRAP, TRAM, and TRIF) and activation of intracellular signal transducing proteins including IRAK/IKK $\alpha$  $\beta$  and TBK-1/IKK $\epsilon$ /IRF3 signalling cascades [modified from Finberg *et al.*, 2007].

#### 1.4.4.1 TLR2

TLR2 has been shown to interact with many different viruses. TLR2 recognises the human cytomegalovirus (HCMV) (a dsRNA virus) envelope glycoproteins B and H [Boehme *et al.*, 2006; Compton *et al.*, 2003], leading to NF- $\kappa$ B activation and the induction of inflammatory cytokines. It is also a receptor in natural killer (NK) cells for murine CMV (MCMV) [Szomolanyi-Tsuda *et al.*, 2006]. The hemagglutinin protein of measles virus stimulates the production of cytokines via TLR2 [Bieback *et al.*, 2002], and the innate immune recognition of vaccinia virus is also mediated by TLR2 [Zhu *et al.*, 2007]. TLR2 is activated in human monocytes and macrophages in response to Varicella-zoster virus (VZV) [Wang *et al.*, 2005], and plays an important role in infections with Herpes Simplex Virus (HSV) Type 1, shown using both transfected cell lines and knockout mice [Kurt-Jones *et al.*, 2004], and in DCs, along with TLR9 [Sato *et al.*, 2006]. Furthermore, infectious and UV-inactivated Epstein-Barr virus (EBV) virions lead to the activation of NF- $\kappa$ B through TLR2 [Gaudreault *et al.*, 2007].

#### 1.4.4.2 TLR3

The role of TLR3 in the antiviral response has not yet been fully elucidated. TLR3 recognises dsRNA, and its synthetic analogue Poly I:C, leading to the activation of NF- $\kappa$ B and the production of Type 1 IFNs [Alexopoulou *et al.*, 2001] *in vitro*, but results are less clear *in vivo* [Edelmann *et al.*, 2004]. TLR3 plays a role in rhinoviral infections in human bronchial epithelial cells [Hewson *et al.*, 2005], in respiratory syncytial virus (RSV) in epithelial cells, mediating inflammatory cytokine and chemokine production [Rudd *et al.*, 2005], in influenza A virus in human lung epithelial cells [Le Goffic *et al.*, 2007], and in MCMV-induced Type 1 IFN production [Tabeta *et al.*, 2004]. Hepatitis B virus (HBV) has been shown to be recognised by TLR3, notably the 3' CCACCA motif of tRNA<sup>Ala</sup> (UGC) [Wang *et al.*, 2006], and hepatitis C virus (HCV) suppresses TLR3 expression, thereby being responsible for the persistence of the virus in chronic HCV infection [Sato *et al.*, 2007]. Interestingly, TLR3 seems to benefit the pathogenesis of West Nile virus (WNV), an ssRNA flavivirus. The dsRNA replication intermediate leads to a TLR3-dependent inflammatory response that disrupts the blood-brain barrier and mediates entry and penetration of WNV into the brain, causing lethal encephalitis [Wang *et al.*, 2004].

#### **1.4.4.3 TLR4**

The main PAMP of TLR4 is bacterial LPS, but it has been shown to interact with several different viruses as well. Using TLR4-deficient mice, it was found that TLR4 is involved in the innate immune response to RSV, through an interaction with the viral envelope fusion protein [Kurt-Jones *et al.*, 2000; Haynes *et al.*, 2001]. Mouse mammary tumour virus (MMTV, a retrovirus) stimulates a TLR4 response, inducing the maturation of bone marrow-derived DCs and the upregulation of CD71 (the MMTV entry receptor) on these cells [Burzyn *et al.*, 2004]. LPS can induce the reactivation of latent MCMV via TLR4 signalling in immunocompetent mice [Cook *et al.*, 2006]. The HBV surface antigen (HBVsAg) is recognised by several TLRs, including TLR4 [Isogawa *et al.*, 2005], whilst the HCV lipo-Viro-particle from chronically infected patients interferes with TLR4 signalling in DCs [Agaugué *et al.*, 2007]. TLR4 has also been shown to be involved in the pathogenesis of CBV3-induced myocarditis [Fairweather *et al.*, 2003], and can mediate CBV4-induced cytokine production in human pancreatic cells [Triantafilou and Triantafilou, 2004].

#### **1.4.4.4 TLR7 and TLR8**

TLR7 and TLR8, located within endosomal compartments, are the primary detectors of viral ssRNA within the cytoplasm. TLR7 and TLR8 within plasmacytoid DCs (pDCs) recognise Vesicular stomatitis virus (VSV) [Lund *et al.*, 2004] and influenza virus [Diebold *et al.*, 2004]. Murine TLR7 and human TLR8 have also been implicated in sensing guanosine- and uridine-rich ssRNA oligonucleotides derived from human immunodeficiency virus-1 (HIV-1), stimulating DCs and macrophages to secrete IFN- $\alpha$  and pro-inflammatory cytokines [Heil *et al.*, 2004]. TLR7 also recognises HSV in human corneal epithelial cells [Li *et al.*, 2006]. TLR8, and to a lesser degree TLR7, mediates the CBV-induced inflammatory response in human cardiac cells [Triantafilou *et al.*, 2005a], and both are involved in the sensing of Sendai virus (SeV) [Melchjorsen *et al.*, 2005] and human parechovirus 1 [Triantafilou *et al.*, 2005b].

#### **1.4.4.5 TLR9**

TLR9 recognises unmethylated CpG DNA in bacteria, and these motifs are also found within several viruses. HSV1 and HSV2 both activate pDCs and DCs to produce Type 1 IFNs through TLR9 [Ashkar *et al.*, 2003; Krug *et al.*, 2004; Lund *et al.*, 2003; Sato *et al.*, 2006], and TLR9 also mediates the recognition of MCMV [Tabeta *et al.*, 2004]. In addition, the recognition of adenovirus in pDCs is mediated by TLR9 and is dependent upon MyD88 [Zhu *et al.*, 2007], but infectivity alone by adenoviruses is not sufficient for TLR9 activation, which are regulated by the specific receptor entry pathway of the virus [Iacobelli-Martinez and Nemerow, 2007]. TLR9 has also been shown to be involved with HIV in pDCs [Mandl *et al.*, 2008].

### 1.4.5 Viral Modulation of Toll-like Receptor Signalling Pathways

All viruses modulate TLR and other PAMP-induced signal transduction pathways, either by activating the PRRs, or suppressing them or their pathways. *Figure 1.13* provides an overview of this battle between virus and host. TLR8 and TLR7 have been shown to mediate the CBV-induced inflammatory response in human cardiac cells [Triantafilou *et al.*, 2005a], though it remains to be found if and where CBV5 modulates the TLR signalling pathway.

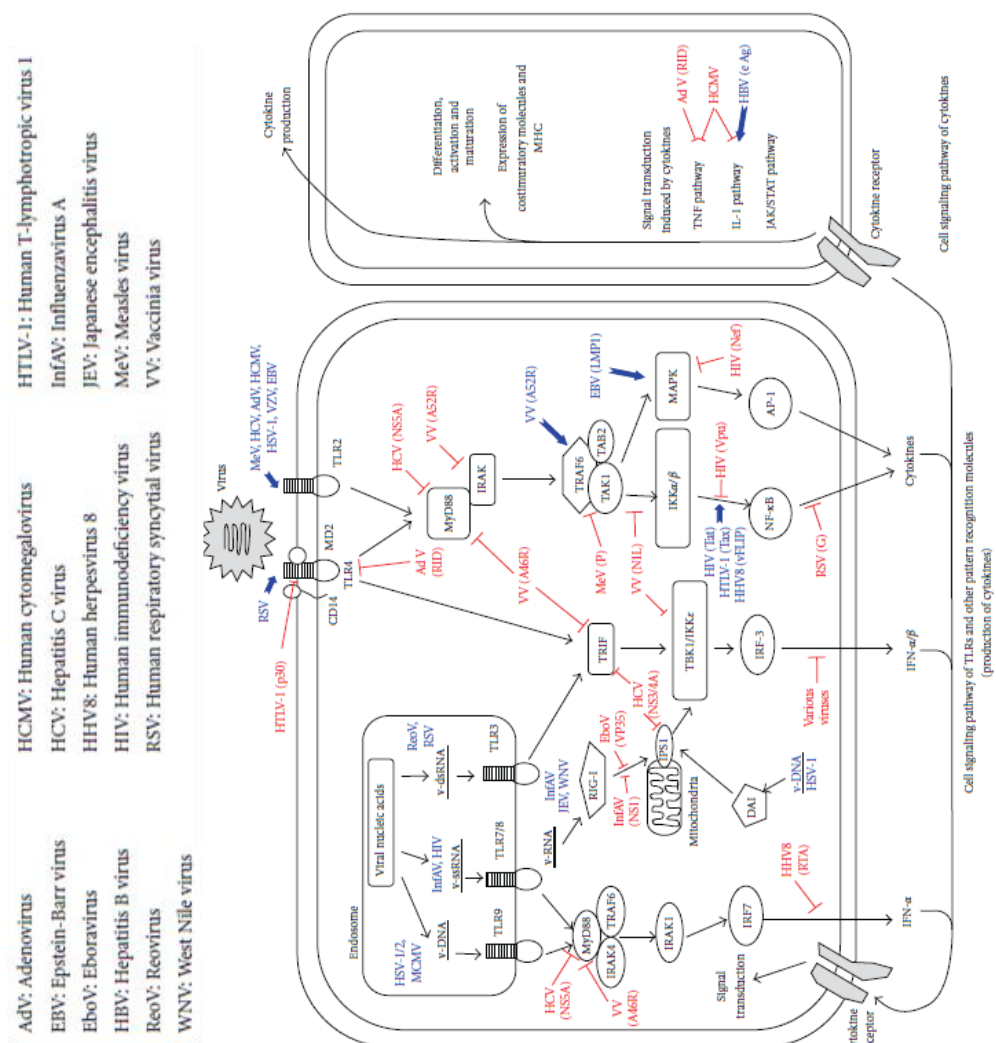


**Figure 1.13: Modulation of TLR and other PAMP-induced signal transduction pathways by virus infection.** Red line indicates suppression by virus. Blue line indicates activation by virus. Parenthesises denote viral proteins or nucleic acids [Yokota *et al.*, 2010].

## **1.5 Innate Immunity and RIG-I-like Receptors**

Along with the TLRs, several new TLR-independent PRRs have been discovered, including the retinoic acid inducible gene-I (RIG-I)-like receptor (RLR) family. There are three known members: RIG-I (also known as DDX58) [Yoneyama *et al.*, 2004], melanoma differentiation-associated gene 5 (MDA5, also known as IFIH1 or Helicard) [Kang *et al.*, 2002], and laboratory of genetics and physiology 2 (LGP2, also known as DHX58) [Rotherfusser *et al.*, 2005].

### **1.5.1 RIG-I, MDA5, and LGP2 Structures**

RIG-I and MDA5 are homologous proteins (925 amino acids long and 1025 amino acids long, respectively) that detect cytoplasmic viral RNA during viral replication [Wilkins and Gale, 2010]. They belong to the superfamily 2 (SF2) helicases, and share seven conserved ‘helicase motifs’ that mediate ATP and nucleic acid binding [Gorbalenya *et al.*, 1988]. MDA5 is distributed throughout the cytoplasm, whereas RIG-I appears to colocalise with F-actin, and is therefore associated with the cytoskeleton [Mukherjee *et al.*, 2009]. Both RIG-I and MDA5 contain an N-terminal region with two caspase activation and recruitment domains (CARDs), a central SF2 type DExD/H-box RNA helicase domain, and a C-terminal repressor domain (RD) [Takeuchi and Akira, 2007]. MDA5 and RIG-I exhibit 23% and 35% amino acid identities in their N-terminal CARD and their RNA helicase domains, respectively [Yoneyama *et al.*, 2005]. The third RLR, LGP2, is 678 amino acids long, and harbours a DExD/H-box RNA helicase domain (which shows 31% and 41% amino acid identities to the RNA helicase domains of RIG-I and MDA5, respectively) and a C-terminal RD, but lacks any

CARDs [Yoneyama *et al.*, 2005]. The representative structures of RIG-I, MDA5, and LGP2 can be seen in *Figure 1.14*.

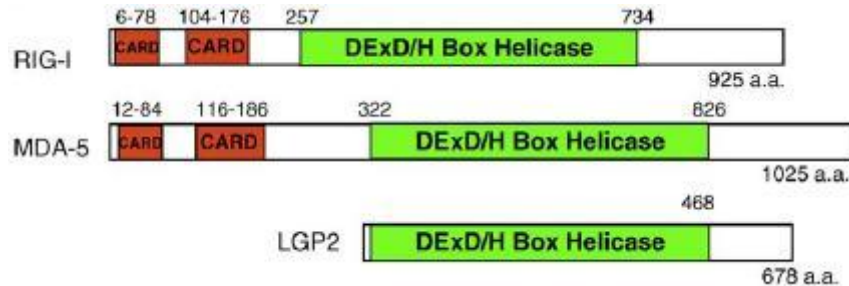


**Figure 1.14: Representative structures of the RLRs.** The position of each CARD and the DExD/H-box helicase is shown. Amino acid positions are indicated [modified from Wilkins and Gale, 2010].

### 1.5.2 CARDs and RLR Dimerisation

CARDs are members of the proapoptotic death domain fold family, which includes death domains, death effector domains, and pyrin domains, and are composed of six antiparallel  $\alpha$  helices [Park *et al.*, 2007]. They are implicated in homophilic interactions (CARD-CARD interactions) that facilitate cell death pathways [Lin *et al.*, 2006], and lead to downstream signalling to activate IRF3/7 and NF- $\kappa$ B. The internal DExD/H-box RNA helicase domain has ATPase activity that is activated by ligand binding. This is necessary for signalling, but does not appear to be required for RNA binding [Yoneyama *et al.*, 2005; Takahasi *et al.*, 2008]. The C-terminal RD of RIG-I contains a zinc-binding site, which is important for controlling RIG-I-mediated IFN responses [Saito *et al.*, 2007]. Research has shown that the C-terminal RD of RIG-I is vital for the binding of uncapped 5'-triphosphate single-stranded RNA (5'-pppRNA), as it contains a partially buried invariant lysine residue that is ideally located to interact with



phosphate. RIG-I has two states; an inactive (closed) one and an active (open) one. In the inactive state, the CARDs and the helicase domain are repressed by RD. Once viral RNA binds to the RD, a conformational change occurs, converting RIG-I to the active state. This results in the dimerisation of RIG-I and the initiation of downstream signalling via the CARDs. Without the RD, RIG-I constitutively activates downstream signalling, whilst overexpression of the RD inhibits the antiviral response [Cui *et al.*, 2008]. The proposed model for 5'-pppRNA activation of RIG-I by ligand-induced dimer formation of RD can be seen in *Figure 1.15*.

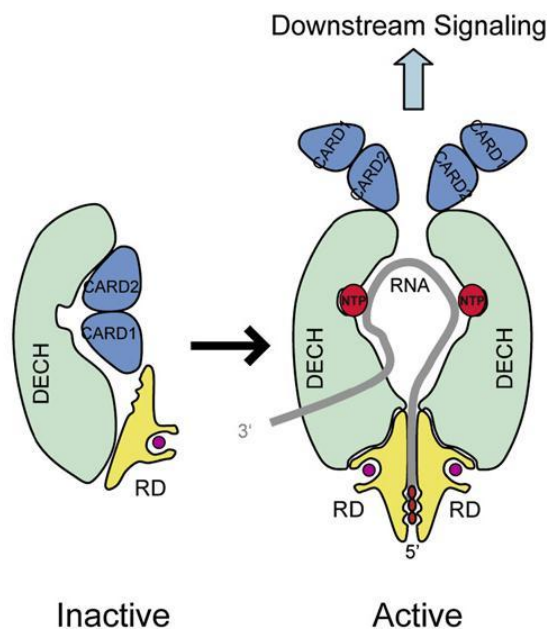


**Figure 1.15: RIG-I dimerisation.** Proposed model for 5'-triphosphate RNA (gray with red phosphates) activation of RIG-I by ligand-induced dimer formation of the repressor domain (RD, yellow with magenta zinc iron). In the inactive state, the RD represses the CARDs and the Helicase domain of RIG-I. Binding of 5'-triphosphate RNA induces a conformational change, resulting in the dimerisation of RIG-I and activation of downstream signalling [modified from Cui *et al.*, 2008].

### 1.5.3 IPS-1

After binding a viral ligand, RIG-I and MDA5 both signal downstream through their CARDs to activate IRF3/7 and NF- $\kappa$ B indirectly, via the protein intermediate IFN- $\beta$  Promoter Stimulator 1 (IPS-1 [Kawai *et al.*, 2005], also known as MAVS (Mitochondrial Antiviral Signalling protein) [Seth *et al.*, 2005], VISA (Virus Induced Signalling Adaptor) [Xu *et al.*, 2005], and Cardif (CARD adaptor inducing IFN- $\beta$ ) [Meylan *et al.*, 2005], listed in order of the acceptance dates of their respective publications, and herein referred to as IPS-1). IPS-1 is the essential adaptor in both RIG-I and MDA5 signalling that mediates effective responses against a variety of RNA viruses [Kumar *et al.*, 2006; Sun *et al.*, 2006]. IPS-1 is 540 amino acids in length, anchored to the mitochondrial outer membrane by means of a short hydrophobic C-terminal region (amino acids 514-535, see *Figure 1.16*) [Seth *et al.*, 2005]. Although anchored there, it moves into a detergent-resistant mitochondrial fraction upon viral infection. The location of IPS-1 suggests a link between recognition of viral infection, development of innate immunity, and mitochondrial function [Hiscott *et al.*, 2006]. IPS-1 contains a single N-terminal CARD-like domain (CLD), homologous to the CARDs of RIG-I and MDA5, a proline-rich region, and a C-terminal effector domain. The crystal structure of the N-terminal CLD of IPS-1 has been determined to 2.1 Angstrom resolution [Potter *et al.*, 2008]. Its structure is typical of that of a member of the death domain superfamily, comprising of a six-helix bundle. It has an asymmetric charge distribution, and shares 25% and 20% sequence homology with the N-terminal CARDs of MDA5 and RIG-I, respectively. The structure of IPS-1 is represented in *Figure 1.16*.

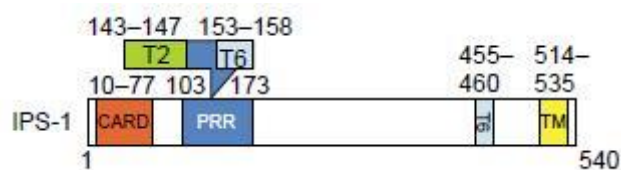


**Figure 1.16: Representative structure of IPS-1.** The position of each significant area is shown. TRAF3 not shown. Abbreviations: T2, TRAF2 binding motif; T6, TRAF6 binding motif; PRR, proline-rich region; TM, mitochondrial transmembrane domain. Amino acid positions are indicated [modified from Johnson and Gale, 2006].

### 1.5.4 Host Response to Viral Infection

RIG-I and MDA5, activated by ligand RNA, interact with IPS-1 via CARD-CARD interactions, which induces the recruitment of downstream signalling molecules, as seen in *Figure 1.17*. TRAF family members are important in this signalling cascade. TRAF3 interacts directly with the TRAF-interacting motif in the proline-rich region of IPS-1, as do TRAF2 and TRAF6 [Xu *et al.*, 2005; Oganessian *et al.*, 2006; Saha *et al.*, 2006]. These TRAF proteins signal downstream, via two pathways, to the protein kinase inhibitor of NF- $\kappa$ B (I $\kappa$ B) kinase (IKK) family members, to activate the transcription factors IRF3/7 and NF- $\kappa$ B.

The first pathway signals via the canonical IKK complex of IKK- $\alpha$ , IKK- $\beta$ , and the regulatory subunit NEMO. This complex phosphorylates I $\kappa$ B, the inhibitor of NF- $\kappa$ B, on serines 32 and 36. Phospho-I $\kappa$ B is then ubiquitinated and targeted to the proteasome for degradation, releasing NF- $\kappa$ B, thereby allowing it to translocate to the nucleus [Karin and Ben-Neriah, 2000]. The second pathway signals via the non-canonical IKK complex of TBK1 and IKK $\epsilon$ . This complex

activates the signal-dependent phosphorylation of IRF3 and IRF7, causing homo- or heterodimerisation, nuclear translocation, and assembly onto the IFN- $\beta$  enhancer, assisted by CBP/p300 [Fitzgerald *et al.*, 2003; Sharma *et al.*, 2003]. TRAF3 interaction with IPS-1 is essential for the recruitment of both IKK complexes, whilst TRAF2 and TRAF6 are more important for NF- $\kappa$ B activation. Crosstalk between the two IKK complexes has been suggested, as NEMO also plays a role in TBK-1/IKK $\epsilon$ -mediated activation of IRFs [Zhao *et al.*, 2007]. The C-terminal effector domain of IPS-1 interacts with Fas-associated death domain (FADD) and receptor interacting protein 1 (RIP1), both death domain-containing proteins. They facilitate NF- $\kappa$ B activation via the interaction and activation of caspase-8 and caspase-10 [Takahashi *et al.*, 2006].

Once in the nucleus, IRF3/7 and NF- $\kappa$ B transcriptionally upregulate type I IFNs (IFN-  $\alpha/\beta$ ), which then signal through the IFN- $\alpha/\beta$  receptor and the Jak-STAT pathway to drive interferon stimulated gene (ISG) expression and an innate immune response. ISGs can function to trigger apoptosis of infected cells, directly inhibit viral infection, and they can also play a role in modulating the adaptive immune response [Lei *et al.*, 2009; Yoneyama and Fujita, 2009]. The overall RLR signalling pathway can be seen in *Figure 1.17*.

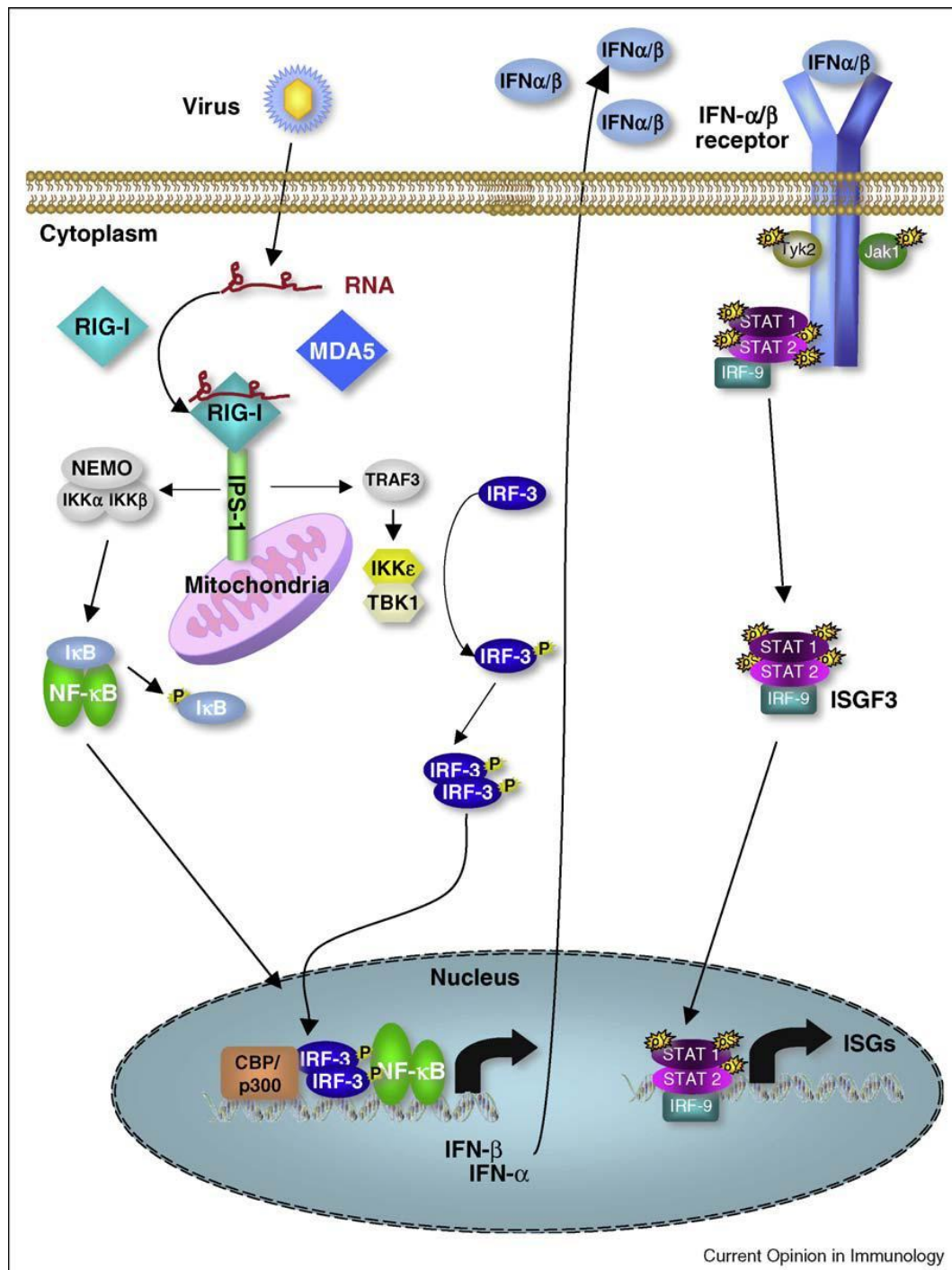


**Figure 1.17: The RLR signalling pathway** showing RIG-I bound to ligand RNA and signalling downstream to IRF3 and NF-κB to induce IFN-α/β production from a virus-infected cell. IFN-α/β is then shown signalling through the IFN-α/β receptor and the Jak-STAT pathway to drive interferon stimulated gene (ISG) expression and an innate immune response [Wilkins and Gale, 2010].

### 1.5.5 Viral Evasion of Host Recognition

To counter the host response to viral infection, several viruses have evolved strategies to inhibit the innate signalling events leading to IFN production. Perhaps the best characterised evasion method is performed by HCV, an infectious agent that mainly infects human hepatocytes. HCV NS3/4A (non-structural 3/4A) is a multifunctional protein harbouring serine protease activity, and has been shown to impair both RIG-I and TLR3 signalling [Foy *et al.*, 2005; Li *et al.*, 2005a]. It does this by cleaving the C-terminal region of IPS-1 at Cys508, thereby disrupting the RIG-I-dependent signalling process by dislodging IPS-1 from the mitochondrial outer membrane [Li *et al.*, 2005b; Loo *et al.*, 2006], and cleaving TRIF at Cys372, resulting in its inability to recruit TBK1 [Li *et al.*, 2005a]. Similar mechanisms are seen in GB virus B (a member of the Flaviviridae family) [Chen *et al.*, 2007], and the 3ABC protease of hepatitis A virus (a member of the Picornaviridae family), which cleaves IPS-1 at Q428 [Yang *et al.*, 2007].

The NS1 protein of influenza A virus has been shown to inhibit RIG-I signalling through direct interaction with RIG-I [Mibayashi *et al.*, 2007], while the V proteins of different paramyxoviruses, including SeV, bind to and inhibit MDA5-dependent type 1 IFN production [Andrejeva *et al.*, 2004]. Another technique is the viral-directed removal of 5'-ppp from the RNA nucleic acid of Hantaan, Crimean-Congo hemorrhagic fever, and Borna disease viruses to evade RIG-I detection [Habjan *et al.*, 2008]. The Vaccinia virus-encoded A46R protein contains a TIR domain that can inhibit TRIF-mediated IRF3 activation, thereby preventing one pathway of TLR3 signalling [Stack *et al.*, 2005]. Understanding these evasion techniques will allow scientists to combat viruses more effectively.

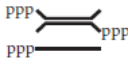













### 1.5.6 RLR Ligands

RIG-I and MDA5 contribute to antiviral signalling in different ways depending on the virus involved [Kato *et al.*, 2006; Loo *et al.*, 2008]. Despite their structural similarities, they show a preferential recognition for different viruses, which may be due to the amino acid sequences of the DExD/H-box RNA helicase domains of RIG-I and MDA5 being only approximately 35% identical, leading to genetic diversity and thus different specificities for distinct RNA conformations [Gitlin *et al.*, 2006].

#### 1.5.6.1 RIG-I Ligands

RIG-I preferentially detects a number of both positive and negative stranded viruses, including: HCV; RSV and related paramyxoviruses; VSV; and influenza A virus [Kato *et al.*, 2006; Loo *et al.*, 2008]. Both RIG-I and MDA5 appear to respond to reoviruses, WNV, and Dengue virus [Fredericksen and Gale, 2006], as well as measles virus [Ikegame *et al.*, 2010]. RIG-I has been shown to be required for the detection of uncapped 5'-ppp RNA [Hornung *et al.*, 2006]. This enables RIG-I to distinguish between host (self) and viral (non-self) RNA, as host RNA is either capped or post-translationally modified to remove the 5'-triphosphate. RIG-I has been reported to detect both dsRNA [Yoneyama *et al.*, 2004] and 5'-ppp ssRNA [Pichlmair *et al.*, 2006], though some form of double-strandedness may be required [Schmidt *et al.*, 2009]. RIG-I can also recognise particular sequences or motifs within viral RNA, such as uridine and adenosine-rich 3'-sequences in 5'-ppp ssRNA (found within HCV and other viruses) [Saito *et al.*, 2008; Uzri and Gehrke, 2009], or short double-stranded blunt-end 5'-pppRNA [Schlee and Hartmann, 2010]. *Table 1.3* lists putative RIG-I ligands.

**Table 1.3: Putative RIG-I ligands generated by enzymatic polymerisation or cleavage. Due to the use of enzymatic polymerisation, the RNA molecules in the table are not molecularly defined, and additional RNA molecules may be present [modified from Schlee and Hartmann, 2010].**

Name	Length (nt)	Structure (source)		5'	3'	Test system	Reference
GFP2	24	ds and ss 3pRNA (phage polymerase IVT)		3p	OH	IFN- $\alpha/\beta$ ELISA in human cell lines (HEK293, HeLa, K562, etc.)	16
Lamin A/C	50–1,000	ds 3pRNA, 5' and 3' blunt end (phage polymerase IVT)		3p	OH	IFN- $\alpha/\beta$ ELISA in murine cDCs, MEFs	7
VSV	11,000	ss 3pRNA (VSV genomic RNA)		3p	OH		
Tri-GFPs	24	ss 3pRNA (phage polymerase IVT)		3p	OH	IFN- $\alpha/\beta$ ELISA in human monocytes, murine cDCs, MEFs	11
SAD $\Delta$ PLp	11,900	ss 3pRNA (Rabies genomic RNA)		3p	OH	IFN- $\beta$ reporter assay in human cell lines (Vero and HEK293)	
Tri-G-AC-U	31	ss 3pRNA (phage polymerase IVT)		3p	OH	Interaction of RIG-I protein with tri-G-AC-U by pulldown assay	
Flu vRNA	890–2,341	ss 3pRNA (Influenza A genomic RNA, 8 segments)		3p	OH	IFN- $\alpha$ ELISA in murine DCs, IFN- $\beta$ reporter assay in human cell line (HEK293), interaction of vRNA with RIG-I-protein (gel shift assay)	12
RNaseL fragments	<200	ss and dsRNA, 5'- or 3'-overhangs (digestion of cellular RNA with RNaseL)		OH	1p	Induction of IFN- $\beta$ in murine MEFs	21
pppRVL	58	ss 3pRNA (phage polymerase IVT)		3p	OH	RIG-I protein by fluorescence anisotropy, RIG-I dimerization by chromatography	29
pppVSVL	60	ss 3pRNA (phage polymerase IVT)		3p	OH	IFN- $\beta$ reporter assay in human cell line (HEK293), pull down assay with RIG-I protein	
ppp-shRNA-luc3	22+24 loop	sh 3pRNA, 2-nt 3'-overhang (phage polymerase IVT)		3p	OH	IFN- $\beta$ ELISA in human cell line (HeLa)	18
PU/UC	105	ss 3pRNA (phage polymerase IVT)		3p	OH	IFN- $\beta$ reporter assay in human cell line (Huh7) and MEFs, IFN- $\beta$ RT-PCR in MEFs, IRF-3 dimerization in Huh7, binding to RIG-I (gel shift), IFN- $\beta$ ELISA of mouse serum	17
Short poly I:C	300	ds 1pRNA, 2-nt 3'-overhang (digestion of poly I:C with RNase III)		1p	OH	IFN- $\beta$ ELISA in MEFs, ATPase assay with RIG-I protein, interaction with RIG-I protein by atomic force microscopy	20
PolyAU	(20–?)	ds 3pRNA, generated <i>in vivo</i> by transcription of transfected DNA poly(dAdT) by cellular RNA polymerase III		3p	OH	Induction of IFN- $\beta$ promoter reporter assay in HEK293 cells and of IFN- $\alpha$ in human monocytes and IFN- $\beta$ in murine MEFs	26,27

Abbreviations: cDC, conventional dendritic cell; ELISA, enzyme-linked immunosorbent assay; IFN, interferon; MEF, mouse embryonic fibroblast; RIG-I, retinoic acid-inducible gene; vRNA, viral RNA.



In addition to these, cleavage products produced by the host endonuclease RNase L during virus infection are recognised by RIG-I, which can amplify the RLR antiviral response [Malathi *et al.*, 2007]. Finally, RIG-I is responsible for binding short dsRNA viral transcripts, less than 1kb in length [Kato *et al.*, 2008]. Despite all this research, there is still debate as to what the RIG-I ligand is, with suggestions that negative sense virus genomic RNA, generated by viral replication, constitutes the major trigger for RIG-I, whilst the other types of RNA mentioned above do not substantially contribute to IFN induction [Rehwinkel *et al.*, 2010]. Figure 1.18 provides an overview of putative RIG-I ligands.

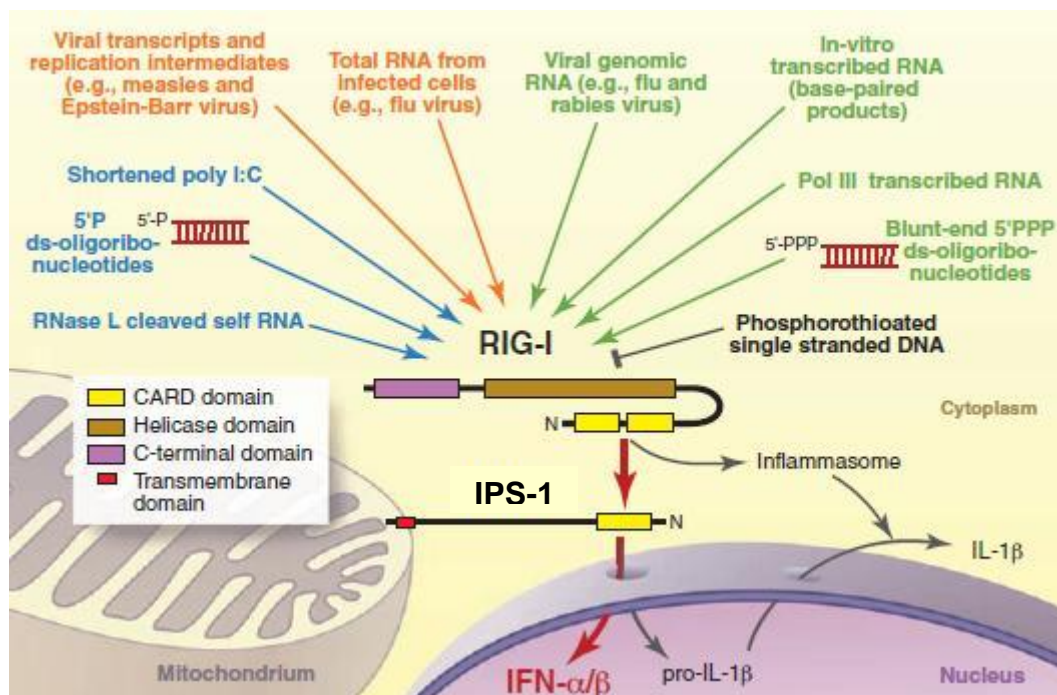


**Figure 1.18: Putative RIG-I ligands.** RIG-I has been reported to be triggered experimentally by a variety of RNA agonists. 5'-ppp-bearing RNAs are shown in green, RNAs without 5'-ppps in blue, and RNAs that may have different 5'-end characteristics in orange. An antagonist is shown in black. Activated RIG-I promotes the induction of interferons and other pro-inflammatory cytokines via the mitochondrial adaptor IPS-1 (bold red arrows). IPS-1-dependent induction of pro-interleukin-1 $\beta$  allows it to be processed into mature interleukin-1 $\beta$  by the inflammasome, which can be directly activated by RIG-I in an IPS-1-independent manner [modified from Rehwinkel and Reis e Sousa, 2010].

#### **1.5.6.2 MDA5 Ligands**

MDA5 has been shown to be critical for Picornaviridae detection, such as encephalomyocarditis virus (EMCV) and Theiler's virus. This is thought to be due to the VPg region at the 5' end of the viral genome. This VPg region blocks the 5'-triphosphate required for RIG-I recognition, but still allows for MDA5 to bind to it [Gitlin *et al.*, 2006; Kato *et al.*, 2006; Pichlmair *et al.*, 2006]. MDA5 is also triggered by reoviruses [Loo *et al.*, 2008] some flaviviruses [Fredericksen *et al.*, 2008], paramyxoviruses [Gitlin *et al.*, 2010], and norovirus [McCartney *et al.*, 2008]. In addition, MDA5 and IPS-1 are crucial in mediating Type 1 IFN responses to CBV3, with the absence of the MDA5-IPS-1 pathway leading to increased mortality in mice after CBV3 infection [Wang *et al.*, 2010; Hühn *et al.*, 2010]. MDA5 has also been shown to be essential for Poly I:C-induced IFN production [Kato *et al.*, 2006; Loo *et al.*, 2008]. Whilst RIG-I is required for the detection of short dsRNA, MDA5 preferentially binds long dsRNA products (greater than 1-2kb in length) [Kato *et al.*, 2008].

### 1.5.6.3 LGP2 Ligands

*In vitro* studies suggest that LGP2 acts as a negative regulator of the RIG-I- and MDA5-mediated antiviral response, as its overexpression inhibits virus-induced IRF3 and NF- $\kappa$ B activation. One possible explanation for this is that LGP2 sequesters dsRNA away from RIG-I and MDA5, thereby preventing activation of the antiviral signal [Rothenfusser *et al.*, 2005]. A second model is that LGP2, via its RD, inhibits dimerisation of RIG-I and its interaction with IPS-1 [Saito *et al.*, 2007], whilst a third possibility is that LGP2 competes with IKK $\epsilon$  for recruitment to IPS-1 [Komuro and Horvath, 2006]. Structural analyses of the RD of LGP2 have also shown that LGP2 can bind to the termini of dsRNA more strongly than MDA5 [Li *et al.*, 2009; Pippig *et al.*, 2009; Takahasi *et al.*, 2009]. However, *in vivo* data suggests that LGP2 can act as a positive regulator of RIG-I- and MDA5-mediated antiviral responses, via its ATPase domain [Venkataraman *et al.*, 2007; Satoh *et al.*, 2010].

## **1.6 Project Aims**

Despite the wealth of research on hunting the RLR ligands, the precise PAMPs recognised by each RLR are, as yet, still undetermined. This project aims to enhance the current knowledge on whether the RNA helicase RIG-I or MDA5 is the primary detector of CBV5. First of all, the extent of RIG-I and MDA5 involvement in CBV5 infection of cardiac cells was investigated. One of the most serious diseases caused by CBV5 is viral myocarditis, which can lead on to dilated cardiomyopathy, and thus cardiac cells were chosen to work on. To further elucidate the role of RIG-I and MDA5 in CBV5 sensing, Huh cells were used, as Huh 7.5.1 cells have a RIG-I mutation that leads to a defect in IFN production. RIG-I has been proposed to dimerise in response to viral ligands, so whether dimerisation between RIG-I, MDA5, and LGP2 occurred after CBV5 infection was observed using immunoprecipitation experiments. Finally, the interaction and colocalisation between RIG-I and MDA5 with IPS-1 (an adaptor protein essential for downstream signalling) was examined using confocal microscopy.

Understanding whether RIG-I or MDA5 is the primary detector of CBV5 will help in the development of novel therapeutic approaches for not only viral myocarditis, but other diseases caused by CBV5 as well.

**Chapter 2**  
**MATERIALS AND METHODS**

## **2.1 Materials**

### **2.1.1 Antibodies**

- Donkey Anti-Goat IgG (H+L) TRITC (Rhodamine), purchased from Jackson Immuno Labs 705-025-003
- IRF-3 (FL-425) Rabbit Polyclonal IgG, purchased from Santa Cruz Biotechnology sc-9082
- LGP2 Goat pAb to DHX58, purchased from Abcam ab82151
- LGP2 (H-159) Rabbit Polyclonal IgG, purchased from Santa Cruz Biotechnology sc-134667
- MAVS (T-20) Goat Polyclonal IgG, purchased from Santa Cruz Biotechnology sc-70096
- MDA5 (C-16) Goat Polyclonal IgG, purchased from Santa Cruz Biotechnology sc-48031
- MDA5 (H-61) Rabbit Polyclonal IgG, purchased from Santa Cruz Biotechnology sc-134513
- Phospho-IkappaBalpha (Ser32) (14D4) Rabbit mAb, purchased from Cell Signaling Technology #2859L
- Rabbit Anti-Goat Polyclonal Immunoglobulins FITC, purchased from DAKO F0250
- RIG-I (C-15) Goat Polyclonal IgG, purchased from Santa Cruz Biotechnology sc-48929

- RIG-I (H-300) Rabbit Polyclonal IgG, purchased from Santa Cruz Biotechnology sc-98911
- Streptavidin-HRP conjugate, purchased from Amersham Biosciences 1058765
- Swine Anti-Rabbit Polyclonal Immunoglobulins FITC, purchased from DAKO F0205
- Swine Anti-Rabbit Polyclonal Immunoglobulins HRP, purchased from DAKO P0217

## **2.2 Tissue Culture**

The following basic tissue culture techniques were used on all the cell lines utilised throughout the project. All tissue culture (TC) was performed in a Microflow Class 2 laminar flow hood in a sterile environment. Aqueous Virkon was used to clean the work area before use, and to clean all the equipment before placing it inside the cabinet, to ensure sterility. A lab coat and disposable gloves and shoes were worn. 25cm<sup>2</sup> Nunclon™  $\Delta$  Surface Flasks and Nunc Falcon tubes were used throughout.

### **2.2.1 Cell Lines**

#### **2.2.1.1 Human Cardiac Cell Line**

Human Cardiac (Girardi) cell line (ECACC – European Collection of Animal Cell Cultures), maintained in 1g/L Glucose Dulbecco's Modified Eagle's Medium (DMEM), containing GlutaMAX, 10% heat-inactivated Foetal Calf Serum (FCS), and 1% non-essential amino acids (Invitrogen (UK)).

#### **2.2.1.2 Huh 7.5 and Huh 7.5.1 Cell Lines**

Human Hepatocellular (Huh) 7.5 cell line (Kindly donated by Dr Chisari, Scripps Research Institute, USA), maintained in 4.5g/L glucose DMEM, containing GlutaMAX, 10% heat-inactivated FCS, and 1% non-essential amino acids (Invitrogen (UK)).

Huh 7.5.1 cell line (Kindly donated by Dr Chisari, Scripps Research Institute, USA), maintained in 4.5g/L glucose DMEM, containing GlutaMAX, 10% heat-inactivated FCS, and 1% non-essential amino acids (Invitrogen (UK)). They contain a RIG-I mutation that leads to a defect in IFN production.



### **2.2.1.3 LLC Cell Line**

LLC (Lewis Lung Carcinoma) cell line (ATCC – American Type Culture Collection), maintained in 1g/L DMEM, containing GlutaMAX, 10% heat-inactivated FCS, and 1% non-essential amino acids (Invitrogen (UK)). The LLC cell line are monkey cells that nearly all viruses are able to propagate on, as they are a very robust cell line.

### **2.2.2 Thawing Cells**

The vial of cells was carefully removed from liquid nitrogen. As soon as they were fully defrosted, the cells were added to 10ml of their appropriate growth medium in a 15ml Falcon tube. This was then centrifuged at 12,000 rpm for 5 minutes at room temperature (RT), after which the supernatant was aspirated off. 5ml growth medium was added, the cells were resuspended, and finally added to a flask and incubated at 37°C 5% CO<sub>2</sub>.

### **2.2.3 Propagating Cells**

Cells have a limited lifespan before they start dying, and thus need propagating to ensure their survival. Fresh growth medium provides new nutrients for the cells, as well as foetal calf serum (FCS; a growth factor) and MEM non-essential amino acids (Sigma). Cells need propagating when they become confluent and cover over 90% of the bottom of the flask. Propagating cells involves splitting down their total number, thereby allowing them the space and nutrients to divide and expand back up again. This way, certain cell lines can be maintained indefinitely, though after a certain number of passages, the overall quality of the cell line decreases.

### **2.2.3.1 Adherent Cell Lines**

Cardiac, Huh 7.5, Huh 7.5.1, and LLC cell lines (adherent cell lines) were propagated by first removing the supernatant, and then washing the cells with 2ml 1X PBS to remove any remaining dead cells. The cells were then incubated with 2ml of trypsin-EDTA solution (1X, Sigma) (a serine protease, which hydrolyses the proteins adhering the cells to the flask bottom), until they could be tapped off the bottom of the flask. After the cells were in suspension, 2ml of the appropriate growth medium was added, to neutralise the trypsin. The cells were then split evenly into separate flasks, and fresh medium was added (to a total of 4ml). The flasks were then incubated at 37°C 5% CO<sub>2</sub>. In some cases, cell lines only required maintaining, rather than propagating. The process is the same, but instead of neutralising the trypsin with medium, 1ml of trypsin was removed, 3ml of fresh growth medium was added, and the flask incubated at 37°C 5% CO<sub>2</sub>.

### **2.2.4 Freezing Cells**

Healthy cells are frozen in liquid nitrogen (-196°C) for long-term cryo-storage. To protect the cells from freezing damage due to ice formation, they are frozen in freezing medium (10% Dimethyl sulfoxide (DMSO) in FCS), with the DMSO acting as a cryoprotectant.

To freeze adherent cell lines, the cells were washed, trypsonised, and neutralised as per propagating them, and then combined into a 15ml Falcon tube and centrifuged at 12,000 rpm for 5 minutes at RT. The supernatant was aspirated off, and 1ml per flask of cells of freezing medium was added (i.e. if two flasks of cells were being frozen, 2ml of freezing medium was added) and the cells resuspended.

In under 10 minutes, the cells were added to labelled cryotubes (Nunc) and stored at  $-80^{\circ}\text{C}$ , allowing the cells to be cooled at a rate of  $1-3^{\circ}\text{C}$  per minute. After 24 hours, they were added to liquid nitrogen for long-term cryo-storage.

## **2.3 Coxsackievirus B5 (CBV5)**

### **2.3.1 Propagating CBV5**

A prototype strain of CBV5 (Faulkner strain) was obtained from the ATCC, and propagated on LLC cells. 100µl CBV5 was added to a flask of 1.5ml LLC cells and incubated at 37°C 5% CO<sub>2</sub> for approximately 24 hours. Once all the cells had been killed, the flasks were freeze-thawed three times, to break open the cells and release the virus. The LLC-CBV5 was then transferred to 50ml Falcon tubes and centrifuged at 12,000 rpm for 5 minutes at RT. The supernatant containing the virions was then added to fresh 50ml Falcon tubes and frozen at -80°C.

### **2.3.2 Purifying CBV5 using a Sucrose Density Gradient**

CBV5 was purified using a sucrose gradient purification procedure. The sucrose gradients were prepared in 40ml Beckmann SW28 ultra-centrifuge tubes. The sucrose solutions were layered into the tubes in the following order (with the boundary between them marked): 7ml 60% sucrose in PBS; 6ml 30% sucrose in PBS; and 3ml 10% sucrose in PBS. 15ml CBV5 was gently loaded onto the gradient, and the tubes were centrifuged at 25,000 rpm for 90 minutes at 4°C. CBV5 bands at the interface between 30% and 60% sucrose. The top layers of sucrose were carefully removed, and the purified CBV5 was pipetted into 15ml Falcon tubes and frozen at -80°C.

### **2.3.3 Isolating Single-Stranded RNA (ssRNA) from Purified CBV5**

In TC, 300µl of purified CBV5 was added to sterile Eppendorfs. Each Eppendorf will end up containing 80µl ssRNA, enough for two indirect immunofluorescence

stimulations of 40µl each. From this point on, all work was performed in a fume hood with sterile Eppendorfs and tips, to ensure the purity of the ssRNA.

2µl vanadyl ribonuclease complex (an RNase inhibitor, which stops the breakdown of RNA) was added to each Eppendorf, followed by 300µl ultrapure phenol (the bottom layer). Phenol dissolves any proteins present. After vortexing for 5-10 seconds, the Eppendorfs were centrifuged at 13,000 rpm for 10 minutes at RT. The upper layer was then transferred to new Eppendorfs. 300µl chloroform / isoamyl alcohol (chloroform dissolves lipids present, and isoamyl alcohol ensures deactivation of RNase) was added to each Eppendorf, followed by another round of vortexing and centrifugation. The upper layer was again transferred into new Eppendorfs. 15µl (1/20<sup>th</sup>) sodium acetate 2M pH 6.5 and 750µl (2.5x vol) of 95% ethanol (both reduce co-precipitation of contaminants) were added, mixed, and the Eppendorfs were then frozen at -80°C for at least 60 minutes. Afterwards, the Eppendorfs (straight from the freezer) were centrifuged at 13,000 rpm for 30 minutes at RT. The excess supernatant was removed, the Eppendorfs were centrifuged at 13,000 rpm for a further minute, and the remaining supernatant was removed, leaving just a pellet of ssRNA. 80µl sterile water (ddH<sub>2</sub>O), or LAL water, was added to each Eppendorf, and the ssRNA was frozen at -80°C.

#### **2.3.4 Preparing UV-Inactivated CBV5**

UV-inactivated CBV5 (UV-CBV5) was prepared by shining UV light upon vials of CBV5 for 30-45 minutes. To test to see if the UV had destroyed the RNA of the CBV5, cardiac cells were stimulated with UV-CBV5 for 24 hours. The UV-CBV5 should have very little effect upon the cells.

## **2.4 Immunofluorescence**

Immunofluorescence is a technique whereby an antigen present within or on a cell can be detected using a specific antibody conjugated to a fluorophore (fluorescent molecule), with the amount of fluorescence emitted equating to the amount of antigen present. Fluorophores absorb light (energy) of a specific wavelength and re-emit energy of a different but specific wavelength. The most commonly used fluorophore is FITC (fluorescein isothiocyanate), which has an excitation wavelength of 495nm (cyan) and an emission wavelength of 519nm (green). Another commonly used fluorophore is TRITC (tetramethylrhodamine isothiocyanate), which has an excitation wavelength of 547nm (green) and an emission wavelength of 572nm (yellow). There are two major types of immunofluorescence: primary (direct) and secondary (indirect).

### **2.4.1 Direct Immunofluorescence**

Direct immunofluorescence utilises a single antigen-specific antibody directly conjugated to a fluorophore (*Figure 2.1*). A specific antigen will be detected by the antibody, and the fluorophore it is attached to can subsequently be detected via microscopy or flow cytometry.

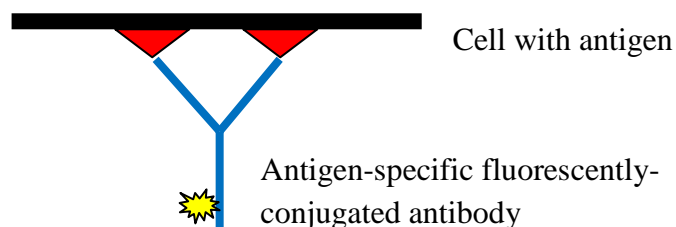


**Figure 2.1: Direct immunofluorescence.** An antigen-specific fluorescently-conjugated antibody binds directly to the antigen.

### 2.4.2 Indirect Immunofluorescence

Indirect immunofluorescence involves two antibodies: an unlabelled primary antibody specific for the antigen of interest; and a fluorescently-conjugated secondary antibody specific for the primary antibody (*Figure 2.2*). The structure of an antibody makes this possible, as it has two regions: an Fc region (fragment crystallisable region); and an Fab region (fragment antigen-binding region). The Fab region contains variable sections that determine which antigen is bound, whilst the Fc region is constant in a class of the same species. Antibodies can be designed in such a way that they contain the same Fc region but different Fab regions. In this way, primary antibodies with the same Fc region can be used to detect various antigens (due to differing Fab regions), and still be detected by a single fluorescently-conjugated secondary antibody specific for the Fc region of the primary antibody.

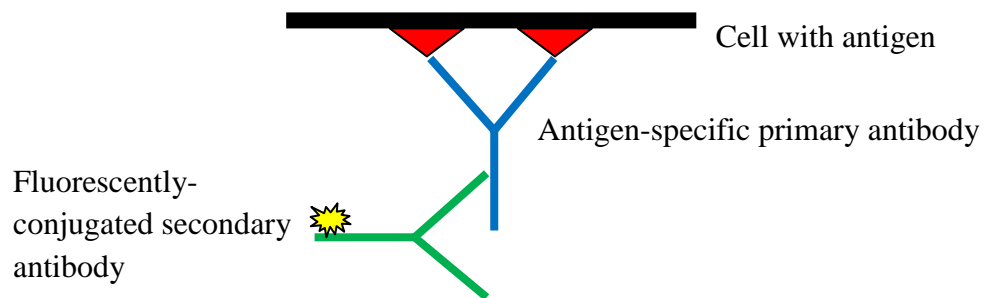


**Figure 2.2: Indirect immunofluorescence.** An antigen-specific primary antibody binds to the antigen, and is itself bound by a fluorescently-conjugated secondary antibody specific to it.

## **2.5 Flow Cytometry**

Flow cytometry is a powerful technique used to analyse cellular characteristics of individual cells in a heterogeneous population. In this project, cells were fluorescently tagged via indirect immunofluorescence and passed through the Becton Dickinson (BD) Fluorescence-Activated Cell Sorting (FACSCalibur™) system (*Figure 2.3*).



***Figure 2.3: BD FACSCalibur™ flow cytometer [BD, URL].***

### **2.5.1 Principles of Flow Cytometry**

A flow cytometer works by passing thousand of cells per second through one or more laser beams, scattering the light onto detectors. The cells must be passed through the laser beams in single file to get accurate readings, and this is achieved using hydrodynamic focusing. The sample of cells merges with a flowing stream of sheath fluid and gets funnelled into a smaller orifice, compressing the cells to roughly one cell in diameter. When the laser strikes a cell, two forms of scattered light occur: forward scatter (FSC), which is the amount of light that is scattered in



the forward direction, quantifies a cell's size; and side scatter (SSC), which is the rest of the light collected on a detector located  $90^{\circ}$  from the laser beam, shows the granularity of a cell. Fluorescence can also be detected. Lasers excite the fluorophores, and the subsequent fluorescent emission travels along the same route as the SSC signal. The light is directed through a series of filters and mirrors, so that the appropriate wavelengths are delivered to the correct detector. All the data is recorded and accessed using the BD CellQuest software.

## **2.6 Determining RIG-I and MDA5 Expression Levels**

Indirect immunofluorescence followed by flow cytometry was used to investigate the expression levels of RIG-I and MDA5 before and after stimulation with either CBV5, UV-CBV5, polyinosinic: polycytidylic acid (Poly I:C, a synthetic double-stranded (dsRNA) analogue), or ssRNA, at 0 hour (unstimulated), 1 hour, 2 hour, 4 hour, and 6 hour time points. Each experiment was performed three separate times. The data of all three experiments were averaged to get the final results (error bars show standard deviation (SD) over all experiments).

Healthy, confluent cells (>90% confluency) were stimulated with either 100µl CBV5, 100µl UV-CBV5, 40µl ssRNA, or 50µl Poly I:C, and incubated for 1, 2, 4, or 6 hours. Three flasks were needed per stimulation per time point.

At each time point, 2ml of the supernatant was added to two screwtop Eppendorfs and frozen at -20°C, for use in the Cytometric Bead Array assay. The rest of the supernatant was discarded, and the cells were quickly washed with 4% Paraformaldehyde (PFA). 1ml X2 SDS-PAGE Reducing Sample Buffer was added to one flask and placed on a rocking table for 1 hour, then transferred to an Eppendorf and frozen at -20°C, for use in discontinuous SDS-PAGE. The other two flasks were fixed with 2.5ml 4% PFA for 15 minutes (4% PFA is used as a fixative, by cross-linking proteins, mainly the residues of the amino acid lysine, to lend rigidity to the cells and prevent further biochemical reactions), the cells were then scraped off and 1ml was transferred to five Eppendorfs (to provide one negative control sample, two MDA5 samples, and two RIG-I samples).

After centrifuging at 13,000 rpm for 2 minutes at RT, the supernatant was aspirated off and the cells were resuspended in 1ml PBS / 0.02%<sub>(w/v)</sub> Bovine Serum Albumin (BSA) / 0.02%<sub>(w/v)</sub> Saponin / 0.02%<sub>(w/v)</sub> Sodium Azide (NaN<sub>3</sub>). BSA is used as a carrier protein to antibodies and as a general protein blocking agent. The amphipathic nature of Saponin makes it act as a surfactant, enhancing the penetration of proteins through the cell membrane. NaN<sub>3</sub> prevents the internalisation of surface antigens, which could produce a loss of fluorescent intensity. The cells were then centrifuged and the supernatant aspirated off again, followed by resuspension in 100µl PBS / BSA / Saponin / NaN<sub>3</sub>, and incubation with 2µl of primary antibody (MDA5 (C-16) Goat pAb or RIG-I (C-15) Goat pAb) for one hour or greater at RT.

After incubation in primary antibody, the cells were washed and resuspended in 100µl PBS / BSA / Saponin / NaN<sub>3</sub>, followed by incubation with 2µl of secondary antibody (pAb Rabbit anti-Goat FITC) for 45 – 60 minutes in the dark (to prevent photobleaching) at RT. The cells were then washed twice in PBS / BSA / Saponin / NaN<sub>3</sub>, then resuspended in 500µl PBS and transferred to flow tubes and run on the FACSCalibur<sup>TM</sup>. 10,000 cells not gated were analysed for each sample.

## **2.7 Phospho-I $\kappa$ B and IRF3 Detection**

### **2.7.1 SDS-PAGE**

SDS-PAGE (Sodium Dodecyl Sulphate Polyacrylamide Gel Electrophoresis) is a technique used to electrophoretically separate proteins according to their Molecular Weight (MW). There are two types of SDS-PAGE; continuous and discontinuous.

#### **2.7.1.1 Continuous SDS-PAGE**

In continuous SDS-PAGE, the identity and concentration of the buffer solutions are the same in both the gel and the tank. This type of SDS-PAGE is easy to prepare and gives adequate resolutions for electrophoresis of DNA and RNA, but for proteins, where a higher resolution is often needed, discontinuous SDS-PAGE is typically used.

#### **2.7.1.2 Discontinuous SDS-PAGE**

Discontinuous SDS-PAGE utilises a different buffer for the tank and the gels, and the gel itself is split into two parts: the upper stacking gel and the lower resolving gel. The 4% stacking gel has a large pore size (low percentage) and low pH (6.8), whilst the 10% resolving gel has smaller pores and a higher pH (8.8). The protein samples are stacked into very thin, sharp zones at the interface between the stacking gel and resolving gel, and are then separated according to their MW as they pass through the resolving gel. Both gels contain chloride ( $\text{Cl}^-$ ) ions as the mobile anion, whilst the running buffer (pH 8.8) has glycine as its anion. When electrophoresis starts, both  $\text{Cl}^-$  and glycinate ions migrate through the stacking gel. The smaller, strongly charged  $\text{Cl}^-$  ions move faster than the glycinate ions. Due to

the low pH in the stacking gel compared to the running buffer, the equilibrium favours the zero net charge zwitterionic form of glycine. The faster  $\text{Cl}^-$  ions leave behind an area of unbalanced, positive counter ions in their wake, creating a steep voltage gradient (the Kohlrausch discontinuity) that pulls the glycinate ions along, resulting in two fronts moving at the same speed. The protein sample molecules, having an intermediate mobility, are carried along between these two fronts through the large pores of the stacking gel, and deposited in a focused narrow band on top of the resolving gel. When the Kohlrausch discontinuity enters the resolving gel, the pH increases, ionising the glycine and increasing its mobility. The faster running glycinate ions dissipate the discontinuity and run past the protein samples, allowing them to separate themselves through the resolving gel [National Diagnostics, URL].

### **2.7.1.3 Discontinuous SDS-PAGE Preparation**

In this project, discontinuous SDS-PAGE followed by western blotting was used to detect the presence of phospho-I $\kappa$ B and IRF3 in the cells' lysate. As explained in the introduction, I $\kappa$ B is an inhibitory protein that regulates NF- $\kappa$ B. RIG-I and MDA5, activated by ligand RNA, interact with IPS-1 via CARD-CARD interactions, which induces the recruitment of downstream signalling molecules. This results in I $\kappa$ B being released from the NF- $\kappa$ B complex and getting phosphorylated, marking it for ubiquitination and degradation by proteosomes, and leads to the activation of NF- $\kappa$ B and IRF3/7. *Figure 2.4* shows the basic setup of the apparatus used for discontinuous SDS-PAGE.

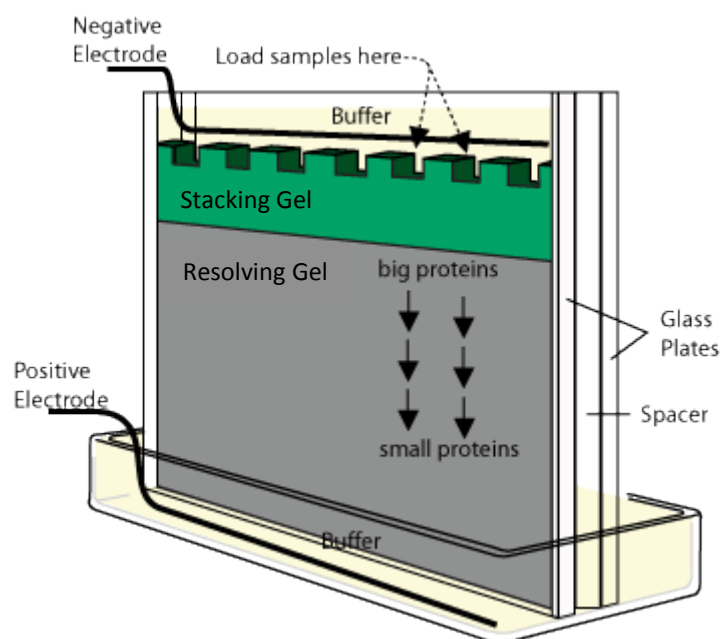


**Figure 2.4: Apparatus used for SDS-PAGE.** A 1mm glass spacer plate and a shorter glass plate are sandwiched together and placed in the holder, forming the cassette. Water is used to test for leaks. A 1mm comb is placed in, and a mark is made approximately 5-10mm below the teeth of the comb, to indicate where the boundary between the resolving gel and the stacking gel should be [modified from The Biotechnology Project at MATC, URL].

Once the apparatus was set up, 10% resolving gel was poured in between the glass plates up to the mark made previously. 10% Ammonium Persulphate (APS) and Tetramethylethylenediamine (TEMED) were only added once the gel was ready to be poured, as they catalyse the polymerisation of the acrylamide gel. A thin strip of saturated isobutanol (top layer) was added to the surface of the resolving gel, to remove any bubbles and even it out, and the gel was then left for approximately 45-60 minutes to polymerise. Once the resolving gel was set, the isobutanol was washed off with  $\text{dH}_2\text{O}$ , and 4% stacking gel was added all the way to the top of the cassette (again, 10% APS and TEMED were added once the gel

was ready to be poured). A comb was inserted at this stage to create the wells, and the stacking gel was left to polymerise for 45-60 minutes.

Once set, the plates were unclipped from the casting stand and slid into a U-shaped gasket electrode assembly, short plate facing inwards, and placed into a tank. Approximately 1 inch (1/3 of the height of the plates) of running buffer was added to the tank and filled between the plates.

#### **2.7.1.4 Sample Preparation for SDS-PAGE**

To prepare the samples for running on the gel, X2 SDS-PAGE Reducing Sample Buffer was added to cells that had been incubated with CBV5, UV-CBV5, ssRNA, or Poly I:C for 0, 1, 2, 4, or 6 hours. The SDS in the reducing sample buffer is an anionic surfactant which both denatures secondary and non-disulphide-linked tertiary structures in proteins, and places a negative charge onto each protein in proportion to its mass. This ensures that each protein is linear and separated only by its MW. The  $\beta$ -mercaptoethanol present further denatures proteins by cleaving their disulphide bonds, thereby disrupting the tertiary and quaternary structure of them. The glycerol helps preserve the proteins at low temperatures, and weighs down the samples when loading them into the wells. The Tris present acts as a buffer (Tris has an effective pH range between 7.0 and 9.2). The addition of Bromophenol Blue allows the samples to be visualised as they pass through the gel.

100 $\mu$ l of each sample was added to separate Eppendorfs and boiled for 10 minutes, along with biotinylated SDS-PAGE standards (2 $\mu$ l + 40 $\mu$ l X2 SDS-PAGE

Reducing Sample Buffer), to help denature the proteins further. The standards are a mixture of biotinylated proteins with consistent molecular weights, allowing for accurate molecular weight determination of immune detected proteins. 40µl of the samples (10µl of standards) were then loaded into the wells, and the apparatus was run at a constant voltage of 200V for 45 minutes, or until the blue dye ran off the bottom of the gel.

### **2.7.2 Western Blot**

Western blotting is a technique used to transfer the proteins that have been separated by SDS-PAGE onto a nitrocellulose membrane, and then probe them with antibodies for further analysis. Using the electroblotting method, a sandwich of the gel (with the stacking gel trimmed off) and the nitrocellulose membrane was compressed in a cassette between two layers of blotting paper and pads pre-soaked in transfer buffer. The gel holder cassette was then placed into a tank transfer system together with an ice block, and the tank filled with transfer buffer. A constant current of 210mA was applied for 60 minutes, electrophoretically transferring the proteins from the gel to the membrane. The principle of western blotting can be seen in *Figure 2.5*.

#### **2.7.2.1 Blocking and Primary Antibody Incubation**

After the transfer was complete, the membrane was washed in 0.1% PBS-Tween. All washes and incubations were performed at RT on a rocking table, to ensure the membrane was fully covered, and the membrane was never left out to dry. At this stage, Ponceau S. dye could be added (for 5-15 minutes) to check if the transfer worked. Ponceau S. is a red stain that rapidly detects protein bands on



membranes, and is easily reversed by multiple washes with 0.1% PBS-Tween. The membrane was then blocked for 60 minutes using 5% blocking reagent, and washed twice for 15 minutes with 0.1% PBS-Tween. The blocking reagent blocks any remaining hydrophobic binding sites, preventing the binding of the primary antibody to the membrane itself and thereby reducing background signal. The membrane was incubated for 60 minutes with a 1:1000 dilution of the primary antibody (either Phospho-I $\kappa$ B $\alpha$  (Ser32) (14D4) Rabbit mAb or IRF-3 (FL-425) Rabbit polyclonal IgG). After use, the primary antibody can be stored at -20°C and reused.

#### **2.7.2.2 Secondary Antibody Incubation**

Two washes of 15 minutes with 0.1% PBS-Tween were then performed to remove excess primary antibody, before the secondary antibody was added. The membrane can be cut at this stage, to separate the standards from the samples. A 1:2000 dilution of polyclonal Swine anti-Rabbit Ig horseradish peroxidase (HRP) was added to the samples, whilst a 1:2000 dilution of streptavidin-HRP conjugate was added to the standards, and left to incubate for 45 – 60 minutes. The membrane was then washed with 0.1% PBS-Tween for 2 hours, changing the solution every 15 minutes, to ensure all excess antibody had been removed before visualising the bands using enhanced chemiluminescence.

#### **2.7.3 Enhanced Chemiluminescence**

The emission of light as a result of the dissipation of energy from a substance in an excited state, caused by a chemical reaction, is termed chemiluminescence. Enhanced chemiluminescence (ECL) involves the use of enhancers (such as

phenols) to increase the light output and extend the light emission duration. The principle of ECL western blotting can be seen in *Figure 2.6*.

Detection of the bands was performed in a dark room, to avoid exposing the autoradiography film to light. Excess 0.1% PBS-Tween was drained from the membrane before placing it, protein side up, on a sheet of cling film in an X-ray cassette. An equal volume of ECL Reagent (Amersham) was mixed together (1ml of each per membrane), added to the membrane, and incubated for 1 minute. Excess reagent was dabbed off, the membrane was turned over (protein side down), and sealed like an envelope in the cling film, smoothing out any air bubbles. The wrapped film was then placed protein side up. A sheet of autoradiography film was placed on top of the membrane, the cassette was closed, and exposed for 2 minutes. The film was then developed immediately, and depending on the intensity and clarity of the bands seen, a new sheet of film could be exposed for a differing length of time.

#### **2.7.4 Stripping and Reprobing Membranes**

A membrane may be stripped of its bound primary and secondary antibodies, allowing it to be reprobed with different antibodies. To strip a membrane, stripping buffer was added (enough to cover the membrane), and incubated for 4 minutes at 37°C in a shaker incubator. After washing at RT with 0.1% PBS-Tween 3 times for 10 minutes each, the membrane was blocked for 60 minutes using 5% blocking reagent, and washed twice for 15 minutes with 0.1% PBS-Tween. A different primary antibody can then be added, following the procedure above.

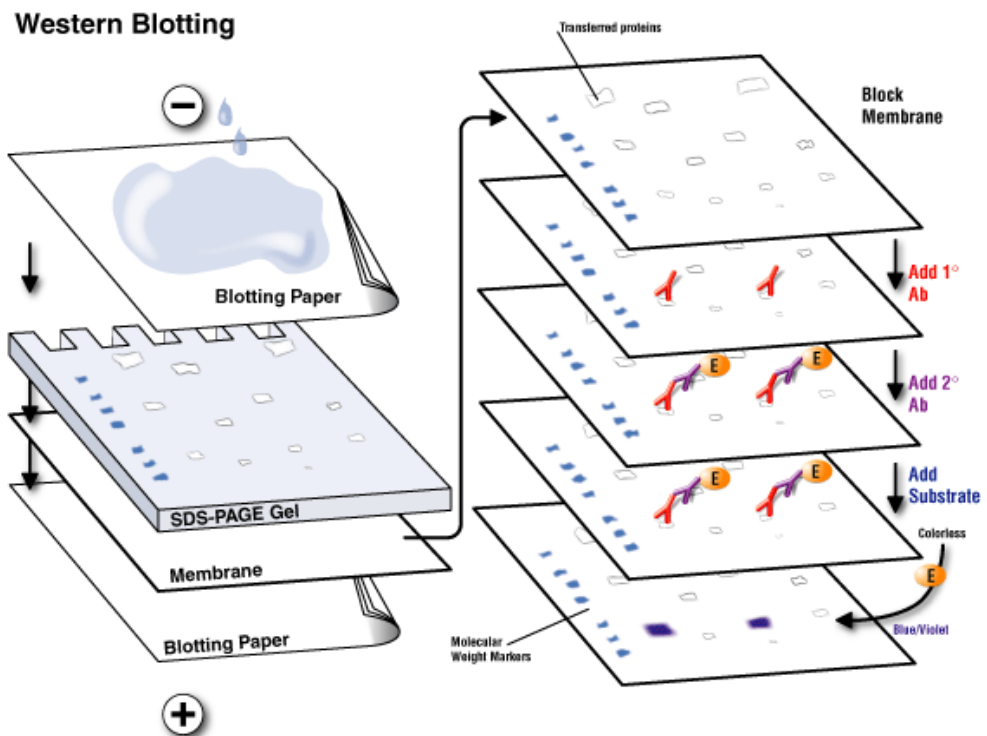


**Figure 2.5: Principle of western blotting.** The proteins are electrophoretically transferred from the SDS-PAGE gel onto the nitrocellulose membrane. The membrane is blocked, and primary and secondary antibodies are added, followed by the substrate, after which the proteins can be visualised using enhanced chemiluminescence [Komabiotek, URL].

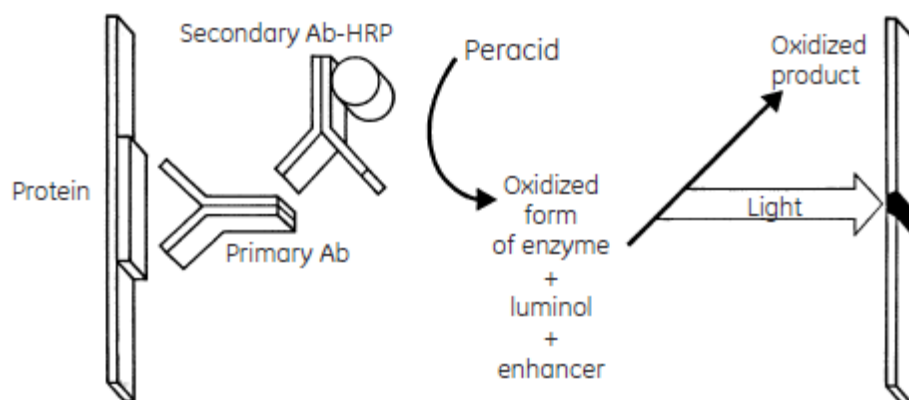


**Figure 2.6: Principle of ECL western blotting.** HRP catalyses the oxidation of luminol to its excited state, and it subsequently decays back to the ground state via a light emitting pathway [GE Healthcare Life Sciences, URL].

## **2.8 Immunoprecipitation**

Immunoprecipitation is a technique used to precipitate a protein out of a lysate using an antibody specific for that protein coupled with beads specific for the antibody. The technique can be used to isolate and concentrate a particular protein, as well as determine if dimerisation between two proteins has occurred. In this project, RIG-I, MDA5, or LGP2 antibodies were used to precipitate out their respective protein, and SDS-PAGE was then used to detect a different protein, i.e. precipitate out MDA5 and perform SDS-PAGE to detect LGP2. If bands appear, this concludes that MDA5 and LGP2 form dimers together.

In TC, 1.5ml of cardiac cells were stimulated with 200µl CBV5 for 1, 2, 4, and 6 hour time points, or left unstimulated (0 hour). 2 flasks were used per time point. At each time point, the medium (plus CBV5) was aspirated off, and the cells washed with 2ml PBS. 1ml lysis buffer was added, and the flasks were placed on a rocking table for over 2 hours, and vortexed every 30 minutes. The lysis buffer was then transferred to Eppendorfs and centrifuged at 13,000 rpm for 20 minutes at RT. The supernatant was transferred to new Eppendorfs, and 25µl resuspended Protein A Sepharose (PAS) beads 10%<sub>(w/v)</sub> was added. The Eppendorfs were then incubated on ice for over 1 hour, with each Eppendorf being flicked every 5-10 minutes to resuspend the PAS beads.

### **2.8.1 Pre-Clearing**

The PAS beads were added at this stage to pre-clear the lysate, before the antibody was added, to prevent non-specific binding of the antibody to unwanted proteins. After incubation on ice, the Eppendorfs were centrifuged at 13,000 rpm

for 5 minutes at RT. The pellet (pre-clear 1 = P1) was kept and stored in the fridge, and the supernatant was transferred to new Eppendorfs. 25µl PAS was then added to the supernatant, and again incubated on ice for over 1 hour, with each Eppendorf being flicked every 5-10 minutes. The Eppendorfs were then centrifuged at 13,000 rpm for 5 minutes at RT, the pellet (P2) kept and stored in the fridge, and the supernatant transferred to new Eppendorfs.

### **2.8.2 Primary Antibody Incubation and Washing**

6µl of MDA5 (C-16) Goat pAb, RIG-I (C-15) Goat pAb, or LGP2 (DHX58) Goat pAb was added, and the Eppendorfs were incubated on ice for over 1 hour, with each Eppendorf being flicked every 5-10 minutes. 30µl PAS beads (or more if required) were added, and again the Eppendorfs were incubated on ice for over 1 hour and flicked every 5-10 minutes. PAS beads have a high affinity for the Fc region of antibodies, so once the antibodies have bound their specific protein, they in turn bind to PAS. The Eppendorfs were then centrifuged at 13,000 rpm for 5 minutes at RT, the pellet (sample = S) was kept, and the supernatant was transferred to new Eppendorfs (to allow a different antibody to be added).

The pellets (P1, P2, and S) were then washed: 500µl lysis buffer was added to each Eppendorf, followed by being vortexed for 1 minute, centrifuged at 13,000 rpm for 2 minutes at RT, and having their supernatant aspirated off. This was repeated four times. After the final centrifugation, 500µl lysis buffer was added to one Eppendorf, mixed, and the whole contents transferred to its duplicate Eppendorf (as there were 2 flasks per time point, resulting in 2 Eppendorfs per time point). An extra 100µl lysis buffer was added to the first Eppendorf, to

retrieve the last few beads of the pellet, and transferred to the duplicate Eppendorf. This results in one Eppendorf with all the contents from the 2 original flasks. The pellet was then dried using a rolled up piece of blue roll.

### **2.8.3 SDS-PAGE**

The final stage involves running an SDS-PAGE and probing with a different antibody to the one bound to the beads, to determine if dimerisation has occurred. The method for the SDS-PAGE and western blot is described above, with the following exceptions. 50µl X2 SDS-PAGE Non-Reducing Sample Buffer was added to each Eppendorf, and incubated for 15 minutes at RT (rather than boiled). After incubation, the Eppendorfs were centrifuged at 13,000 rpm for 1 minute at RT before loading onto the gel. As a control, X2 SDS-PAGE Reducing Sample Buffer was added to samples, followed by boiling for 10 minutes. The procedure then continues exactly as described in section 2.7, using MDA5 (H-61) Rabbit pAb, RIG-I (H-300) Rabbit pAb, or LGP2 (H-159) Rabbit pAb as the primary antibody.

## **2.9 Confocal Microscopy**

Confocal microscopy is a technique used to visualise the interaction and location of different proteins within cells. A confocal microscope can create sharp images of specimens by using a spatial pinhole that excludes out-of-focus light in specimens which are thicker than the focal plane. This increases the micrograph contrast and enables reconstruction of three-dimensional images. A confocal microscope works by scanning one or more focused beams of light, usually from a laser or arc-discharge source, across the specimen to create illumination. The principle light pathways in confocal microscopy can be seen in *Figure 2.7*.

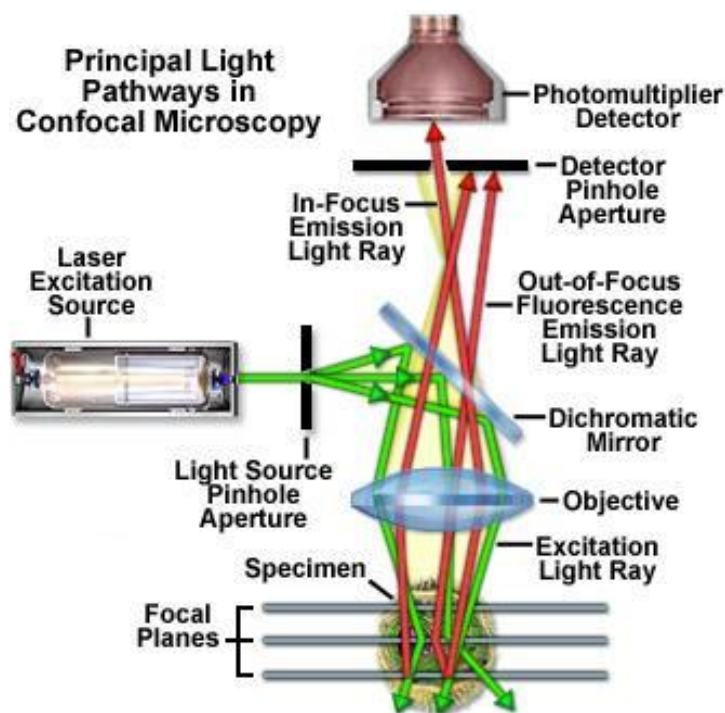


**Figure 2.7: Principle light pathways in confocal microscopy.** The point of illumination is brought to focus by the objective lens, and laterally scanned using a scanning device under computer control. This is detected by a photomultiplier detector through a detector pinhole, and the output from the photomultiplier detector is built into an image and displayed by the computer [Nikon MicroscopyU, URL].

### 2.9.1 Slide Preparation

In this project, cardiac cells were stimulated with CBV5 and the colocalisation of RIG-I or MDA5 with IPS-1 was investigated. Lab-Tek 8-well chamber slides were used, and 2.5 slides were used per stimulation. Five time points were used per stimulation: 0 hour (unstimulated), 1 hour, 2 hours, 4 hours, and 6 hours. Two wells were used per time point. The slides were divided up as shown in *Figure 2.8*.

Unstimulated	Unstimulated	Unstimulated	Unstimulated
RIG-I	RIG-I	MDA5	MDA5
IPS-1	IPS-1	IPS-1	IPS-1
2 hour CBV5	2 hour CBV5	2 hour CBV5	2 hour CBV5
RIG-I	RIG-I	MDA5	MDA5
IPS-1	IPS-1	IPS-1	IPS-1
4 hour CBV5	4 hour CBV5	4 hour CBV5	4 hour CBV5
RIG-I	RIG-I	MDA5	MDA5
IPS-1	IPS-1	IPS-1	IPS-1
6 hour CBV5	6 hour CBV5	6 hour CBV5	6 hour CBV5
RIG-I	RIG-I	MDA5	MDA5
IPS-1	IPS-1	IPS-1	IPS-1
1 hour CBV5	1 hour CBV5	1 hour CBV5	1 hour CBV5
RIG-I	RIG-I	RIG-I	RIG-I
IPS-1	IPS-1	IPS-1	IPS-1
1 hour CBV5	1 hour CBV5	1 hour CBV5	1 hour CBV5
MDA5	MDA5	MDA5	MDA5
IPS-1	IPS-1	IPS-1	IPS-1

**Figure 2.8: Layout of Lab-Tek 8-well chamber slides stimulated with CBV5 at different time points.** Cells were grown to confluency and stimulated. After fixing, the cells were incubated with the primary antibody, washed, and incubated with the corresponding secondary antibody: Donkey Anti-Goat TRITC (red) for RIG-I and MDA5, and Swine Anti-Rabbit FITC (green) for IPS-1. TOPRO was used as a nuclear stain.



To prepare the slides, 300µl DMEM was added to each well. One flask of cells was trypsonised, 10,000 cells were added to each well, and the slides were incubated overnight, making sure that they did not reach 100% confluency before carrying on with the stimulations. To determine the Xµl of cells, the cells were counted using a haemocytometer, as explained in *Figure 2.9*.

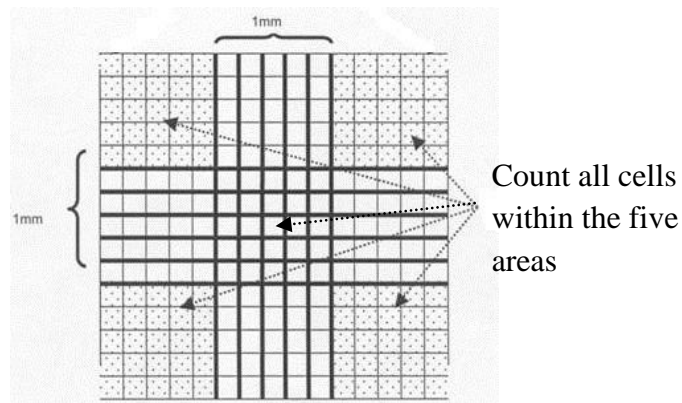


**Figure 2.9: Layout of a haemocytometer.** Divide the number of cells in the five areas by 5 to get the average, and multiply by  $10^4$  to get cells / ml. The following equation was used to work out Xµl of cells: Number of cells counted / 10,000 cells = 1000µl of medium / Xµl [modified from WHO, URL].

The medium was aspirated from each well, and the slides were stimulated with 150µl DMEM and 10µl CBV5 and incubated at 37°C 5% CO<sub>2</sub> for 1, 2, 4, or 6 hours. All aspirations and additions to the wells were made from the same corner, to minimise damage to the cells. At each time point, the cells were fixed with 300µl 4% PFA for 15 minutes, washed with 300µl PBS, and left in 300µl PBS until the whole slide was ready.

Once ready, the 300µl PBS was aspirated off and 150µl PBS / BSA / Saponin / NaN<sub>3</sub> was added to each well. 4µl primary antibody was added to each well (as

detailed in *Figure 2.8*), and incubated for 1 hour at RT. The primary antibodies used were: MDA5 (C-16) Goat pAb; RIG-I (C-15) Goat pAb; and MAVS (H-135) Rabbit pAb.

The cells were then washed twice with 300µl PBS / BSA / Saponin / NaN<sub>3</sub>, and 150µl PBS / BSA / Saponin / NaN<sub>3</sub> was added to each well. 5µl secondary antibody (Donkey Anti-Goat TRITC (red) and Swine Anti-Rabbit FITC (green)) was added to each well and incubated for 45-60 minutes in the dark at RT. The cells were then washed twice with 300µl PBS / BSA / Saponin / NaN<sub>3</sub>, and 150µl PBS / BSA / Saponin / NaN<sub>3</sub> was added to each well. 1µl TOPRO (a nuclear stain) was added to each well and incubated for 10 minutes. The cells were finally washed three times with 300µl PBS / BSA / Saponin / NaN<sub>3</sub>, and all the liquid was removed.

The chambers and gasket were removed from the slide, and a few drops of SlowFade Gold Antifade Reagent were added to each well, and left for 10 minutes. This reagent suppresses photobleaching and preserves the signal of the fluorescently labelled secondary antibody. A coverslip was then placed over the wells and any air bubbles were gently pushed out from underneath them. Excess SlowFade Gold Antifade Reagent was removed using blue roll, and the coverslips were sealed down using a thin layer or two of clear nail varnish. Slides were then imaged on an LSM510 confocal microscope under a 63x / 1.4 Oil DIC objective, utilising the three fluorescent wavelengths of 488 (Argon – green), 543 (red), and 633 (blue).

### **2.9.2 Confocal Image Analysis**

Once confocal images have been taken, the extent of colocalisation needs to be statistically determined. It is no longer sufficient to merely overlay the red and green images, and say that where yellow appears is where colocalisation has occurred. User bias can play a large role in determining the amount of yellow colour present, leading to false positives as a result of increasing the background values. An imbalance of red and green pixel ratios can lead to wildly varying results. To eliminate user bias and provide a quantitative value of the extent of colocalisation, the images are automatically thresholded and the interdependency of the red and green channels is measured. A correlation coefficient is used to calculate the interdependence of the two variables, which equates to the extent of colocalisation that may be occurring.

#### **2.9.2.1 LSM Image Browser and AxioVision LE**

LSM Image Browser software [free software available from Zeiss, [URL](#)] was used to adjust the contrast and brightness of the confocal images taken. This does not affect the statistical analysis of the images, as the ImageJ and JACoP software (detailed below) automatically thresholds images, removing user bias. When images are taken, they are saved as an LSM file, which is essentially an extension of the TIFF multiple image stack file format, containing instrument specific hardware settings metadata and a thumbnail image. Before they can be analysed using ImageJ and JACoP, they need to be converted to TIF files, using AxioVision LE [free software available from Zeiss, [URL](#)]. The steps involved are detailed below:

- Open AxioVision LE
- Click on “Open Image” (Ctrl-I)
- Select an image (located in the .mdb folder, as an .lsm file)
- Image will appear in the main window
- Click “File – Export” (Ctrl-6)
- Choose “Save In” location, tick “Use color for channel images”, change File Type to TIF Tagged Image File, keep “Convert to 8 bit” and “Apply display mappings” ticked (can also tick “Burn-in annotations” as well if required)
- Click on “Start”
- The image will be saved in the location chosen as a TIF File

#### **2.9.2.2 ImageJ and JACoP**

Having converted the images to TIF files, they can then be analysed using ImageJ and JACoP. ImageJ software [free download from either MacBiophotonics, URL, or ImageJ, URL] is an image processing and analysis in Java piece of software used to analyse confocal images. JACoP (Just Another Colocalisation Plugin) [available from ImageJ Plugins, URL] then needs to be downloaded to the Plugins folder of ImageJ [Bolte and Cordelieres, 2006]. The steps performed to run the colocalisation analysis are detailed below:

- Open MacBiophotonics ImageJ
- Drag and drop a .TIF image onto the ImageJ bar, opening the image in ImageJ

- Click “Image – Color – Split Channels” to get three 8-bit split channels (Red, Green, Blue) in grey (the images should already be in 8-bit since they were exported from AxioVision; if not, need to convert each of the three images to 8-bit by clicking “Image – Type – 8-bit” for each one)
- Click “Plugins – JACoP”, bringing up the JACoP window and automatically selecting the Red and Green image.
- The images to analyse can be changed using the drop down menu for Image A and Image B
- Under “Analysis to perform”, make sure Pearson’s coefficient, M1 & M2 coefficients, Costes’ automatic threshold, Cytofluorogram, and Costes’ randomization are all checked. Van Steensel’s CCF, Li’s ICA, Objects based methods, and Overlap coeff., k1 & k2 are not required
- Click on the Micro. tab, select Confocal rather than Wide-Field
- If wanted, in the Costes’ rand<sup>o</sup> tab, can change the Nb of random. rounds, depending on computing power (any value between 200-1000)
- Click on Analyze to run the analysis

Once the analysis has run, several windows pop up. The log is the most important window, as it provides all of the statistical data. It details which two images have been compared, Pearson’s coefficient, Mander’s Coefficients (original and threshold values), Costes’ randomisation based colocalisation, Costes’ automatic threshold values, and the Cytofluorogram’s parameters. The most important values to note are the  $r(\text{obs})$ ,  $r(\text{rand})$ , and the p-value. These three values are required for each set of images taken, to statistically determine the extent of colocalisation between two images (i.e., between RIG-I and IPS-1).

### **2.9.2.3 Pearson's Correlation Coefficient**

Pearson's correlation coefficient ( $r(\text{obs})$ , also referred to as  $R_r$ ) measures the covariance between the intensities of each channel in each pixel, and is not sensitive to background or colocalised pixel intensity. It has a linear regression range of -1 to 1, with -1 being total negative correlation (whereby no pixels overlap), 0 being a random correlation, and 1 being total positive correlation (where all the pixels overlap). Values of approximately 0.5 and above are considered reasonable Pearson's coefficients. The values obtained can then be compared across multiple samples.

### **2.9.2.4 Mander's Overlap Coefficient**

Mander's overlap coefficient is calculated from the Pearson's coefficient. It is sensitive to background intensity (therefore images require thresholding), but is easier to interpret than Pearson's coefficient, as it ranges from 0 (total negative correlation) to 1 (total positive correlation). Manders' overlap coefficient is strongly influenced by the ratio of red:green pixels (ch1:ch2), so they need to be roughly 1:1 to use this method.

### **2.9.2.5 Mander's Colocalisation Coefficients**

Mander's colocalisation coefficients ( $M1$  and  $M2$ ) show the extent that green pixels in one channel overlap red pixels in the other channel, and vice versa. Each value represents the percentage of the total pixels in each channel that overlap with pixels in the other channel. It is sensitive to background intensity, but not to overlapping pixel intensities (i.e., bright red – bright green is equivalent to faint

red – bright green). Values range from 0 to 1, with 1 representing 100% colocalisation.

#### 2.9.2.6 Costes' Randomisation Method

Costes' randomisation method calculates the statistical significance of the Pearson's correlation coefficient. It returns a significance (p-value) expressed as a percentage, which is inversely correlated to the probability of getting  $r(\text{obs})$  by chance. A p-value of 1 indicates that there is a >95% certainty that colocalisation exists. Costes' randomisation method is achieved by creating a random image (*Figure 2.10*) for both

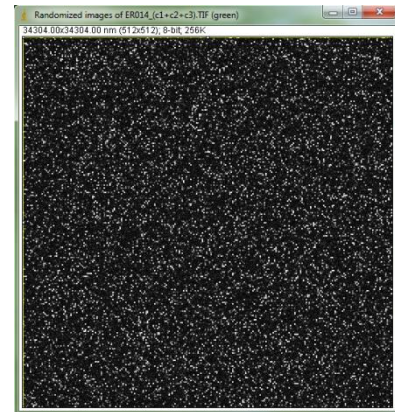


***Figure 2.10: Random image obtained using Costes' randomisation method.***

channels by shuffling pixel blocks, and calculating the  $r(\text{obs})$  compared to one of the original images. This is repeated 200-1000 times (depending on value set) and averaged to obtain the  $r(\text{rand})$ , and this is then compared against the original  $r(\text{obs})$  to obtain the p-value.

#### 2.9.2.7 Costes' Threshold

Costes' Threshold is an algorithm designed to calculate the 'perfect' threshold, thereby eliminating user bias from the thresholding procedure. The limit values for each channel start at the maximum intensity, and are progressively decremented. The Pearson's coefficient is calculated for each decrement until it reaches a value of 0, which equates to a random pixel correlation. At this point, the threshold has been reached for each image.

## **2.10 Plasmid DNA**

### **2.10.1 Plasmid DNA Preparation**

#### **2.10.1.1 Transformation**

All procedures were performed with sterile tips and next to a bunsen burner, to ensure sterility. Agar plates containing Zeocin, a selection antibiotic, were first prepared, by adding 40µl Zeocin to 100ml agar. psiRNA-RIG-I (Invivogen) or psiRNA-MDA5 (Invivogen) plasmids (*Figure 2.11*) were then transformed into a competent *Escherichia.coli* strain (*E.coli* GT116). 5µl of the plasmid was added to 100µl of *E.coli* GT116 and incubated on ice for 30 minutes. This was followed by heat shocking the tubes at 42°C for 45 seconds, then placing them back on ice for 2 minutes. 500µl of Luria Broth (LB) was then added to each tube, and placed on a shaker incubator at 225 rpm at 37°C for 1 hour. 100µl of the transformed *E.coli* in LB was then added to a Zeocin agar plate, evenly spread until absorbed, and placed in an incubator at 37°C overnight to grow. The plasmids contain a Zeocin-resistance gene, so only the *E.coli* that have taken up the plasmid will survive on the Zeocin agar plates.

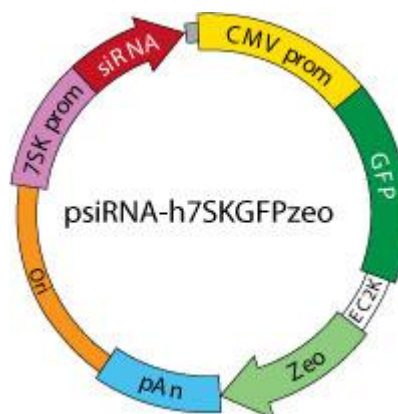


**Figure 2.11:** The *psiRNA-h7SK GFPzeo* plasmid from the human 7SK RNA polymerase III promoter. The plasmids contain the GFP:zeo fusion gene that allows for simple monitoring of transfection efficiency and selection in both *E. coli* and mammalian cells [Invivogen, URL].



After growing up the *E.coli* colonies, the transformed *E.coli* and plasmids were expanded. 25µl Zeocin was added to 25ml LB in bottles, and individual colonies were added to separate bottles, as well as being added to a reference plate, and incubated overnight in a shaker incubator at 225 rpm at 37°C.

#### **2.10.1.2 DNA Isolation**

The broths were centrifuged at 4000 rpm for 10 minutes, and the supernatant discarded. 400µl STET buffer was added, the samples vortexed, and transferred to sterile Eppendorfs. 10µl lysozyme (50mg/ml; damages bacterial cell walls) was added to each tube, immediately after which the tubes were boiled for 1 minute until the lids pop open. The samples were then placed on ice for 5 minutes, then centrifuged at 13,000 rpm for 30 minutes. The pellet was removed (by 'stabbing' it with a sterile toothpick), and 5µl of RNase A (20µg/ml; degrades RNA) was added and the samples incubated at 37°C - 42°C for 30 minutes. 400µl of phenol / chloroform / isoamyl alcohol (bottom layer) was then added, the samples vortexed, and centrifuged for 15 minutes at 13,000 rpm.

The supernatant was transferred to a fresh sterile Eppendorf, and 400µl of chloroform / isoamyl alcohol was added, the samples vortexed, and centrifuged again for 15 minutes at 13,000 rpm. The supernatant was again transferred into new Eppendorfs. 20µl (1/20<sup>th</sup>) sodium acetate 2M pH 6.5 and 1ml (2.5x vol) of 95% ethanol were added, mixed, and the Eppendorfs were then frozen at -80°C for at least 1 hour. Afterwards, the Eppendorfs (straight from the freezer) were centrifuged at 13,000 rpm for 20 minutes at RT. The excess supernatant was removed, the Eppendorfs were centrifuged at 13,000 rpm for a further minute, and

the remaining supernatant was removed. 80µl sterile water (ddH<sub>2</sub>O), or LAL water, was added to each Eppendorf, and the samples frozen at -20°C.

#### **2.10.1.3 Agarose Gel Electrophoresis**

To check the purity of the plasmid preparations, the samples were run on an agarose gel. A 1%<sub>w/v</sub> agarose gel was prepared (1g agarose in 100ml of 1X ELFO), and 10µl of the sample (with 5µl of ELFO Loading Buffer) was run on it at 100V for 45 minutes. A 1kb DNA ladder was run alongside the samples. Once run, the bands were observed using a Stratagene eagle eye UV imaging system.

#### **2.10.2 Silencing**

Silencing is a method used to downregulate or entirely suppress a particular gene via the introduction of antisense RNA, such as small interfering RNA (siRNA). Once transfected into a cell, siRNA binds to and cleaves specific messenger RNA and decreases its activity. In this project, psiRNA-hMDA5 (Invivogen) or psiRNA-hRIG-I (Invivogen) plasmids (*Figure 2.11*) were introduced into cells to knockdown (KD) MDA5 or RIG-I activity, respectively. psiRNA-hMDA5 is a psiRNA vector expressing short hairpin RNA (shRNA) targeting the human MDA5 gene, and psiRNA-hRIG-I is the same but targets the human RIG-I gene. This allows the other protein (RIG-I or MDA5) to be studied, to help determine which one is the primary detector of CBV5.

The method takes 5 days to perform: the dishes are prepared on day 1; the plasmid DNA (containing the siRNA) is transfected into the cells on day 2; the medium is replaced with selection medium on day 3; SDS-PAGE and western blotting are

used to check the KD on day 4; and if the KD worked, the cells are stimulated and a CBA assay is performed on day 5.

#### **2.10.2.1 Day 1 – Cell Preparation**

On day 1, the dishes for each transfection were prepared. 9 dishes per transfection were required, to meet the following criteria: three time points per stimulation with CBV5 (3 dishes); duplicates (6 dishes); 2 dishes for the unstimulated (0 hour) time point (8 dishes); and 1 dish for control (9 dishes total). As both a RIG-I and MDA5 transfection were being performed, 9 dishes were required for each of them. In each dish, 500µl cardiac cells was added to 1.5ml DMEM, to ensure 50-60% confluency by day 2.

#### **2.10.2.2 Day 2 – Transfection Reagent Preparation**

Using sterile Eppendorfs and tips, jetPRIME™ Transfection Reagent was prepared on day 2 in the afternoon. For each dish, 1µl plasmid DNA (psiRNA-hMDA5 or psiRNA-hRIG-I) was added to 100µl jetPRIME™ Buffer and 2µl jetPRIME™ Reagent. 1ml medium was removed from each dish, and the 103µl jetPRIME™ Transfection Reagent and plasmid DNA was added and incubated at 37°C 5% CO<sub>2</sub> overnight.

#### **2.10.2.3 Day 3 – Switch to Selection Medium**

The DMEM of each dish was replaced with 2ml Zeocin-DMEM selection medium (200ml DMEM / FCS / NA + 200µl Zeocin) on the morning of day 3. This ensures that only cells that have taken up the plasmid DNA containing the Zeocin resistance gene (and therefore the siRNA) survive.

#### **2.10.2.4 Day 4 – Check Knockdown**

On day 4, the KD of RIG-I and MDA5 was checked using SDS-PAGE and western blotting. If RIG-I siRNA (or MDA5 siRNA) was successfully transfected into the cells, it should KD the function of RIG-I (or MDA5), and the expression levels of RIG-I (or MDA5) obtained in transfected cells should be lower than the expression levels of RIG-I (or MDA5) in untransfected cells.

#### **2.10.2.5 Day 5 – Stimulation of Cells**

If the KD worked, then 1ml of cells was stimulated on day 5 with 100 $\mu$ l CBV5 for 2 hours, 4 hours, or 6 hours, or left unstimulated (0 hour). At each time point, the supernatant was transferred to two screwtop Eppendorfs and frozen at -20°C. An IFN- $\beta$  flex set bead system assay was performed on the stored supernatant.

## **2.11 Cytometric Bead Array**

A cytometric bead array (CBA) human soluble protein flex set bead system (Becton Dickinson) was used to quantitatively measure IFN- $\beta$  production in cells. The flex set bead system is a bead-based immunoassay capable of measuring soluble IFN- $\beta$  in cell culture supernatant samples. The beads, of known size and fluorescence, are coated with a capture antibody specific for IFN- $\beta$ . The detection reagent is a mixture of phycoerythrin (PE)-conjugated secondary antibodies, which provides a fluorescent signal in proportion to the amount of bound IFN- $\beta$ . When the beads are incubated with cell supernatant, sandwich complexes (capture bead, IFN- $\beta$ , and PE) are formed, and can be measured using flow cytometry.

### **2.11.1 Assay Procedure**

The standards and detection reagents were prepared according to the BD CBA Human Soluble Protein Master Buffer Kit manual. 50 $\mu$ l of the tissue culture supernatant prepared previously was added to flow tubes, followed by the addition of 50 $\mu$ l of the IFN- $\beta$  beads, mixed, and incubated for 1 hour at RT. 50 $\mu$ l of the PE detection reagent was then added and mixed, followed by a further 2 hour incubation at RT in the dark. 1ml of Wash Buffer was added to each tube, centrifuged at 200g for 5 minutes, and then the supernatant was carefully aspirated off and discarded. The bead pellets were resuspended in 300 $\mu$ l of Wash Buffer, and the samples were analysed using flow cytometry, with the data acquired being analysed using the FCAP Array software (Becton Dickinson).

### **Chapter 3**

## **RNA HELICASE INVOLVEMENT IN CBV5 INFECTION OF CARDIAC CELLS**

### **3.1 Introduction**

The RLR family, consisting of the three known family members RIG-I, MDA5, and LGP2, are pattern recognition receptors which detect a range of different viruses. RIG-I (retinoic acid inducible gene-I) and MDA5 (melanoma differentiation-associated gene 5) are homologous cytoplasmic proteins containing an N-terminal region with two caspase activation and recruitment domains (CARDs), a central SF2 type DExD/H-box RNA helicase domain, and a C-terminal repressor domain (RD) [Takeuchi and Akira, 2007]. LGP2 (laboratory of genetics and physiology 2) harbours a DExD/H-box RNA helicase domain and a C-terminal RD, but lacks any CARDs [Yoneyama *et al.*, 2005].

Once a viral ligand has been detected and bound by RIG-I and MDA5, both signal downstream through their CARDs to activate IRF3/7 and NF- $\kappa$ B indirectly, via the protein intermediate IPS-1 (IFN- $\beta$  promoter stimulator 1) [Kawai *et al.*, 2005]. After interaction with RIG-I and MDA5, IPS-1 goes on to recruit and activate a variety of other proteins, including TRAF2, TRAF3, and TRAF6 [Xu *et al.*, 2005; Oganessian *et al.*, 2006; Saha *et al.*, 2006]. These TRAF proteins then signal further downstream to the I $\kappa$ B kinase (IKK) family members, to activate the transcription factors IRF3/7 and NF- $\kappa$ B, and initiate an immune response.

RIG-I and MDA5 contribute to antiviral signalling in different ways depending on the virus involved [Kato *et al.*, 2006; Loo *et al.*, 2008]. Although a lot of research has gone into determining the precise pathogen associated molecular patterns (PAMPs) recognised by each RLR, the results are still far from conclusive.

RIG-I has been shown to detect a wide variety of different viruses and PAMPs, with uncapped 5'-triphosphate RNA (5'-pppRNA) found to be important for RIG-I activation [Hornung *et al.*, 2006]. Other motifs found to induce RIG-I-mediated IFN production include: double-stranded RNA [Yoneyama *et al.*, 2004]; 5'-ppp single-stranded RNA [Pichlmair *et al.*, 2006]; uridine and adenosine-rich 3'-sequences in 5'-ppp ssRNA [Saito *et al.*, 2008; Uzri and Gehrke, 2009]; short double-stranded blunt-end 5'-pppRNA [Schlee and Hartmann, 2010]; cleavage products produced by the host endonuclease RNase L during viral infection [Malathi *et al.*, 2007]; and short dsRNA viral transcripts, less than 1kb in length [Kato *et al.*, 2008]. There are also suggestions that negative sense virus genomic RNA, generated by viral replication, constitutes the major trigger for RIG-I, whilst the other types of RNA mentioned above do not substantially contribute to IFN induction [Rehwinkel *et al.*, 2010].

MDA5, on the other hand, has been shown to be critical for Picornaviridae detection, due to the VPg region at the 5' end of the viral genome [Gitlin *et al.*, 2006; Kato *et al.*, 2006; Pichlmair *et al.*, 2006]. MDA5 has also been shown to be essential for Poly I:C-induced IFN production [Kato *et al.*, 2006; Loo *et al.*, 2008]. Whilst RIG-I is required for the detection of short dsRNA, MDA5 preferentially binds long dsRNA products (greater than 1-2kb in length) [Kato *et al.*, 2008].

Coxsackievirus B5 (CBV5), a member of the Picornaviridae family, belongs to the *Enterovirus* genus and the *Human enterovirus B* species. One of the most serious diseases caused by CBV5 is viral myocarditis, which can lead on to dilated cardiomyopathy (DCM). Viral myocarditis is an inflammatory disease of



the myocardium characterised by leukocyte infiltrate and necrosis of the myocytes [Bohn and Benson, 2002]. Some patients can develop chronic myocarditis, whilst myocardial destruction can lead on to DCM. DCM is characterised by dilation and impaired contraction of the left or both ventricles of the heart, and is the major reason for cardiac transplantation in Europe and the USA [Manolio *et al.*, 1992]. Determining the primary detector of CBV5 in cardiac cells is therefore vital in developing treatments for CBV5 infection.

## **3.2 Results**

### **3.2.1 MDA5 and RIG-I Expression Levels**

Indirect immunofluorescence coupled with flow cytometry was used to investigate the expression levels of RIG-I and MDA5 in human cardiac cells in response to stimulation with purified CBV5, UV-CBV5 (UV-inactivated CBV5 has the ability to bind to cellular receptors, but is unable to cause a productive infection), purified genomic CBV5 ssRNA, and Poly I:C. The stimuli were incubated at 1, 2, 4, and 6 hour time points (0 hour = unstimulated). Once stimulated, the cells were harvested, fixed and permeabilised. They were then incubated with Goat pAb antibodies against either MDA5 (*Figure 3.1*) or RIG-I (*Figure 3.2*), followed by incubation with FITC-conjugated secondary antibody.

The expression levels of MDA5 (*Figure 3.1*) in response to Poly I:C stimulation increased, with a maximum increase at 2 hours. Furthermore, after CBV5 stimulation, there is a marked increase in MDA5 expression after the first two hours, which tails off after 4 and 6 hours of infection. The UV-CBV5 stimulation showed no response in MDA5 expression levels. Likewise, stimulation with ssRNA resulted in no effect in MDA5 expression.

The expression levels of RIG-I in human cardiac cells in response to the four different stimulations can be seen in *Figure 3.2*. The Poly I:C had no effect on the expression levels of RIG-I, and neither did the UV-CBV5. Likewise, ssRNA stimulation had little effect upon the expression levels of RIG-I. CBV5 stimulation resulted in an initial strong response by RIG-I after 1 hour, which gradually decreased over the remaining hours.

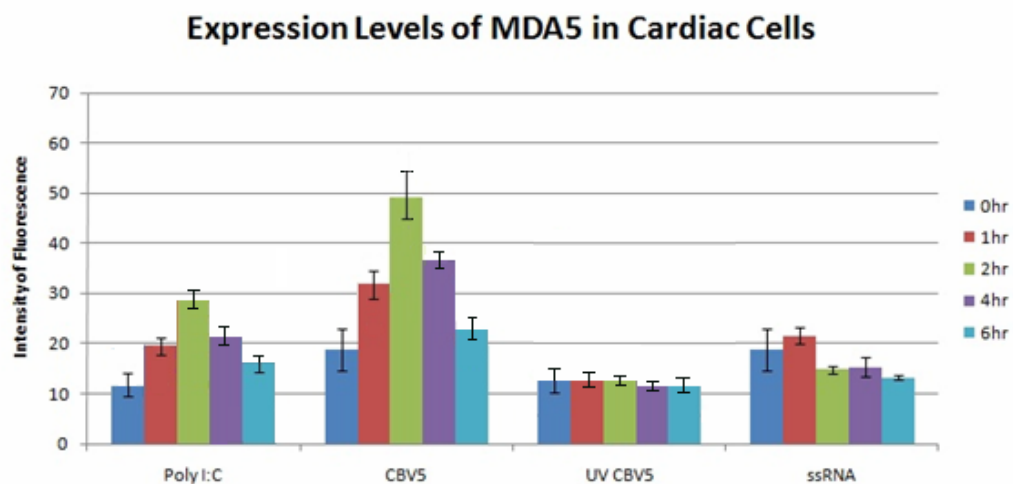


**Figure 3.1: Expression levels of MDA5 in human cardiac cells.** Cardiac cells were stimulated with Poly I:C, CBV5 virions, UV-CBV5, or ssRNA, at 1, 2, 4, and 6 hour time points (0hr = unstimulated), measured by intensity of fluorescence. Confluent cells were stimulated, harvested, fixed and permeabilised, followed by incubation with MDA5 Goat pAb primary antibody and pAb Rabbit anti-Goat FITC secondary antibody. Fluorescence was detected using a FACSCalibur (BD) counting 10,000 cells not gated. Isotype controls were performed, with values similar to unstimulated samples. Data show means  $\pm$  SD and are representative of three independent experiments.

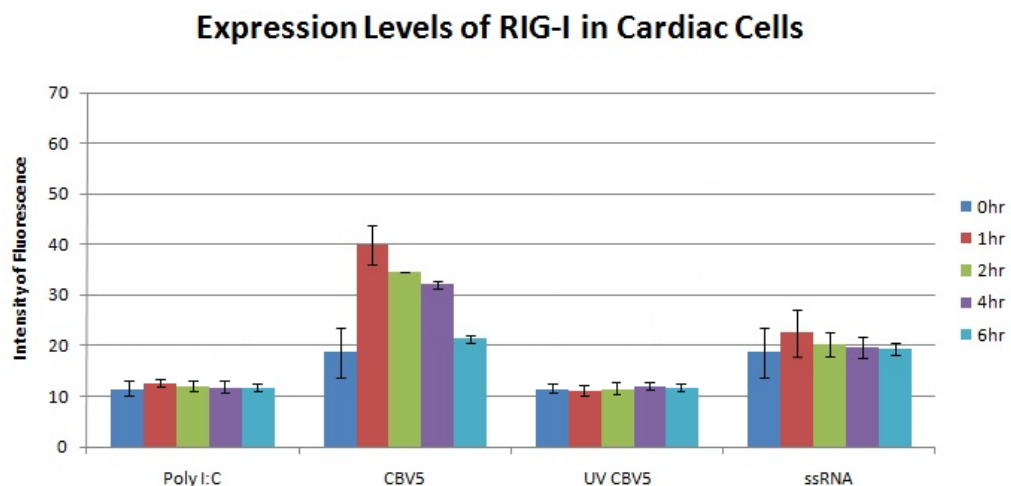


**Figure 3.2: Expression levels of RIG-I in human cardiac cells.** Cardiac cells were stimulated with Poly I:C, CBV5 virions, UV-CBV5, or ssRNA, at 1, 2, 4, and 6 hour time points (0hr = unstimulated), measured by intensity of fluorescence. Confluent cells were stimulated, harvested, fixed and permeabilised, followed by incubation with RIG-I Goat pAb primary antibody and pAb Rabbit anti-Goat FITC secondary antibody. Fluorescence was detected using a FACSCalibur (BD) counting 10,000 cells not gated. Isotype controls were performed, with values similar to unstimulated samples. Data show means  $\pm$  SD and are representative of three independent experiments.

### 3.2.2 Signalling Detection Upon Infection With CBV5

RIG-I and MDA5, activated by ligand RNA, interact with IPS-1 via CARD-CARD interactions, which induces the recruitment of downstream signalling molecules. This results in I $\kappa$ B being released from the NF- $\kappa$ B complex and getting phosphorylated, marking it for ubiquitination and degradation by proteosomes. The transcription factors NF- $\kappa$ B and IRF3 transcriptionally upregulate type I IFNs to mediate induction of the innate immune response. The detection of phospho-I $\kappa$ B therefore corresponds to NF- $\kappa$ B activation.

Human cardiac cells were stimulated with Poly I:C, ssRNA, CBV5 virions, or UV-CBV5 at 1, 2, 4, and 6 hour time points, or left unstimulated (0 hour). Discontinuous SDS-PAGE combined with western blotting using Phospho-I $\kappa$ B mAb or IRF3 mAb was used to detect the presence of phospho-I $\kappa$ B (*Figure 3.3*) or IRF3 (*Figure 3.4*), respectively. The bands were visualised using enhanced chemiluminescence.

The blots for phospho-I $\kappa$ B detection in human cardiac cells stimulated with Poly I:C, ssRNA, CBV5 virions, or UV-CBV5 can be seen in *Figure 3.3*. Phospho-I $\kappa$ B was detected in the lysate of cardiac cells stimulated with Poly I:C at all time points. ssRNA induced a similar response, with a slightly weaker presence of phospho-I $\kappa$ B at the 6 hour time point. Interestingly, stimulation with CBV5 resulted in a delayed phospho-I $\kappa$ B detection occurring from 2 hours onwards, with no phospho-I $\kappa$ B presence after 1 hour. Upon stimulation with UV-CBV5, phospho-I $\kappa$ B was detected at all time points, with the weakest presence occurring at the 6 hour time point.

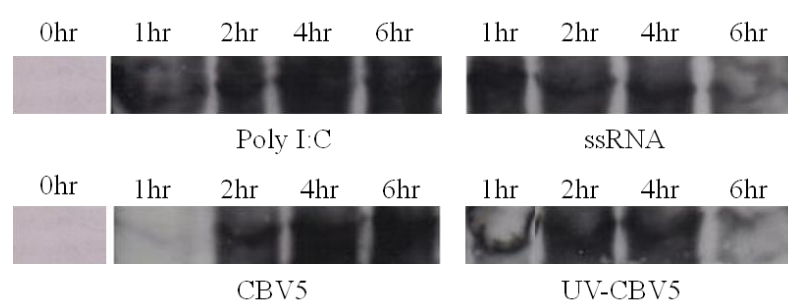


**Figure 3.3: Phospho-I $\kappa$ B detection.** Human cardiac cells were stimulated with Poly I:C, ssRNA, CBV5 virions, or UV-CBV5 for 1, 2, 4, or 6 hour time points (0 hr = unstimulated). Discontinuous SDS-PAGE followed by western blotting using Phospho-I $\kappa$ B Rabbit mAb and a Swine Anti-Rabbit Ig HRP was used to detect the presence of phospho-I $\kappa$ B. The bands were visualised using the ECL procedure. Representative of three independent experiments.

As well as NF- $\kappa$ B, IRF3 is another indicator of MDA5 and RIG-I activation. *Figure 3.4* shows IRF3 detection in human cardiac cells stimulated with Poly I:C, ssRNA, CBV5 virions, or UV-CBV5. IRF3 is being detected at all time points in response to Poly I:C, ssRNA, and UV-CBV5 stimulation. Again, CBV5 stimulation results in IRF3 being detected after 2 hours, with no IRF3 present after 1 hour.

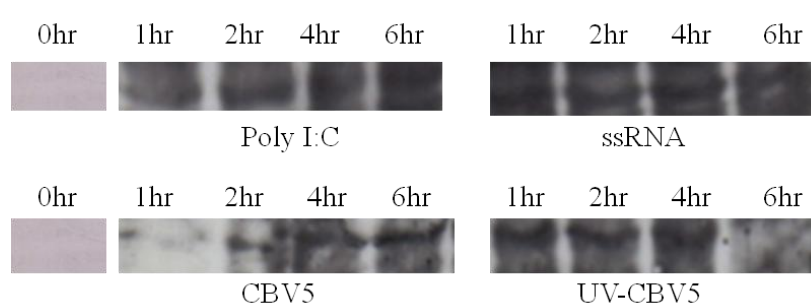


**Figure 3.4: IRF3 detection.** Human cardiac cells were stimulated with Poly I:C, ssRNA, CBV5 virions, or UV-CBV5 for 1, 2, 4, or 6 hour time points (0 hr = unstimulated). Discontinuous SDS-PAGE followed by western blotting using IRF3 Rabbit pAb and a Swine Anti-Rabbit Ig HRP was used to detect the presence of IRF3. The bands were visualised using the ECL procedure. Representative of three independent experiments.

### 3.2.3. IFN- $\beta$ Production

Using a flow cytometric flex set bead system (Becton Dickinson), the IFN- $\beta$  production in human cardiac cells stimulated with CBV5, ssRNA, or Poly I:C was measured, and can be seen in *Figure 3.5*. IFN- $\beta$  is a type I IFN, which signals through the IFN- $\alpha/\beta$  receptor and the Jak-STAT pathway to drive interferon stimulated gene (ISG) expression and an innate immune response (*Figure 1.17*). In response to CBV5 stimulation, compared to the basal unstimulated level, IFN- $\beta$  production is greatly upregulated after 2 hours (over 5 times greater; 300 pg/ml vs. 1600 pg/ml) and 4 hours (6 times greater; 300 pg/ml vs. 1800 pg/ml), but drops down slightly after 6 hours (only 2.5 times greater; 300 pg/ml vs 800 pg/ml). Stimulation with ssRNA and Poly I:C both had a similar, though much less pronounced, effect on IFN- $\beta$  production. In both cases, IFN- $\beta$  production was increased after 2 hours, and slowly drops down after 4 and 6 hours.

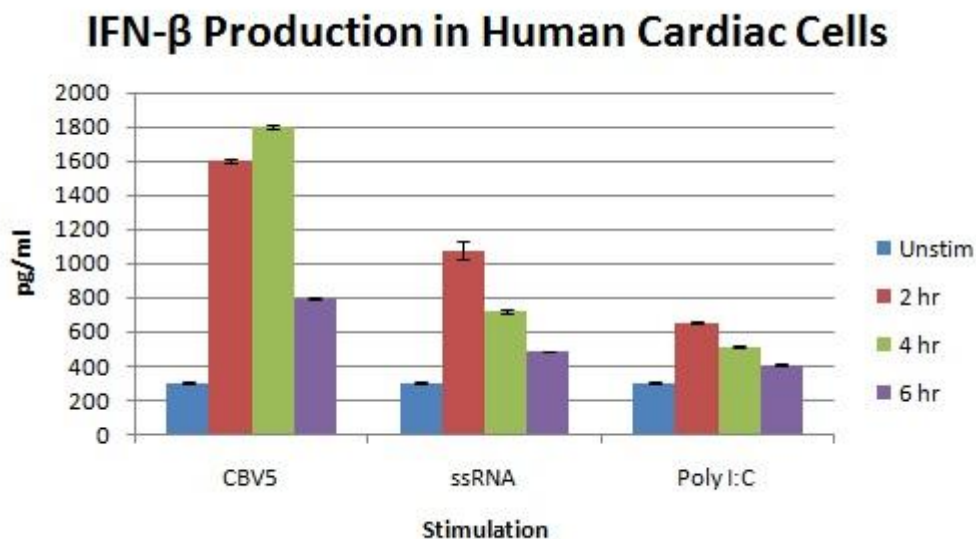


**Figure 3.5: IFN- $\beta$  production in human cardiac cells.** Confluent cardiac cells were stimulated with CBV5, ssRNA, or Poly I:C for 2, 4, or 6 hours, or left unstimulated, measured using a flow cytometric flex set bead system (Becton Dickinson). Data show means  $\pm$  SD and are representative of three independent experiments.

### 3.2.4 Silencing of RIG-I and MDA5

In order to verify the involvement of RIG-I and MDA5 in CBV5 innate immune recognition, RIG-I and MDA5 expression was knocked down using psiRNA-RIG-I and psiRNA-MDA5. Reduction in expression was confirmed using SDS-PAGE and western blotting. The role of CBV5 and its capability of activating an innate immune response in RIG-I or MDA5 silenced cardiac cells was investigated.

#### 3.2.4.1: psiRNA Purification

psiRNA-RIG-I and psiRNA-MDA5 were transformed into a competent *E.coli* strain (*E.coli* GT116), which was expanded and lysed. The plasmids were then purified from the lysate, concentrated and sterilised. To check the purity of the plasmid preparations, 10µl of the sample was run on a 1%<sub>w/v</sub> agarose gel at 100V for 45 minutes (*Figure 3.6*).

Agarose gel analysis of the purified plasmid samples revealed plasmids illustrating a very high level of purity.

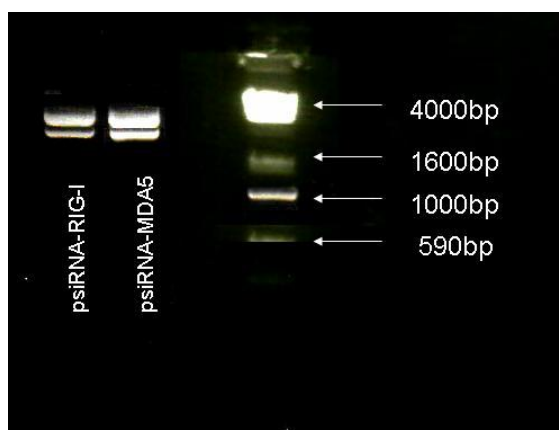


**Figure 3.6** Agarose gel of purified *psiRNA-RIG-I* and *psiRNA-MDA5*. The plasmids are approximately 3000bp. The positions of the 1kb DNA ladder fragments are indicated on the right. The plasmid sample was run on a 1%<sub>w/v</sub> agarose gel for 45 minutes at 100V. Bands were observed using a Stratagene eagle eye UV imaging system. Representative of two independent experiments.



### 3.2.4.2: RIG-I Silenced and MDA5 Silenced Cardiac Response to CBV5

Cellular expression of RIG-I or MDA5 was reduced by transfecting cardiac cells with psiRNA-RIG-I or psiRNA-MDA5. A 70% reduction in MDA5 expression and an 80% reduction in RIG-I expression was achieved (*Figure 3.7*). Controls using TLR7 were also performed, to show that psiRNA-MDA5 and psiRNA-RIG-I are specific and do not affect other genes. No TLR7 expression reduction was observed.

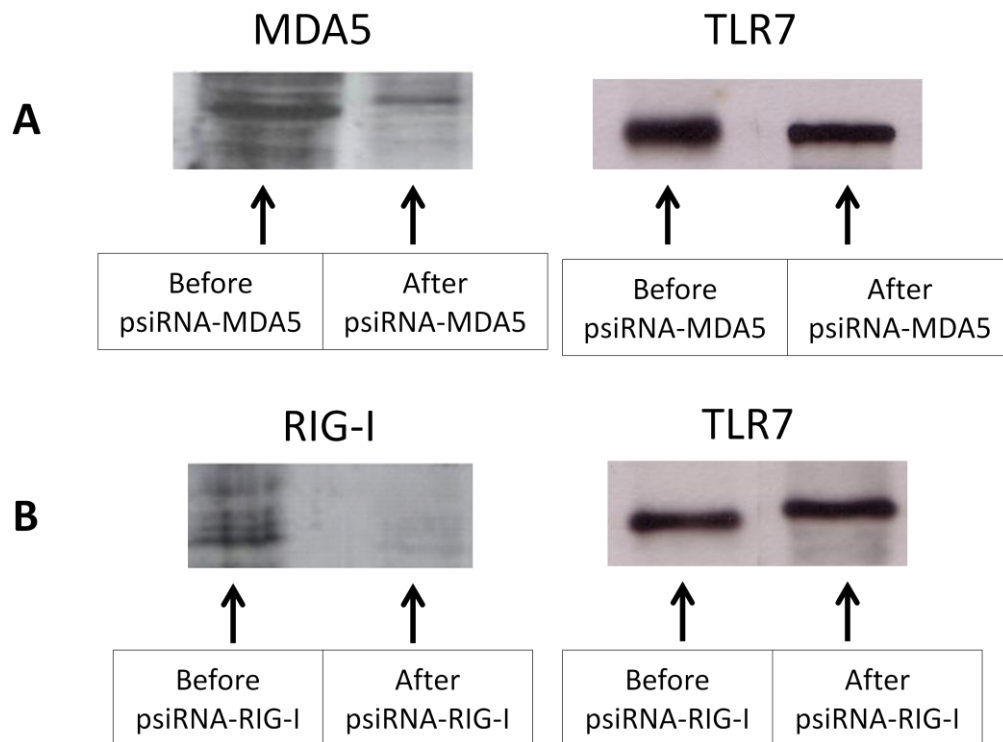


**Figure 3.7. RIG-I, MDA5, and TLR7 expression after use of psiRNA.** Lysates from cells transfected before and after with (A) psiRNA-MDA5 or (B) psiRNA-RIG-I were separated by SDS-PAGE and transferred onto a nitrocellulose membrane. The membrane was probed for MDA5, RIG-I, or TLR7 using specific primary antibodies followed by the appropriate secondary antibody conjugated to HRP and imaged via enhanced chemiluminescence. The gels were analysed via densitometry using Quantity One 1-D analysis software from Biorad to calculate area and pixel value. Representative of three independent experiments.

Silenced cells were stimulated with CBV5 for 2, 4, and 6 hour time points (0 hour = unstimulated). The cell supernatant was collected post-stimulation for IFN- $\beta$  analysis using the IFN- $\beta$  flex set bead system. The release of IFN- $\beta$  was significantly decreased in cardiac cells with reduced RIG-I expression (*Figure 3.8*), and even more decreased in cardiac cells with reduced MDA5 expression (*Figure 3.9*).

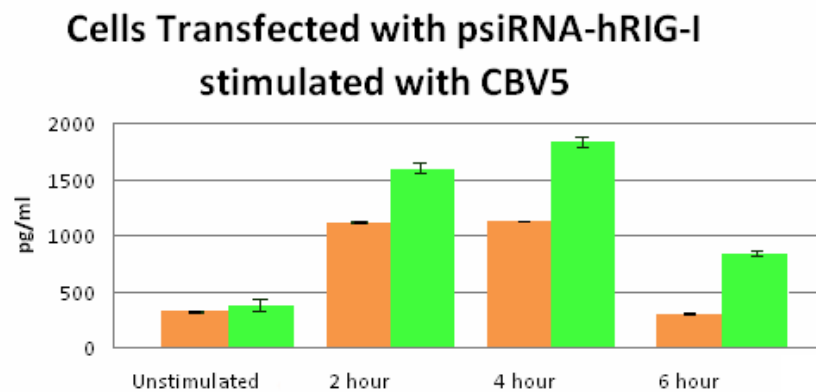


**Figure 3.8: IFN- $\beta$  expression in human cardiac cells.** IFN- $\beta$  release from untransfected cardiac cells (green) and RIG-I silenced cardiac cells (light brown) in response to CBV5 stimulation at different time points. The cell supernatant was used for IFN- $\beta$  detection using a flow cytometric IFN- $\beta$  flex set bead system (Becton Dickinson). Data show means  $\pm$  SD and are representative of three independent experiments.

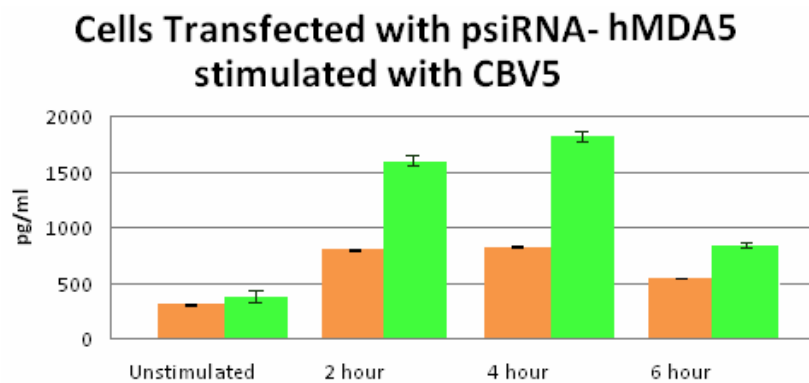


**Figure 3.9: IFN- $\beta$  expression in human cardiac cells.** IFN- $\beta$  release from untransfected cardiac cells (green) and MDA5 silenced cardiac cells (light brown) in response to CBV5 stimulation at different time points. The cell supernatant was used for IFN- $\beta$  detection using a flow cytometric IFN- $\beta$  flex set bead system (Becton Dickinson). Data show means  $\pm$  SD and are representative of three independent experiments.

### **3.3 Conclusion**

To determine RIG-I and MDA5 involvement in cardiac cells in response to CBV5 infection, the expression levels of both RLRs were measured, and phospho-I $\kappa$ B and IRF3 were detected, along with IFN- $\beta$  production. Both RIG-I and MDA5 expression levels increased within the first two hours of CBV5 infection, and dropped off slightly after 4 and 6 hours of infection. MDA5 expression was higher than RIG-I overall.

The initial strong response by both RLRs, however, shows that both are involved in CBV5 sensing. Since the genomic ssRNA by itself failed to upregulate MDA5 or RIG-I, this suggests that MDA5 and RIG-I sense the replicative intermediate dsRNA form that occurs during the viral replication cycle. The presence of phospho-I $\kappa$ B and IRF3 being detected in response to stimulation with ssRNA, as well as IFN- $\beta$  production, is perhaps due to ssRNA detection by TLR7 or TLR8, both of which could trigger activation and cytokine secretion.

CBV5 infection causes an intense cytokine secretion of IFN- $\beta$ , similar to that seen during CBV3 infection [Wang *et al.*, 2010; Hühn *et al.*, 2010]. In response to RIG-I and MDA5 being silenced in cardiac cells and stimulated with purified CBV5, there was a decrease in IFN- $\beta$  production in cells with silenced RIG-I, and a more significant reduction in IFN- $\beta$  production when MDA5 was silenced. This indicates that both RLRs play a role in CBV5 detection; however, MDA5 might be more involved in viral sensing.

Both RLRs have increasingly been shown to interact with the same virus, indicating that they are not solely responsible for the detection of one type of virus. For example, both RIG-I and MDA5 appear to respond to reoviruses, WNV, and Dengue virus [Fredericksen and Gale, 2006], as well as measles virus [Ikegame *et al.*, 2010]. Despite the fact that CBV5 is a picornavirus, RIG-I is still able to detect it. The VPg region at the 5' end of the picornaviral genome is critical for MDA5 detection [Gitlin *et al.*, 2006; Kato *et al.*, 2006; Pichlmair *et al.*, 2006], whereas RIG-I requires 5'pppRNA [Hornung *et al.*, 2006]. In this case, because CBV5 has a VPg 5' region rather than a 5'pppRNA, perhaps RIG-I is detecting a different part of the CBV5 RNA, or is being upregulated in a different manner.

RIG-I has been shown to be degraded in cells infected with a variety of picornaviruses [Barral *et al.*, 2009], and MDA5 is cleaved in poliovirus-infected cells [Barral *et al.*, 2007], although CBV5 does not appear to have this effect. RIG-I also appears to be associated with the cytoskeleton [Mukherjee *et al.*, 2009], and many viruses, including poliovirus and CBV3, cause massive reorganisation of the cytoskeleton. This alteration of the cytoskeleton could potentially act as a RIG-I-mediated sensor of infection [Coyne *et al.*, 2007, Ju *et al.*, 2007].

## **Chapter 4**

# **DETERMINING THE ROLE OF RIG-I AND MDA5 IN CBV5 SENSING USING HUH CELLS**

#### **4.1 Introduction**

RLRs were initially thought to recognise the same ligand, dsRNA, but it has since become apparent that RIG-I and MDA5 possess distinct virus specificities. It has been shown that they each recognise different viruses and different viral RNAs [Kato *et al.*, 2006; Loo *et al.*, 2008]. RIG-I recognises single-stranded RNA (ssRNA) containing a terminal 5'-triphosphate (ppp) [Pichlmair *et al.*, 2006], as well as linear dsRNA no longer than 23 nucleotides in length [Kato *et al.*, 2008]. MDA5 recognises long strands of dsRNA, but the mechanism by which this occurs is less clear [Kato *et al.*, 2008].

RIG-I recognises negative sense ssRNA viruses, including influenza virus, Newcastle disease virus, Sendai virus, and Hepatitis C virus, whilst positive sense ssRNA viruses, such as picornaviruses, and more specifically encephalomyocarditis virus and Coxsackievirus B3, have been shown to activate MDA5 [Kato *et al.*, 2006; Loo *et al.*, 2008; Wang *et al.*, 2010].

In order to determine the involvement of RIG-I in CBV5 recognition, Huh cells were used. The Huh (human hepatoma) cell lines are established from a hepatocellular carcinoma [Nakabayashi *et al.*, 1982]. They possess a highly useful property for studying RIG-I, namely that Huh 7.5.1 cells have an inactivating mutation in RIG-I, which leads to a defect in IFN production.

## 4.2 Results

### 4.2.1. Expression Levels in Huh 7.5 Cells

Huh 7.5 cells were stimulated with Poly I:C, CBV5 virions, UV-CBV5, or ssRNA, at 1, 2, 4, and 6 hour time points, or left unstimulated (0 hour). MDA5 expression was measured by indirect immunofluorescence (*Figure 4.1*). In all cases, MDA5 expression levels in these cells was low. Poly I:C, which is a known MDA5 agonist, had little effect upon MDA5 expression levels, and neither did CBV5 and ssRNA.

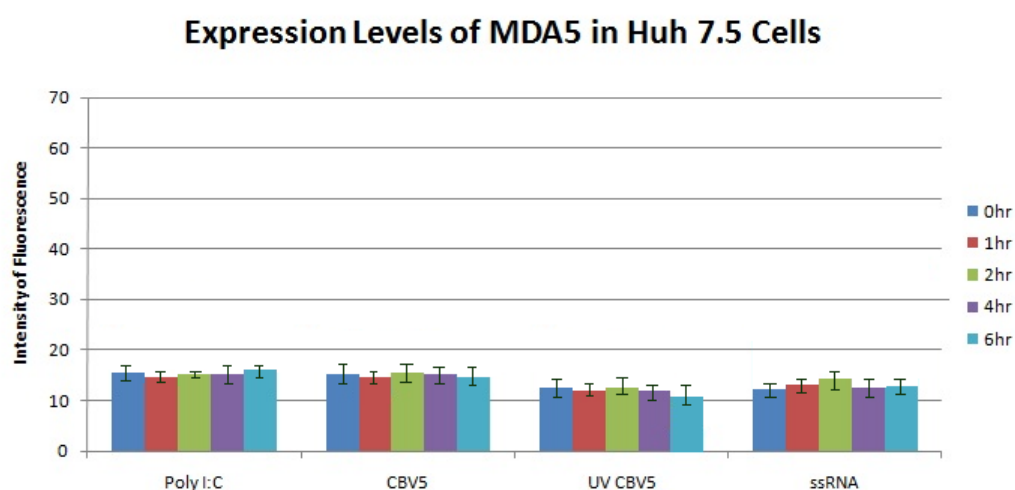


**Figure 4.1: MDA5 expression in Huh 7.5 cells.** Cells were stimulated with Poly I:C, CBV5 virions, UV-CBV5, or ssRNA, at 1, 2, 4, and 6 hour time points (0hr = unstimulated), measured by intensity of fluorescence. Confluent cells were stimulated, harvested, fixed and permeabilised, followed by incubation with MDA5 Goat pAb primary antibody and pAb Rabbit anti-Goat FITC secondary antibody. Fluorescence was detected using a FACSCalibur (Becton Dickinson) counting 5,000 cells not gated. Isotype controls were performed, with values similar to unstimulated samples. Data show means  $\pm$  SD and are representative of three independent experiments.

The expression levels of RIG-I in response to the same stimulations were also tested (Figure 4.2). Poly I:C, UV-CBV5, and ssRNA stimulation had little effect on RIG-I expression levels. However, CBV5 induced RIG-I expression at all time points, with the greatest response occurring after 2 hour.

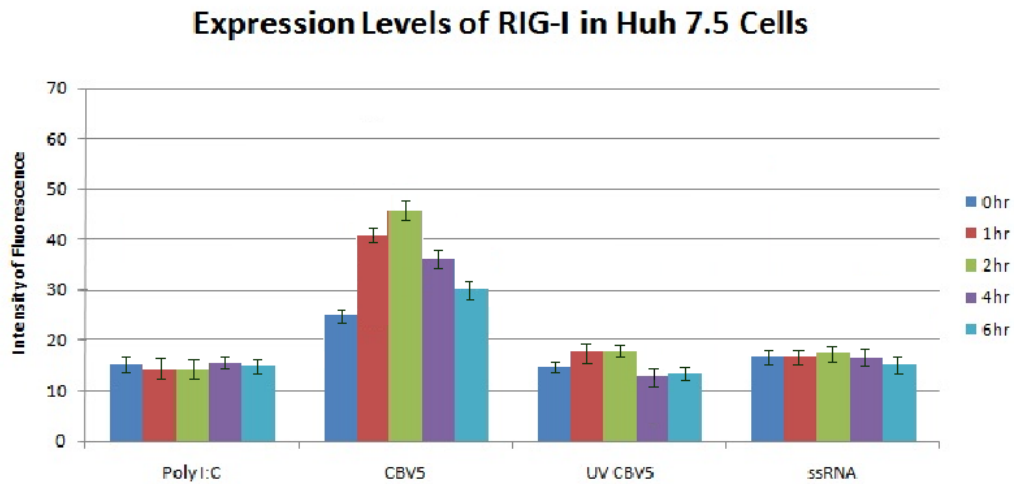


**Figure 4.2: RIG-I expression in Huh 7.5 cells.** Expression levels of RIG-I in Huh 7.5 cells stimulated with Poly I:C, CBV5 virions, UV-CBV5, or ssRNA, at 1, 2, 4, and 6 hour time points (0hr = unstimulated), measured by intensity of fluorescence. Confluent cells were stimulated, harvested, fixed and permeabilised, followed by incubation with RIG-I Goat pAb primary antibody and pAb Rabbit anti-Goat FITC secondary antibody. Fluorescence was detected using a FACSCalibur (Becton Dickinson) counting 5,000 cells not gated. Isotype controls were performed, with values similar to unstimulated samples. Data show means  $\pm$  SD and are representative of three independent experiments.



#### 4.2.2 Expression Levels in Huh 7.5.1 Cells

The Huh 7.5.1 cells have a RIG-I mutation that results in its inactivation. They were therefore used to investigate the importance of MDA5 and in particular RIG-I in CBV5 innate immune recognition. The expression levels of MDA5 in Huh 7.5.1 cells in response to Poly I:C, CBV5 virions, UV-CBV5, or ssRNA stimulation at 1, 2, 4, and 6 hour time points were measured by indirect immunofluorescence (*Figure 4.3*). There was a very low MDA5 expression in unstimulated cells, and there was no response to Poly I:C, CBV5, UV-CBV5, or ssRNA, indicating that the minimal expression of MDA5 was not sufficient to detect viral stimuli.

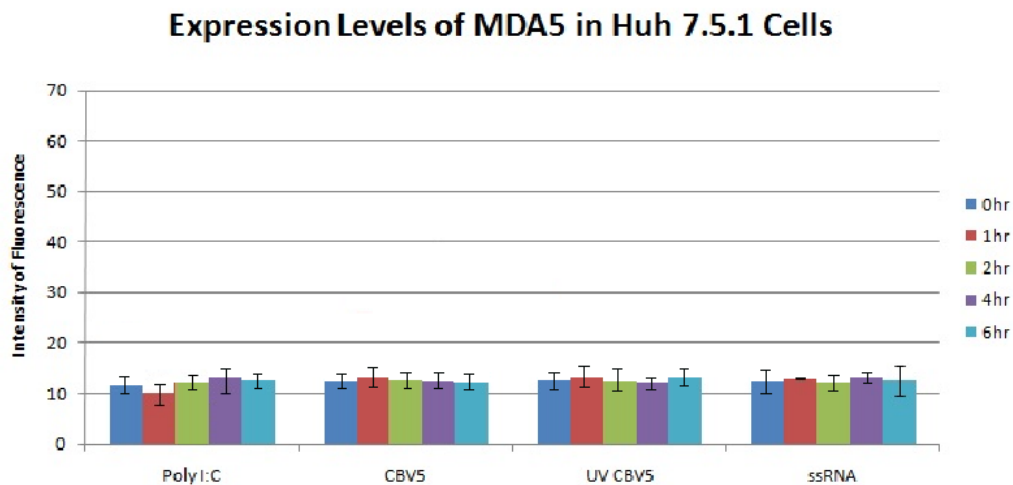


**Figure 4.3: Expression levels of MDA5 in Huh 7.5.1 cells.** Cells were stimulated with Poly I:C, CBV5 virions, UV-CBV5, or ssRNA, at 1, 2, 4, and 6 hour time points (0hr = unstimulated), measured by intensity of fluorescence. Confluent cells were stimulated, harvested, fixed and permeabilised, followed by incubation with MDA5 Goat pAb primary antibody and pAb Rabbit anti-Goat FITC secondary antibody. Fluorescence was detected using a FACSCalibur (Becton Dickinson) counting 5,000 cells not gated. Isotype controls were performed, with values similar to unstimulated samples. Data show means  $\pm$  SD and are representative of three independent experiments.

The expression levels of RIG-I in Huh 7.5.1 cells was minimal, as expected (Figure 4.4). The different stimulations with Poly I:C, CBV5, UV-CBV5 and ssRNA had little effect upon RIG-I expression, although there was a very slight response to CBV5.

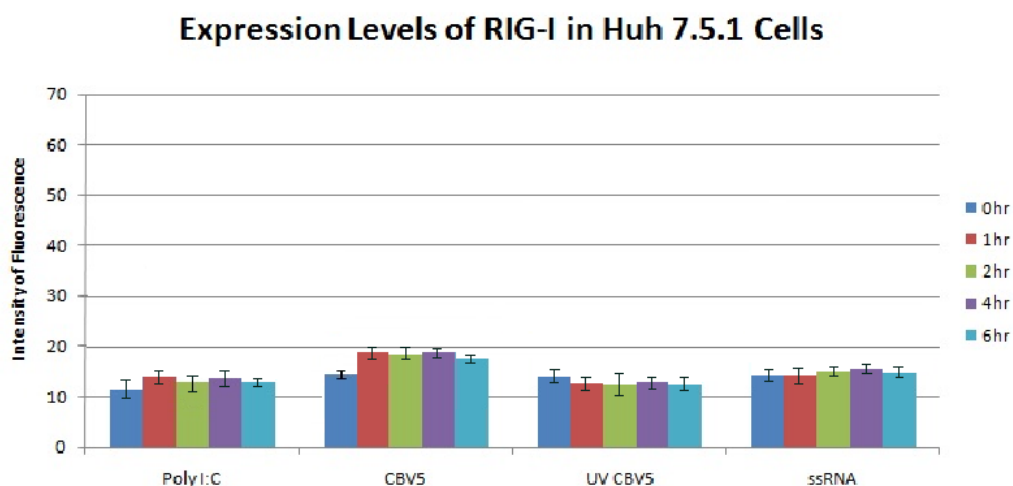


**Figure 4.4: Expression levels of RIG-I in Huh 7.5.1 cells.** Cells stimulated with Poly I:C, CBV5 virions, UV-CBV5, or ssRNA, at 1, 2, 4, and 6 hour time points (0hr = unstimulated), measured by intensity of fluorescence. Confluent cells were stimulated, harvested, fixed and permeabilised, followed by incubation with RIG-I Goat pAb primary antibody and pAb Rabbit anti-Goat FITC secondary antibody. Fluorescence was detected using a FACSCalibur (Becton Dickinson) counting 5,000 cells not gated. Isotype controls were performed, with values similar to unstimulated samples. Data show means  $\pm$  SD and are representative of three independent experiments.

### 4.2.3 Phospho-I $\kappa$ B and IRF3 Detection in Huh 7.5 Cells

Phospho-I $\kappa$ B detection corresponds with NF- $\kappa$ B activation, which, coupled with IRF3 detection, gives an indication of MDA5 and RIG-I activity in response to different stimulations. *Figure 4.5* shows phospho-I $\kappa$ B detection in Huh 7.5 cells stimulated with Poly I:C, ssRNA, CBV5 virions, or UV-CBV5 for 1, 2, 4, or 6 hour time points. In response to Poly I:C stimulation, phospho-I $\kappa$ B was detected after 1 hour, but from 2 hours onwards, very little phospho-I $\kappa$ B could be seen. ssRNA and UV-CBV5 both induced a similar response, with phospho-I $\kappa$ B being detected at all time points, but least so at 6 hours. CBV5 stimulation resulted in phospho-I $\kappa$ B being present at all time points, and most strongly after 6 hours.

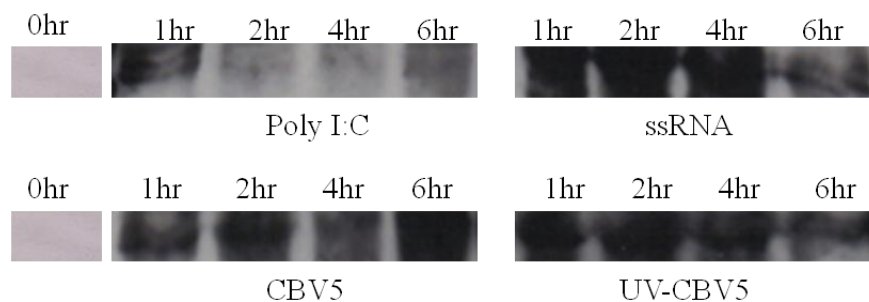


**Figure 4.5: Phospho-I $\kappa$ B detection in Huh 7.5 cells.** Huh 7.5 cells were stimulated with Poly I:C, ssRNA, CBV5 virions, or UV-CBV5 for 1, 2, 4, or 6 hour time points (0 hr = unstimulated). Discontinuous SDS-PAGE followed by western blotting using Phospho-I $\kappa$ B Rabbit mAb and a Swine Anti-Rabbit Ig HRP secondary antibody was used to detect the presence of phospho-I $\kappa$ B. The bands were visualised using the ECL procedure. Representative of three independent experiments.

IRF3 detection in Huh 7.5 cells in response to the four stimulations can be seen in *Figure 4.6*. Overall, the extent of IRF3 detection was fairly minor. Similar to phospho-I $\kappa$ B detection, Poly I:C stimulation resulted in IRF3 being detected most strongly after 1 hour, but dropping off after that. CBV5 stimulation resulted in no IRF3 being present after 1 hour, with a gradual, though minimal increase in detection after 2, 4, and 6 hours. ssRNA stimulation resulted in minor IRF3 detection, with the strongest presence occurring at 2 hours. Stimulation with UV-CBV5 caused IRF3 to be detected over the first 4 hours, but no IRF3 present after 6 hours.

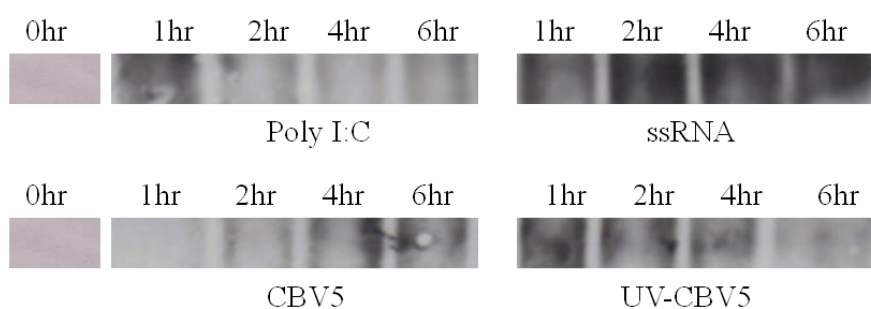


**Figure 4.6: IRF3 detection in Huh 7.5 cells.** Huh 7.5 cells were stimulated with Poly I:C, ssRNA, CBV5 virions, or UV-CBV5 for 1, 2, 4, or 6 hour time points (0 hr = unstimulated). Discontinuous SDS-PAGE followed by western blotting using IRF3 Rabbit pAb and a Swine Anti-Rabbit Ig HRP secondary antibody was used to detect the presence of IRF3. The bands were visualised using the ECL procedure. Representative of three independent experiments.

#### 4.2.4 Phospho-I $\kappa$ B and IRF3 Detection in Huh 7.5.1 Cells

To determine whether stimulations with CBV5, ssRNA, UV-CBV5 and Poly I:C can lead to an NF- $\kappa$ B-driven transcription response, or IRF3 activation, Huh 7.5.1 cells were subject to stimulation for 1, 2, 4, and 6 hours, and the presence of phospho-I $\kappa$ B (Figure 4.7) or IRF3 (Figure 4.8) was investigated.

In Figure 4.7, Poly I:C stimulation induced the greatest response, with phospho-I $\kappa$ B present at all time points. Similarly, ssRNA stimulation resulted in phospho-I $\kappa$ B being detected at all time points. Stimulation with CBV5 again resulted in phospho-I $\kappa$ B being detected at all time points. Phospho-I $\kappa$ B was detected at low levels at 1, 2, and 4 hour time points in response to UV-CBV5 stimulation, and very low levels after 6 hours.

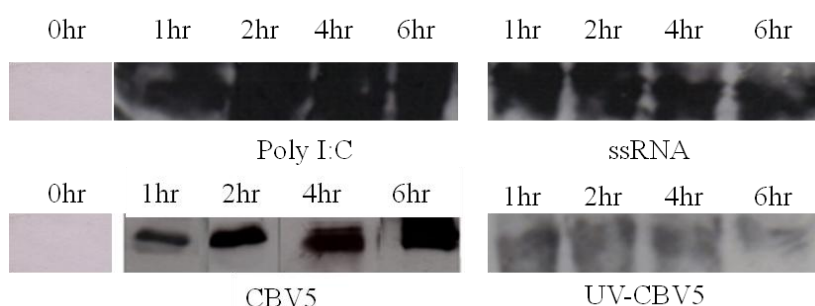


**Figure 4.7: Phospho-I $\kappa$ B detection in Huh 7.5.1 cells.** Huh 7.5.1 cells were stimulated with Poly I:C, ssRNA, CBV5 virions, or UV-CBV5 for 1, 2, 4, or 6 hour time points (0 hr = unstimulated). Discontinuous SDS-PAGE followed by western blotting using Phospho-I $\kappa$ B Rabbit mAb and a Swine Anti-Rabbit Ig HRP secondary antibody was used to detect the presence of phospho-I $\kappa$ B. The bands were visualised using the ECL procedure. Representative of three independent experiments.

Figure 4.8 shows IRF3 detection in Huh 7.5.1 cells stimulated with the four different stimulations. IRF3 is detected at all time points in response to Poly I:C, and ssRNA. There is a minimal detection of IRF3 upon UV-CBV5 stimulation. However, stimulation with CBV5 results in IRF3 being detected at the 2 and 4 hour time points, with no IRF3 present after 1 hour. The amount of IRF3 present decreases at the 6 hour time point, but is still detectable.

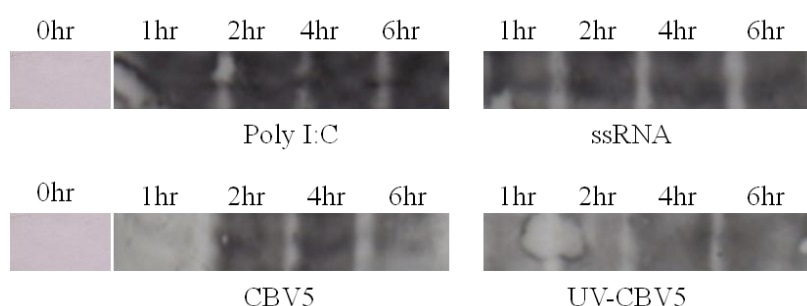


**Figure 4.8: IRF3 detection in Huh 7.5.1 cells.** Huh 7.5.1 cells were stimulated with Poly I:C, ssRNA, CBV5 virions, or UV-CBV5 for 1, 2, 4, or 6 hour time points (0 hr = unstimulated). Discontinuous SDS-PAGE followed by western blotting using IRF3 Rabbit pAb and a Swine Anti-Rabbit Ig HRP secondary antibody was used to detect the presence of IRF3. The bands were visualised using the ECL procedure. Representative of three independent experiments.

#### **4.2.5 IFN- $\beta$ Production**

IFN- $\beta$  production in Huh 7.5 and Huh 7.5.1 cells stimulated with CBV5 was measured using a flow cytometric flex set bead system (Becton Dickinson), and can be seen in *Figure 4.9* and *Figure 4.10*, respectively. IFN- $\beta$  production is greater in Huh 7.5 cells than in Huh 7.5.1 cells, which is to be expected, as Huh 7.5.1 cells have an inactivating mutation in RIG-I leading to a defect in IFN production. In both cases, the greatest response can be seen after 2 and 4 hours of stimulation with CBV5. At the 2 hour time point, Huh 7.5.1 cells have a near 70% reduction in IFN- $\beta$  production compared to Huh 7.5 cells (1022 pg/ml vs. 1721 pg/ml). After 4 hours, IFN- $\beta$  production in Huh 7.5 cells is still over 50% greater than that seen in Huh 7.5.1 cells (1884 pg/ml compared to 1212 pg/ml). IFN- $\beta$  production in Huh 7.5 cells after 6 hours of stimulation with CBV5 is less than half that seen at the 4 hour time point (903 pg/ml compared to 1884 pg/ml), but still over 25% greater than IFN- $\beta$  production seen in Huh 7.5.1 cells (714 pg/ml).

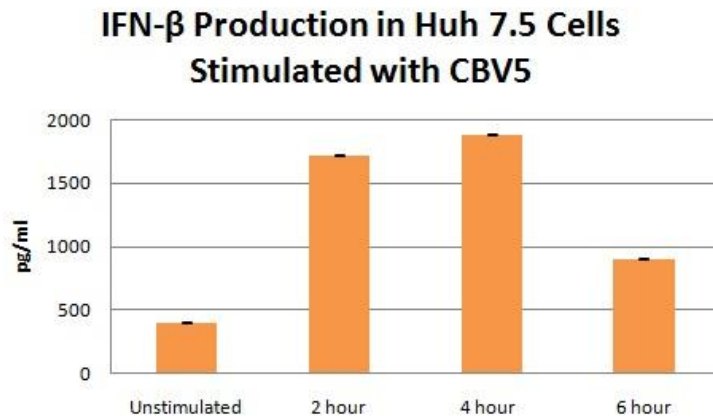


**Figure 4.9: IFN- $\beta$  production in Huh 7.5 cells.** Confluent cells were stimulated with CBV5 for 2, 4, or 6 hours, or left unstimulated. IFN- $\beta$  was measured in the cell supernatant using a flow cytometric flex set bead system (Becton Dickinson). Data show means  $\pm$  SD and are representative of three independent experiments.

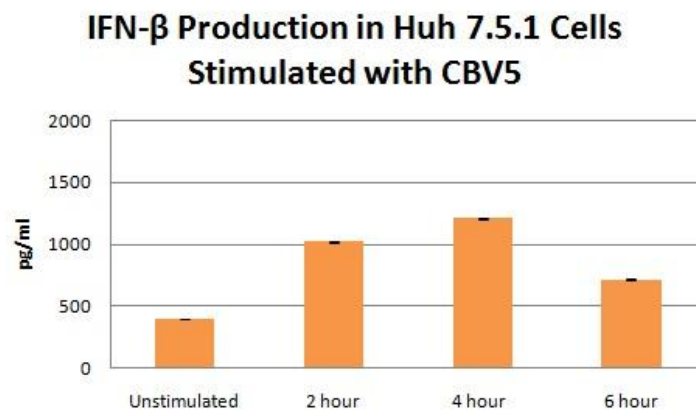


**Figure 4.10: IFN- $\beta$  production in Huh 7.5.1 cells.** Confluent cells were stimulated with CBV5 for 2, 4, or 6 hours, or left unstimulated. IFN- $\beta$  was measured in the cell supernatant using a flow cytometric flex set bead system (Becton Dickinson). Data show means  $\pm$  SD and are representative of three independent experiments.



### **4.3 Conclusion**

The IFN- $\beta$  production in Huh 7.5 cells and Huh 7.5.1 cells are the most significant results here. Huh 7.5.1 cells have an inactivating mutation in RIG-I that leads to a defect in IFN production. As less IFN- $\beta$  production is seen in Huh 7.5.1 cells, this indicates that RIG-I plays a role in CBV5 detection. If detection was performed solely by MDA5, it would be expected that IFN- $\beta$  production in both Huh 7.5 cells and Huh 7.5.1 cells would remain the same, as the RIG-I mutation would have no effect, due to RIG-I not being involved. Because a decrease in IFN- $\beta$  production is detected, RIG-I plays a role alongside MDA5 in sensing CBV5.

In Huh 7.5 cells and Huh 7.5.1 cells, the expression levels of RIG-I become greater than those of MDA5 in response to CBV5 stimulations, again suggesting that RIG-I plays an important role in CBV5 sensing.

Huh cells have been used in a variety of experiments to determine the role of RIG-I during infection. It has been shown that HSV-1 and adenovirus DNA induce IFN- $\beta$  mRNA production when they are transfected into Huh 7 but not Huh 7.5.1 cells [Cheng *et al.*, 2007], that RIG-I and MDA5 synergistically mediate an antiviral response to Dengue virus [Nasirudeen *et al.*, 2011], and that RIG-I is essential for HCV detection in Huh 7 cells [Sumpter *et al.*, 2005]. A meta-analysis of Huh cells has also been performed to reveal factors that influence susceptibility to HCV infection [MacPherson *et al.*, 2011]. These all show the importance of Huh cells in the research of viruses.

**Chapter 5**  
**RLR DIMERISATION**

## **5.1 Introduction**

The RLR family, consisting of the three known family members RIG-I, MDA5, and LGP2, are pattern recognition receptors which detect a range of different viruses. RIG-I (retinoic acid inducible gene-I) and MDA5 (melanoma differentiation-associated gene 5) are homologous cytoplasmic proteins containing an N-terminal region with two caspase activation and recruitment domains (CARDs), a central SF2 type DExD/H-box RNA helicase domain, and a C-terminal repressor domain (RD) [Takeuchi and Akira, 2007]. LGP2 (laboratory of genetics and physiology 2) harbours a DExD/H-box RNA helicase domain and a C-terminal RD, but lacks any CARDs [Yoneyama *et al.*, 2005].

Once a viral ligand has been detected and bound by RIG-I and MDA5, both signal downstream through their CARDs to activate IRF3/7 and NF- $\kappa$ B indirectly, via the protein intermediate IPS-1 (IFN- $\beta$  promoter stimulator 1) [Kawai *et al.*, 2005]. After interaction with RIG-I and MDA5, IPS-1 goes on to recruit and activate a variety of other proteins, including TRAF2, TRAF3, and TRAF6 [Xu *et al.*, 2005; Oganessian *et al.*, 2006; Saha *et al.*, 2006]. These TRAF proteins then signal further downstream to the I $\kappa$ B kinase (IKK) family members, to activate the transcription factors IRF3/7 and NF- $\kappa$ B, and initiate an immune response.

RIG-I, MDA5, and LGP2 have been proposed to homo- and heterodimerise upon viral ligand detection. This process involves the C-terminal RD, which is important for controlling RLR-mediated IFN responses. RIG-I has two states; an inactive (closed) one and an active (open) one. In the inactive state, the CARDs and the helicase domain are repressed by RD. Once a viral ligand binds to the RD,

a conformational change occurs, converting RIG-I to the active state. This results in the dimerisation of RIG-I and the initiation of downstream signalling via the CARDs. Without the RD, RIG-I constitutively activates downstream signalling, whilst overexpression of the RD inhibits the antiviral response [Cui *et al.*, 2008]. The proposed model for 5'-triphosphate single-stranded RNA activation of RIG-I by ligand-induced dimer formation of RD can be seen in *Figure 1.15*.

Dimerisation of the RLRs is essential for them to function correctly. LGP2 has been suggested as a negative regulator of the RIG-I- and MDA5-mediated antiviral response, as its overexpression inhibits virus-induced IRF3 and NF- $\kappa$ B activation [Rothenfusser *et al.*, 2005; Saito *et al.*, 2007; Komuro and Horvath, 2006]. LGP2 has been proven to be a regulator for RIG-I- and MDA5-dependent signalling via its RD. Although it was previously thought that LGP2 inhibits dimerisation of RIG-I and its interaction with IPS-1, it has now been shown that LGP2 augments MDA5-dependent signalling [Pippig, *et al.*, 2009].

## **5.2 Results**

To test whether RIG-I, MDA5, and LGP2 homo- or heterodimerise together, immunoprecipitation experiments were performed. Immunoprecipitation is a technique used to precipitate a protein out of a lysate using an antibody specific for that protein coupled with beads specific for the antibody. The technique can be used to isolate and concentrate a particular protein, as well as determine if dimerisation between two proteins has occurred. In this project, RIG-I, MDA5, or LGP2 antibodies were used to precipitate out their respective protein, and SDS-PAGE was then used to detect a different protein, i.e. precipitate out MDA5 and perform SDS-PAGE to detect LGP2.

Cardiac cells were stimulated with CBV5 for 1, 2, 4, and 6 hours, or left unstimulated (0 hour). At each time point, the cells were washed, lysis buffer was added for over 2 hours, followed by centrifugation and transferral of the supernatant to new Eppendorfs. The cell lysate was then pre-cleared twice in Protein A Sepharose (PAS) beads, to prevent non-specific binding of the antibody to unwanted proteins, followed by incubation with primary antibody and more PAS beads. PAS beads have a high affinity for the Fc region of antibodies, so once the antibodies have bound their specific protein, they in turn bind to PAS. After washing the resulting pellet in lysis buffer, the samples were analysed using SDS-PAGE and western blotting, using X2 SDS-PAGE Non-Reducing Sample Buffer.

### 5.2.1 MDA5 Homodimerisation

Cardiac cells were stimulated with CBV5 for 1, 2, 4, or 6 hours, or left unstimulated, and an MDA5 Goat pAb was used to precipitate MDA5 out of the cell lysate. The western blot results after incubating with MDA5 Rabbit pAb and detecting using polyclonal Swine anti-Rabbit Ig HRP are shown in *Figure 5.1*. The MDA5 immunoprecipitation indicates that MDA5 is present as a dimer at all time points after stimulation with CBV5, signified by the thick bands at approximately 200 kDa. The amount of MDA5 present decreases slightly after 6 hours, shown by the less intense band. A few MDA5 monomers can also be seen at the approximate 110 kDa mark. A boiled control using X2 SDS-PAGE Reducing Sample Buffer was performed to illustrate that reducing conditions disrupt protein structure.

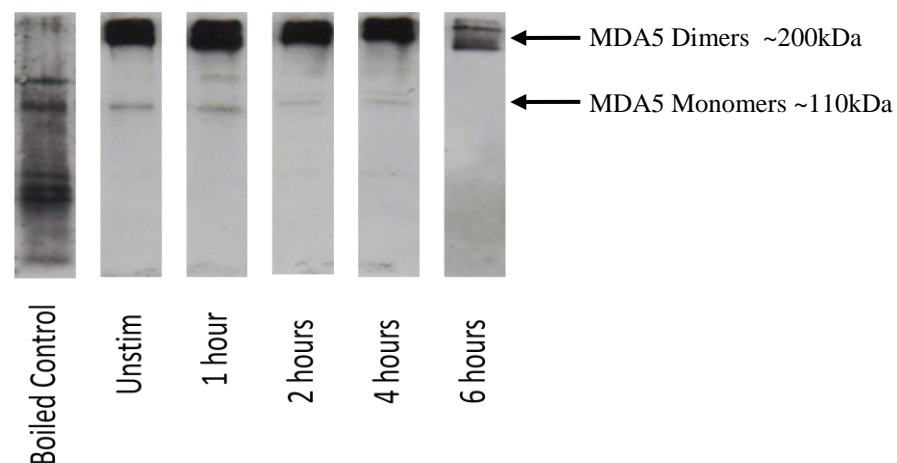


**Figure 5.1: Homodimerisation of MDA5.** MDA5 homodimers and MDA5 monomers can be seen at all time points. Cardiac cells were stimulated with CBV5 for 1, 2, 4, or 6 hours, or left unstimulated, and the cell lysate was pre-cleared twice with PAS beads. Incubation with MDA5 Goat pAb and PAS beads followed, to precipitate MDA5 out of the lysate. The resulting pellets were washed in lysis buffer and analysed using SDS-PAGE (using X2 SDS-PAGE Non-Reducing Sample Buffer) and western blotting with MDA5 Rabbit pAb primary antibody followed by polyclonal Swine anti-Rabbit Ig HRP. A boiled control using X2 SDS-PAGE Reducing Sample Buffer was also performed. Enhanced chemiluminescence was used to visualise the protein bands. kDa: kiloDalton. Representative of three independent experiments.

### 5.2.2 RIG-I Homodimerisation

Cardiac cells were stimulated with CBV5 for 1, 2, 4, or 6 hours, or left unstimulated, and a RIG-I Goat pAb was used to precipitate RIG-I out of the cell lysate. The western blot results after incubating with RIG-I Rabbit pAb and detecting using polyclonal Swine anti-Rabbit Ig HRP are shown in *Figure 5.2*. Similar to that seen by MDA5 in *Figure 5.1*, homodimerisation of RIG-I appears to occur at all time points after stimulation with CBV5. RIG-I even appears to be a dimer in unstimulated cells, which is not consistent with a study performed by Cui *et al.*, 2008. A few RIG-I monomers can also be seen. A boiled control using X2 SDS-PAGE Reducing Sample Buffer was performed to illustrate that reducing conditions disrupt protein structure.

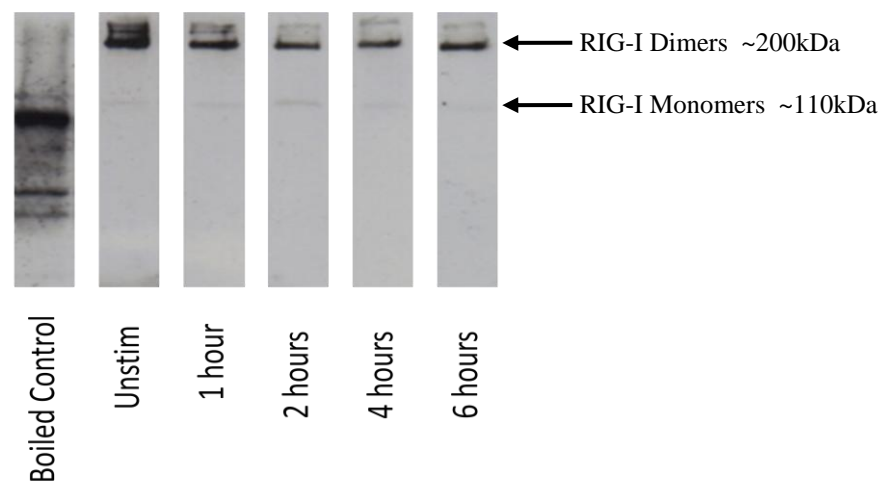


**Figure 5.2: Homodimerisation of RIG-I.** RIG-I dimers and a few RIG-I monomers can be seen at all time points. Cardiac cells were stimulated with CBV5 for 1, 2, 4, or 6 hours, or left unstimulated, and the cell lysate was pre-cleared twice with PAS beads. Incubation with RIG-I Goat pAb and PAS beads followed, to precipitate RIG-I out of the lysate. The resulting pellets were washed in lysis buffer and analysed using SDS-PAGE (using X2 SDS-PAGE Non-Reducing Sample Buffer) and western blotting with RIG-I Rabbit pAb primary antibody followed by polyclonal Swine anti-Rabbit Ig HRP. A boiled control using X2 SDS-PAGE Reducing Sample Buffer was also performed. Enhanced chemiluminescence was used to visualise the protein bands. kDa: kiloDalton. Representative of three independent experiments.

### 5.2.3 LGP2 Monomers

Cardiac cells were stimulated with CBV5 for 1, 2, 4, or 6 hours, or left unstimulated, and a LGP2 Goat pAb was used to precipitate LGP2 out of the cell lysate. The western blot results after incubating with LGP2 Rabbit pAb and detecting using polyclonal Swine anti-Rabbit Ig HRP can be seen in *Figure 5.3*. At each time point, monomers of LGP2 are detected, indicated by the thick band located around the 60 kDa mark. A boiled control using X2 SDS-PAGE Reducing Sample Buffer was performed to illustrate that reducing conditions disrupt protein structure.

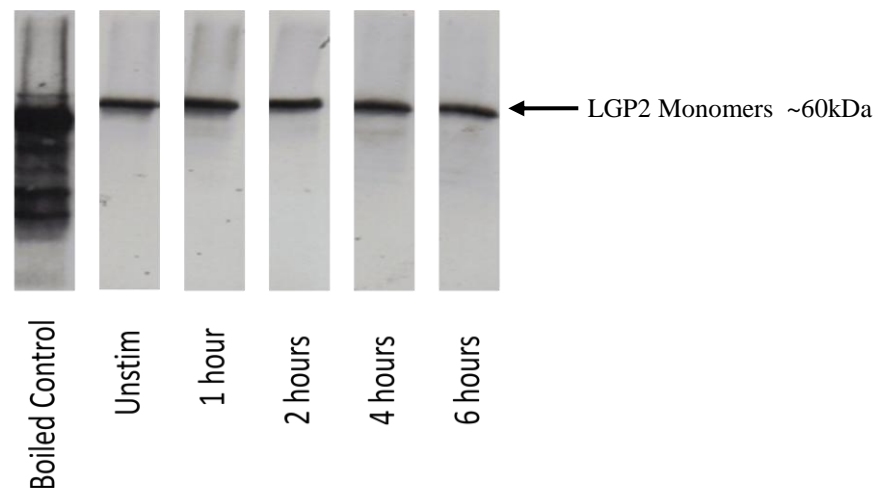


**Figure 5.3: Monomers of LGP2.** LGP2 monomers can be seen at all time points. Cardiac cells were stimulated with CBV5 for 1, 2, 4, or 6 hours, or left unstimulated, and the cell lysate was pre-cleared twice with PAS beads. Incubation with LGP2 Goat pAb and PAS beads followed, to precipitate LGP2 out of the lysate. The resulting pellets were washed in lysis buffer and analysed using SDS-PAGE (using X2 SDS-PAGE Non-Reducing Sample Buffer) and western blotting with LGP2 Rabbit pAb primary antibody followed by polyclonal Swine anti-Rabbit Ig HRP. A boiled control using X2 SDS-PAGE Reducing Sample Buffer was also performed. Enhanced chemiluminescence was used to visualise the protein bands. kDa: kiloDalton. Representative of three independent experiments.



#### 5.2.4 MDA5 – LGP2

MDA5 Goat pAb was used to precipitate MDA5 out of the cell lysate, then western blotting was performed using a LGP2 Rabbit pAb followed by a polyclonal Swine anti-Rabbit Ig HRP (*Figure 5.4*). Very faint bands can be seen, possibly suggesting the presence of a small amount of LGP2. From this blot, it appears that LGP2 does not dimerise with MDA5 upon CBV5 stimulation.

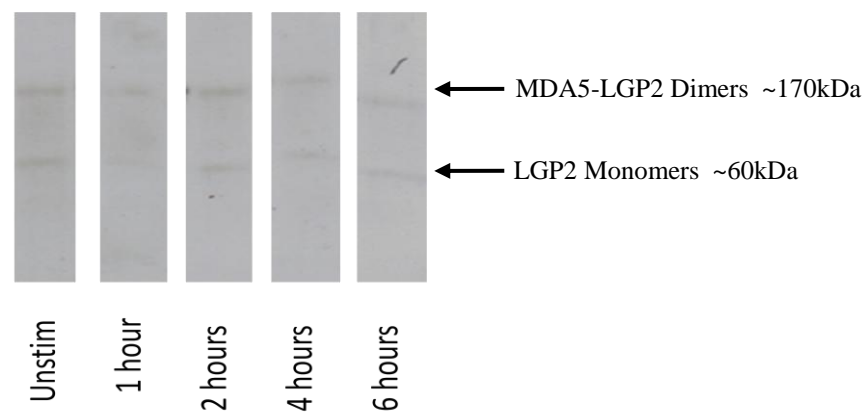


**Figure 5.4: Association between MDA5 and LGP2.** Minor MDA5-LGP2 dimerisation occurs, and a few LGP2 monomers can be seen. Cardiac cells were stimulated with CBV5 for 1, 2, 4, or 6 hours, or left unstimulated, and the cell lysate was pre-cleared twice with PAS beads. Incubation with MDA5 Goat pAb and PAS beads followed, to precipitate MDA5 out of the lysate. The resulting pellets were washed in lysis buffer and analysed using SDS-PAGE (using X2 SDS-PAGE Non-Reducing Sample Buffer) and western blotting with LGP2 Rabbit pAb primary antibody followed by polyclonal Swine anti-Rabbit Ig HRP. Enhanced chemiluminescence was used to visualise the protein bands. kDa: kiloDalton. Representative of three independent experiments.

### 5.2.5 LGP2 – MDA5

The association between LGP2 and MDA5 can be seen in *Figure 5.5*. LGP2 Goat pAb was used to precipitate LGP2 out of the cell lysate, then western blotting was performed using a MDA5 Rabbit pAb followed by a polyclonal Swine anti-Rabbit Ig HRP. Heterodimerisation between LGP2 and MDA5 appears to occur at all time points, indicated by the bands appearing near the 170 kDa mark. The bands around the 110 kDa mark imply that MDA5 monomers are also present. It seems that only a percentage of LGP2 is required to associate with MDA5, as MDA5 appears much more prevalently as a monomer. Treatment with SDS could have disrupted the bond between LGP2 and MDA5, thereby allowing the detection of MDA5 monomers.

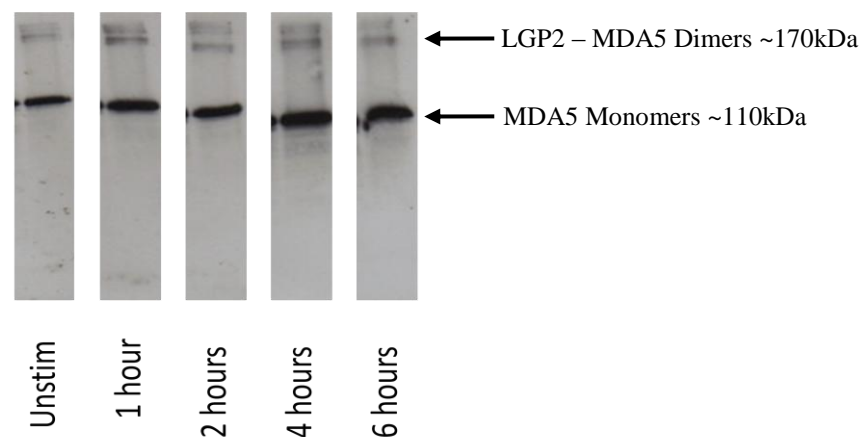


**Figure 5.5: Association between LGP2 and MDA5.** MDA5 monomers can be seen at all time points, as can LGP2 – MDA5 heterodimers. Cardiac cells were stimulated with CBV5 for 1, 2, 4, or 6 hours, or left unstimulated, and the cell lysate was pre-cleared twice with PAS beads. Incubation with LGP2 Goat pAb and PAS beads followed, to precipitate LGP2 out of the lysate. The resulting pellets were washed in lysis buffer and analysed using SDS-PAGE (using X2 SDS-PAGE Non-Reducing Sample Buffer) and western blotting with MDA5 Rabbit pAb primary antibody followed by polyclonal Swine anti-Rabbit Ig HRP. Enhanced chemiluminescence was used to visualise the protein bands. kDa: kiloDalton. Representative of three independent experiments.

### 5.2.6 RIG-I – LGP2

RIG-I Goat pAb was used to precipitate RIG-I out of the cell lysate, then western blotting was performed using a LGP2 Rabbit pAb followed by a polyclonal Swine anti-Rabbit Ig HRP to determine the presence of LGP2 (*Figure 5.6*). Bands were located around the 60 kDa mark, suggesting that monomers of LGP2 were present, and thereby verifying that LGP2 does not heterodimerise with RIG-I. The SDS treatment could have broken the bond between RIG-I and LGP2, resulting in only LGP2 monomers being seen.

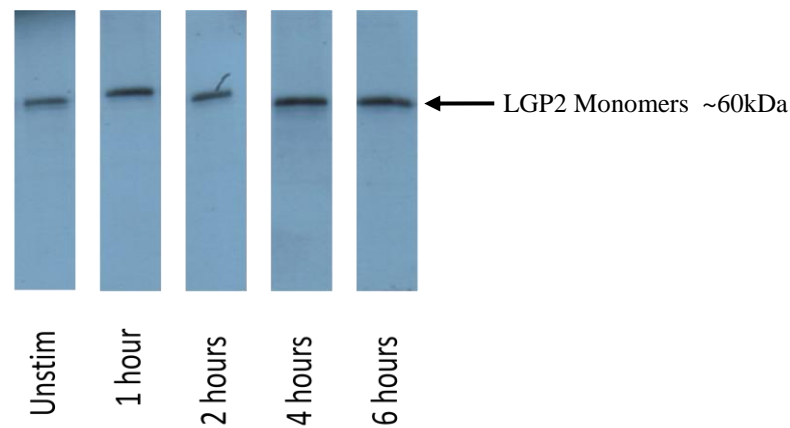


**Figure 5.6: Association between RIG-I and LGP2.** LGP2 monomers can be seen at all time points. Cardiac cells were stimulated with CBV5 for 1, 2, 4, or 6 hours, or left unstimulated, and the cell lysate was pre-cleared twice with PAS beads. Incubation with RIG-I Goat pAb and PAS beads followed, to precipitate RIG-I out of the lysate. The resulting pellets were washed in lysis buffer and analysed using SDS-PAGE (using X2 SDS-PAGE Non-Reducing Sample Buffer) and western blotting with LGP2 Rabbit pAb primary antibody followed by polyclonal Swine anti-Rabbit Ig HRP. Enhanced chemiluminescence was used to visualise the protein bands. kDa: kiloDalton. Representative of three independent experiments.

### 5.2.7 LGP2 – RIG-I

The association between LGP2 and RIG-I can be seen in *Figure 5.7*. LGP2 Goat pAb was used to precipitate LGP2 out of the cell lysate, then western blotting was performed using a RIG-I Rabbit pAb followed by a polyclonal Swine anti-Rabbit Ig HRP. Similar to *Figure 5.5*, heterodimerisation between LGP2 and RIG-I can be seen at all time points, indicated by the top bands near the 170 kDa mark. Monomers of RIG-I can also be seen, as indicated by the bands around the 110 kDa mark, which could be caused by the treatment with SDS, disrupting the LGP2 – RIG-I dimers.

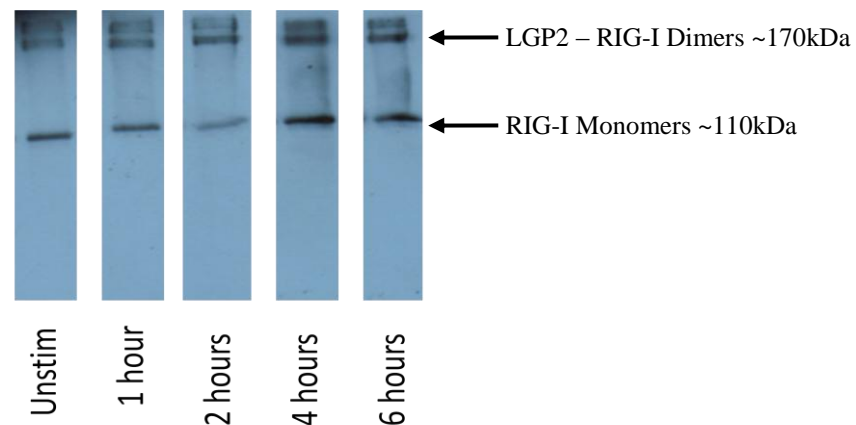


**Figure 5.7: Association between LGP2 and RIG-I.** RIG-I monomers can be seen at all time points, as can LGP2 – RIG-I heterodimers. Cardiac cells were stimulated with CBV5 for 1, 2, 4, or 6 hours, or left unstimulated, and the cell lysate was pre-cleared twice with PAS beads. Incubation with LGP2 Goat pAb and PAS beads followed, to precipitate LGP2 out of the lysate. The resulting pellets were washed in lysis buffer and analysed using SDS-PAGE (using X2 SDS-PAGE Non-Reducing Sample Buffer) and western blotting with RIG-I Rabbit pAb primary antibody followed by polyclonal Swine anti-Rabbit Ig HRP. Enhanced chemiluminescence was used to visualise the protein bands. kDa: kiloDalton. Representative of three independent experiments.

### **5.3 Conclusion**

The function and mechanism of LGP2 in innate immunity is still puzzling. So far, it is known that the LGP2 RD can regulate RIG-I- and MDA5-dependent signalling. This study aimed to determine whether the RLRs dimerise. It can be seen that RIG-I and MDA5 exist primarily as homodimers, but also as monomers, in cardiac cells, whilst LGP2 exists as a monomer. RIG-I and MDA5 can also heterodimerise with a percentage of LGP2.

The perplexing question is that although heterodimers between LGP2 and RIG-I or MDA5 are present in the LGP2 immunoprecipitations, in the MDA5 or RIG-I immunoprecipitations, LGP2 presence is only detected as a monomer. These results could be due to the higher affinity of the LGP2 RD with the other RLRs, enabling it to bind and precipitate RIG-I or MDA5, whereas MDA5 or RIG-I have a lower affinity, and may therefore not be able to bind a detectable percentage of higher LGP2 aggregates.

Overall, this study concludes that LGP2 and RIG-I or MDA5 associate in cardiac cells, and that there is a synergistic mechanism of RLR association for viral detection. Whether LGP2 is acting as a positive or negative regulator of RIG-I and MDA5 in response to CBV5 infection remains to be determined, although in the case of many picornaviruses, including EMCV, as well as other RNA viruses, LGP2 acts as a positive regulator of MDA5- and RIG-I-mediated viral recognition [Sato *et al.*, 2010].

**Chapter 6**  
**IMAGING OF RLR INTERACTIONS**

## **6.1 Introduction**

It is important to know the extent of colocalisation between RIG-I and MDA5 with IPS-1 in response to viral infection, to determine when RIG-I and MDA5 are most active. The RLR family, consisting of the three known family members RIG-I, MDA5, and LGP2, are pattern recognition receptors that detect a range of different viruses. RIG-I (retinoic acid inducible gene-I) and MDA5 (melanoma differentiation-associated gene 5) are homologous cytoplasmic proteins containing an N-terminal region with two caspase activation and recruitment domains (CARDs), a central SF2 type DExD/H-box RNA helicase domain, and a C-terminal repressor domain (RD). LGP2 (laboratory of genetics and physiology 2) harbours a DExD/H-box RNA helicase domain and a C-terminal RD, but lacks any CARDs.

Once a viral ligand has been detected and bound by RIG-I and MDA5, both signal downstream through their CARDs to activate IRF3/7 and NF- $\kappa$ B indirectly, via the protein intermediate IPS-1 (IFN- $\beta$  promoter stimulator 1). After interaction with RIG-I and MDA5, IPS-1 goes on to recruit and activate a variety of other proteins, including TRAF2, TRAF3, and TRAF6. These TRAF proteins then signal further downstream to the I $\kappa$ B kinase (IKK) family members, to activate the transcription factors IRF3/7 and NF- $\kappa$ B, and initiate an immune response. The CARD-CARD interaction between RIG-I and MDA5 with IPS-1 is an essential step in the antiviral process. If this interaction is disrupted, then the whole signalling cascade will fail to initiate.

## **6.2 Results**

Confocal microscopy was used to visualise the interaction and colocalisation between IPS-1 and MDA5 (*Figure 6.1*) and between IPS-1 and RIG-I (*Figure 6.2*) in human cardiac cells in response to CBV5 stimulation. The cells were incubated with two species of primary antibody: RIG-I and MDA5 were incubated with goat pAb; whilst IPS-1 was incubated with rabbit pAb. Using two different species of primary antibody allows for the use of different fluorescently-conjugated secondary antibodies, each specific for a particular species of primary antibody. RIG-I and MDA5 were incubated with Donkey anti-Goat TRITC (red) secondary antibody, whilst IPS-1 was incubated with Swine anti-Rabbit FITC (green) secondary antibody. This ensures that both MDA5 and RIG-I appear as red under the confocal microscope, whilst IPS-1 appears green. The nucleus was stained blue using TOPRO.

Once the confocal images were taken, the extent of colocalisation needed to be statistically determined. This was achieved using a variety of different software, including LSM Image Browser, AxioVision LE, ImageJ, and JACoP. The ImageJ and JACoP pieces of software automatically threshold images, removing user bias and providing a quantitative value of the extent of colocalisation. The Pearson's correlation coefficient,  $r(\text{obs})$ , measures the covariance between the intensities of each channel in each pixel, and is not sensitive to background or colocalised pixel intensity. It has a linear regression range of -1 to 1, with -1 being total negative correlation (whereby no pixels overlap), 0 being a random correlation, and 1 being total positive correlation (where all the pixels overlap). Values of approximately 0.5 and above are considered reasonable Pearson's coefficients.



In both cases, the greatest response to CBV5 can be seen within the first 2 hours of infection. RIG-I and MDA5 are both present in the cytoplasm only, and not in the nucleus, and this is clearly seen in all the images. The same goes for IPS-1, which is located on mitochondrial membranes within the cytoplasm.

### **6.2.1 Colocalisation between IPS-1 and MDA5**

*Figure 6.1* shows the colocalisation between IPS-1 and MDA5 in cardiac cells in response to CBV5 stimulation. In unstimulated cells (panel A), MDA5 and IPS-1 activity are at a basal level, with a Pearson's correlation coefficient,  $r(\text{obs})$ , of 0.683. This shows that there is minimal colocalisation between IPS-1 and MDA5, but even when no viral infection is present, there is some colocalisation going on. Panel B depicts cells that have been incubated with CBV5 for 1 hour. There is an immediate antiviral response by MDA5, with the  $r(\text{obs})$  increasing to 0.91, showing massive colocalisation between IPS-1 and MDA5. Such a high  $r(\text{obs})$  value suggests that nearly all available MDA5 is linked with IPS-1, to ensure a rapid antiviral response. This response continues in panel C, in which cells have been incubated for 2 hours with CBV5. The  $r(\text{obs})$  is 0.912, again showing extreme colocalisation between IPS-1 and MDA5.

In cells stimulated with CBV5 for 4 hours (panel D), the colocalisation between MDA5 and IPS-1 is slightly decreased, with an  $r(\text{obs})$  of 0.802. Although this is not as high as the  $r(\text{obs})$  found after 1 hour and 2 hour CBV5 stimulations, the extent of colocalisation between IPS-1 and MDA5 is still greater than that found in cells left unstimulated ( $r(\text{obs})$  of 0.802 compared to 0.683). After 6 hours of CBV5 stimulation (panel E), the extent of colocalisation increases slightly back

up to 0.877, which, although lower than the  $r(\text{obs})$  found after 1 hour and 2 hour CBV5 stimulations, still shows extensive colocalisation between IPS-1 and MDA5.

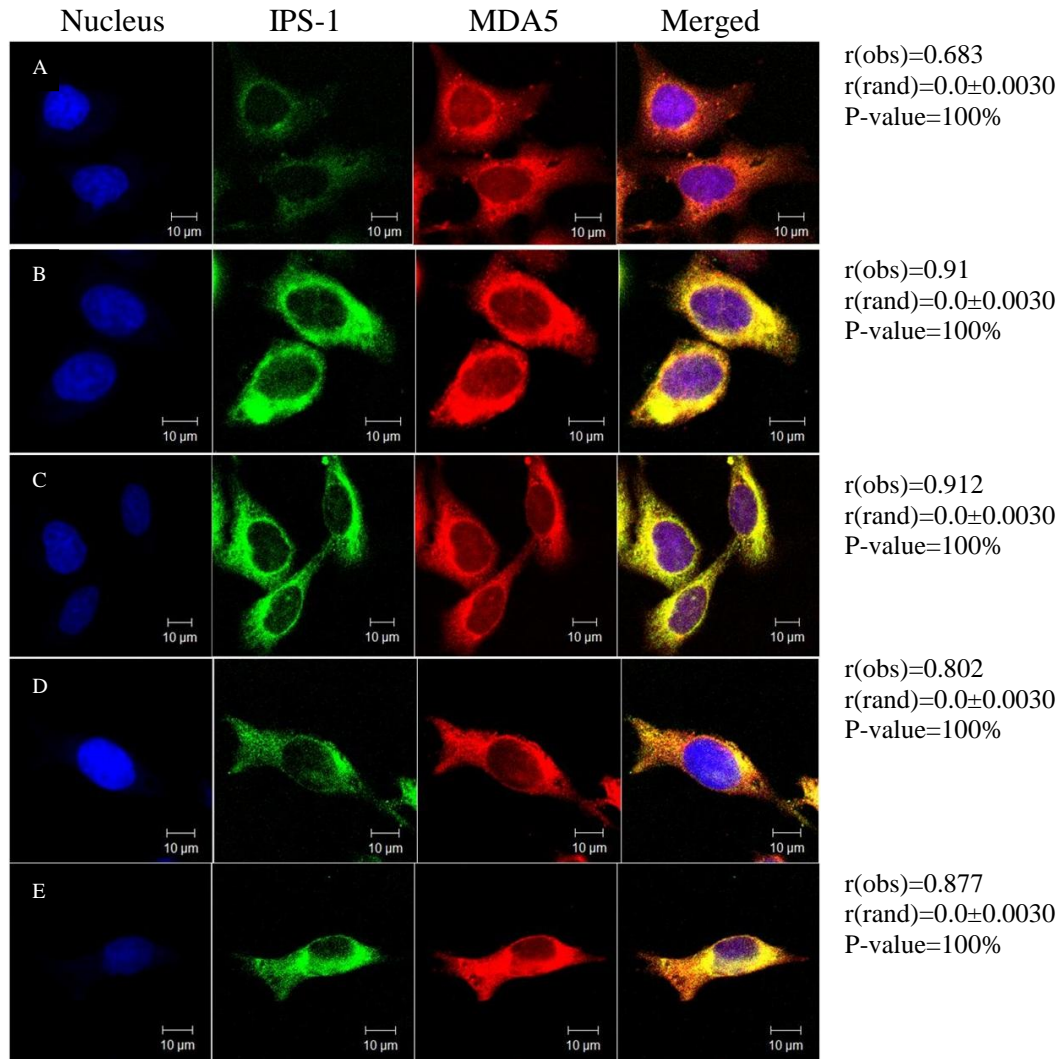


**Figure 6.1: Colocalisation of IPS-1 and MDA5 in cardiac cells in response to CBV5 stimulation.** Confluent cells were left unstimulated (A), or incubated with 100 $\mu$ l CBV5 for 1 hour (B), 2 hours (C), 4 hours (D), or 6 hours (E). IPS-1 and MDA5 were labelled using indirect immunofluorescence with FITC and TRITC conjugated probes, respectively. TOPRO was used to stain the nucleus. The cells were imaged using a Carl Zeiss LSM510 confocal microscope. The merged images show extensive colocalisation between IPS-1 and MDA5, determined using ImageJ software. (Scale bar = 10 $\mu$ m). Representative cell samples shown.

### 6.2.2 Colocalisation between IPS-1 and RIG-I

*Figure 6.2* shows the colocalisation between IPS-1 and RIG-I in cardiac cells in response to CBV5 stimulation. The extent of colocalisation is very similar to that seen between IPS-1 and MDA5 in *Figure 6.1*. In unstimulated cells (panel A), the  $r(\text{obs})$  is 0.567, showing a small amount of colocalisation between IPS-1 and RIG-I. Maybe because RIG-I has been shown to associate with the cytoskeleton, this  $r(\text{obs})$  is lower than that of MDA5 with IPS-1, although both values still show minor colocalisation. In panel B, showing cells stimulated for 1 hour with CBV5, the  $r(\text{obs})$  is 0.877. RIG-I can be seen to colocalise strongly with IPS-1 to initiate an immune response, though the colocalisation is slightly lower than that of MDA5 and IPS-1 ( $r(\text{obs})$  of 0.91). After 2 hours of stimulation with CBV5 (panel C), the colocalisation between IPS-1 and RIG-I increased to 0.918, equalling that seen by MDA5 and IPS-1. Both MDA5 and RIG-I are extensively bound to IPS-1 during this stage of viral infection.

In panel D, the RIG-I antiviral response to CBV5 stimulation after 4 hours decreases down to an  $r(\text{obs})$  of 0.724. This effect is similar to that seen in the MDA5 response, although the MDA5 response appears to be slighter greater ( $r(\text{obs})$  of 0.802 for MDA5 compared to 0.724 for RIG-I). The colocalisation between IPS-1 and RIG-I in response to 4 hour CBV5 infection is still greater than that seen in unstimulated cells (panel A). After 6 hours of CBV5 stimulation (panel E), the  $r(\text{obs})$  increases back up to 0.896, again showing extensive colocalisation between IPS-1 and RIG-I. Interestingly, the colocalisation between IPS-1 and RIG-I at this stage of infection is slightly greater than that shown between IPS-1 and MDA5 ( $r(\text{obs})$  of 0.896 versus 0.877), as well as that shown

between RIG-I and IPS-1 after 1 hour of CBV5 stimulation ( $r(\text{obs})$  again of 0.896 versus 0.877), suggesting RIG-I potentially plays a greater role later on during the infection.

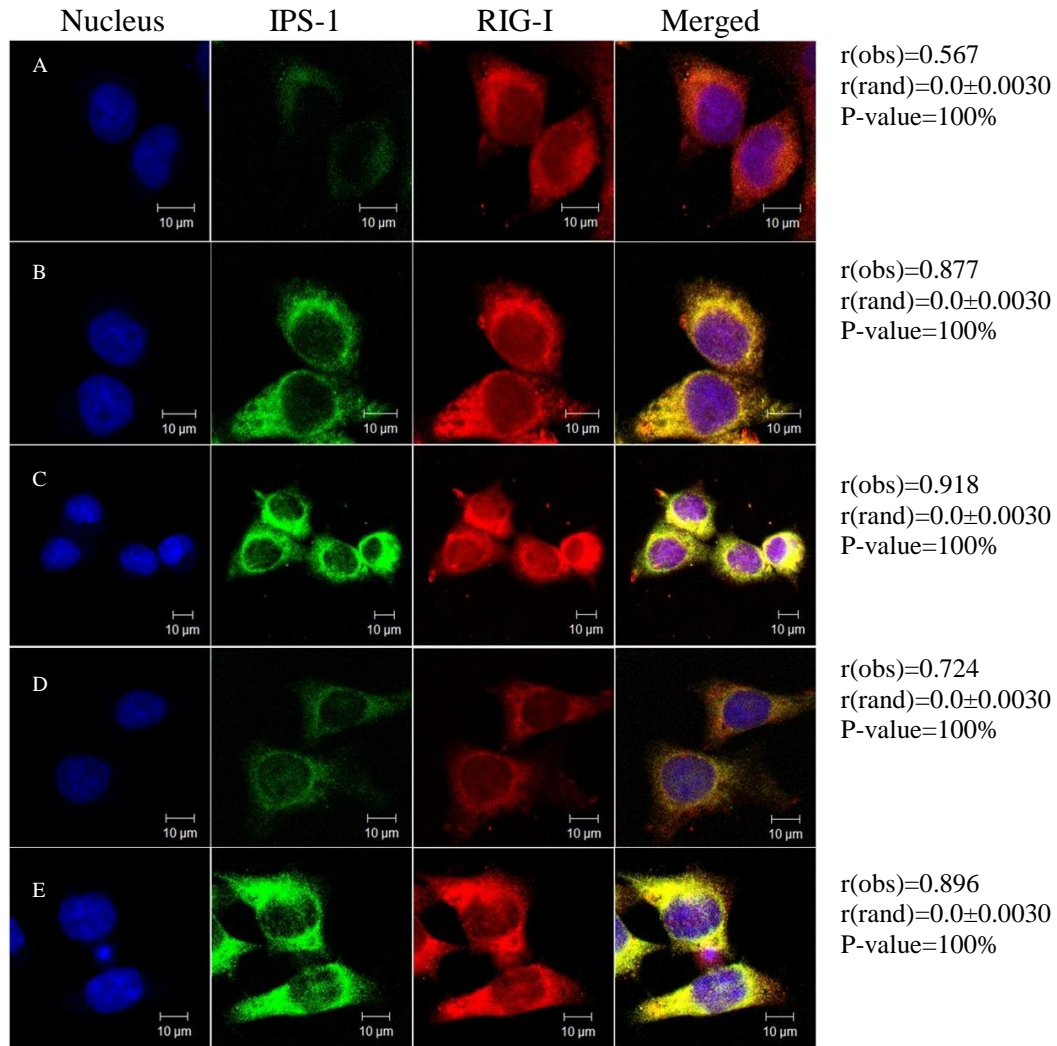


**Figure 6.2: Colocalisation of IPS-1 and RIG-I in cardiac cells in response to CBV5 stimulation.** Cells were left unstimulated (A), or incubated with 100 $\mu$ l CBV5 for 1 hour (B), 2 hours (C), 4 hours (D), or 6 hours (E). IPS-1 and RIG-I were labelled using indirect immunofluorescence with FITC and TRITC conjugated probes, respectively. TOPRO was used to stain the nucleus. The cells were imaged using a Carl Zeiss LSM510 confocal microscope. The merged images show extensive colocalisation between IPS-1 and RIG-I, determined using ImageJ software. (Scale bar = 10 $\mu$ m). Representative cell samples shown.

### **6.3 Conclusion**

Both MDA5 and RIG-I show extensive colocalisation with IPS-1 in cardiac cells in response to CBV5 stimulation, determined using ImageJ software. The ImageJ and JACoP pieces of software remove user bias from images and provide a quantitative value of the extent of colocalisation. From the values obtained, it can be seen that the greatest response occurs within the first two hours of infection, drops down slightly in the fourth hour, but picks up again at six hours post-infection. MDA5 shows marginally greater colocalisation with IPS-1 earlier on during CBV5 infection, whilst RIG-I appears to play a greater role later on during infection. Overall, both act synergistically with IPS-1 to initiate downstream signalling in response to CBV5 infection.

The RLRs have been shown to interact with IPS-1 in response to various other viral infections. Influenza A virus infection in human primary macrophages results in the translocation of actin and RIG-I / IPS-1 signalling components to the mitochondria to initialise the production of type I IFNs and inflammatory cytokines [Ohman *et al.*, 2009]. The RSV NS1 protein colocalises with IPS-1 following infection, blocking RIG-I – IPS-1 signalling [Boyapalle *et al.*, 2012]. In response to Rhinovirus infection in primary bronchial epithelial cells, TLR3, RIG-I, and MDA5 coordinate together to elicit an antiviral response [Slater *et al.*, 2010].

**Chapter 7**  
**DISCUSSION**

Coxsackievirus B5 (CBV5), belonging to the *Enterovirus* genus and Picornaviridae family, consists of a non-enveloped icosahedral capsid enclosing a naked single-stranded, positive sense, polyadenylated RNA genome. CBV5 can cause a range of diseases, with the most serious including viral myocarditis (which can lead on to dilated cardiomyopathy, DCM), aseptic meningitis, and pancreatitis. Viral myocarditis is an inflammatory disease of the myocardium characterised by leukocyte infiltrate and necrosis of the myocytes [Bohn and Benson, 2002], and results in a high mortality rate in newborns. Myocardial destruction can lead on to DCM, characterised by dilation and impaired contraction of the left or both ventricles of the heart, and is the major reason for cardiac transplantation in Europe and the USA [Manolio *et al.*, 1992].

The immune system, consisting of two main branches of immunity (innate and acquired), defends the human body against invading pathogens. Innate immunity is the first line of defence against pathogens, and responds rapidly to invading microbes. It does this via pattern recognition receptors (PRRs) which can distinguish self from non-self, and recognise certain microbial components, termed pathogen-associated molecular patterns (PAMPs), to initiate an appropriate immune response. Recognition of PAMPs by PRRs leads to the rapid activation of latent transcription factors (such as NF- $\kappa$ B and IRF3) to stimulate the expression of antimicrobial genes and the production of type I interferons (IFN) [Akira and Takeuchi, 2007].

The Toll-like receptors (TLRs) are an important class of PRRs. The 13 currently known members within the TLR family recognise a wide range of different

PAMPs, and initiate appropriate downstream signalling (via two different pathways: the MyD88-dependent pathway; and the MyD88-independent (TRIF-dependent) pathway) to activate the innate and adaptive immune response. Several TLRs are important for the recognition of different viruses, including TLR2, TLR3, TLR4, TLR7/8, and TLR9.

Along with the TLRs, several new TLR-independent PRRs have been discovered, including the retinoic acid inducible gene-I (RIG-I)-like receptor (RLR) family. There are three known members: RIG-I [Yoneyama *et al.*, 2004], melanoma differentiation-associated gene 5 (MDA5) [Kang *et al.*, 2002], and laboratory of genetics and physiology 2 (LGP2) [Rotherfusser *et al.*, 2005]. The RLRs detect cytoplasmic viral RNA during viral replication, and preferentially recognise different viruses. RIG-I has been shown to detect a number of both positive and negative stranded viruses, as well as several different viral PAMPs, whilst MDA5 has been shown to be critical for Picornaviridae detection, including CBV3. Despite the wealth of research on hunting the RLR ligands, the precise PAMPs recognised by each RLR are, as yet, still undetermined.

In this regard, this project aimed to enhance the current knowledge on whether the RNA helicase RIG-I or MDA5 is the primary detector of CBV5. To determine this, the extent of RIG-I and MDA5 involvement in CBV5 infection of cardiac cells was investigated. As one of the leading causes of viral myocarditis is CBV5, work was performed upon cardiac cells. To further elucidate the role of RIG-I and MDA5 in CBV5 sensing, Huh cells were used, as Huh 7.5.1 cells have an inactivating RIG-I mutation that leads to a defect in IFN production. RIG-I has



been proposed to dimerise in response to viral ligands, so whether dimerisation between RIG-I, MDA5, and LGP2 occurred after CBV5 infection was observed using immunoprecipitation experiments. Finally, the interaction and colocalisation between RIG-I and MDA5 with IPS-1 (an adaptor protein essential for downstream signalling) was examined using confocal microscopy.

Understanding whether RIG-I or MDA5 is the primary detector of CBV5 will help in the development of novel therapeutic approaches for not only viral myocarditis, but for other diseases caused by CBV5 as well.

### **7.1 RNA Helicase Involvement in CBV5 Infection of Cardiac Cells**

To determine RIG-I and MDA5 involvement in human cardiac cells in response to CBV5 infection, a number of different experiments were performed. To start off with, indirect immunofluorescence coupled with flow cytometry was used to investigate the expression levels of RIG-I and MDA5 in human cardiac cells in response to stimulation with purified CBV5, UV-CBV5, purified genomic CBV5 ssRNA, and Poly I:C.

Neither MDA5 nor RIG-I showed any response to stimulation with UV-CBV5, which is to be expected. UV-inactivation destroys the viral RNA, whilst leaving the capsid intact. This allows CBV5 to maintain its ability to bind to cellular receptors, but its viral RNA is unable to cause a productive infection. As both MDA5 and RIG-I are located within the cytoplasm, if the viral RNA is inactivated, they will not be upregulated. Poly I:C, a synthetic dsRNA analogue, has been shown to induce MDA5 expression [Kato *et al.*, 2006; Loo *et al.*, 2008], and results here confirm that, with only MDA5 expression levels being upregulated in response to Poly I:C stimulation.

Both RIG-I and MDA5 expression levels increased within the first two hours of CBV5 infection, and dropped off slightly after 4 and 6 hours of infection. The overall response by MDA5 was higher than that of RIG-I, suggesting that MDA5 is the primary detector of CBV5, but the fact that RIG-I expression levels also increased indicates that RIG-I plays a role in CBV5 sensing too. Since the genomic ssRNA by itself failed to upregulate either MDA5 or RIG-I, this suggests

that these RLRs sense the replicative intermediate dsRNA form that occurs during the viral replication cycle.

Following on from showing that both RIG-I and MDA5 expression levels are upregulated in response to CBV5 stimulation, discontinuous SDS-PAGE combined with western blotting was performed to detect the presence of phospho-I $\kappa$ B and IRF3. The detection of phospho-I $\kappa$ B corresponds to NF- $\kappa$ B activation, as RIG-I and MDA5, once activated by ligand RNA, interact with IPS-1 via CARD-CARD interactions, inducing the recruitment of downstream signalling molecules. This results in I $\kappa$ B being released from the NF- $\kappa$ B complex and getting phosphorylated, marking it for ubiquitination and degradation by proteosomes [Karin and Ben-Neriah, 2000]. The transcription factors NF- $\kappa$ B and IRF3 transcriptionally upregulate type I IFNs to mediate induction of the innate immune response.

The same four stimulations (Poly I:C, ssRNA, CBV5, and UV-CBV5) and time points (0, 1, 2, 4, and 6 hours) were used as before, and both phospho-I $\kappa$ B and IRF3 were found to be present in all cases. Interestingly, ssRNA stimulation resulted in phospho-I $\kappa$ B and IRF3 being detected, which is perhaps due to ssRNA detection by TLR7 or TLR8, both of which could trigger activation [Triantafilou *et al.*, 2005a]. The presence of phospho-I $\kappa$ B and IRF3 in response to Poly I:C stimulation is likely due to MDA5 being upregulated, and the same is true for stimulation with CBV5.

Using a flow cytometric flex set bead system (Becton Dickinson), the IFN- $\beta$  production in human cardiac cells stimulated with CBV5, ssRNA, or Poly I:C was measured. IFN- $\beta$  is a type I IFN, which, once upregulated by IRF3 and NF- $\kappa$ B, signals through the IFN- $\alpha/\beta$  receptor and the Jak-STAT pathway to drive interferon stimulated gene (ISG) expression and an innate immune response [Lei *et al.*, 2009; Yoneyama and Fujita, 2009]. IFN- $\beta$  was upregulated in response to all three stimulations, though most greatly by CBV5, and the greatest response occurred after 2 and 4 hours of stimulation, and dropped down after 6 hours. This result shows that CBV5 infection causes an intense cytokine secretion of IFN- $\beta$ , similar to that seen during CBV3 infection [Wang *et al.*, 2009; Hühn *et al.*, 2010]. Even though MDA5 and RIG-I expression levels are not upregulated in response to ssRNA, IFN- $\beta$  production occurs, again suggesting that TLR7 or TLR8 are detecting the purified genomic CBV5 ssRNA and initiating cytokine secretion.

Finally, in order to verify the involvement of RIG-I and MDA5 in CBV5 innate immune recognition in human cardiac cells, RIG-I and MDA5 expression was knocked down using psiRNA-RIG-I and psiRNA-MDA5 plasmids, and IFN- $\beta$  production was measured. In response to RIG-I and MDA5 being silenced in cardiac cells and stimulated with purified CBV5, there was a decrease in IFN- $\beta$  production in cells with silenced RIG-I, and a more significant reduction in IFN- $\beta$  production when MDA5 was silenced.

Overall, in human cardiac cells, both RLRs play a role in CBV5 detection. However, MDA5 appears to be more involved in viral sensing than RIG-I.

## **7.2 Determining the Role of RIG-I and MDA5 in CBV5 Sensing Using Huh Cells**

In order to more fully determine the involvement of RIG-I in CBV5 recognition, Huh cells were used. Established from a hepatocellular carcinoma, the Huh cell line possesses a highly useful property for studying RIG-I, specifically that Huh 7.5.1 cells have an inactivating mutation in RIG-I, which leads to a defect in IFN production. The same set of experiments that were performed on the cardiac cells were performed on Huh 7.5 (wild type) cells and Huh 7.5.1 cells, namely: determining the expression levels of MDA5 and RIG-I; detecting phospho-I $\kappa$ B and IRF3; and determining IFN  $\beta$  production.

The expression levels of both RIG-I and MDA5 in response to Poly I:C, CBV5, UV-CBV5, and ssRNA stimulation at various time points was minimal in both Huh 7.5 cells and Huh 7.5.1 cells in all cases, with the one exception of CBV5 stimulation in Huh 7.5 resulting in the upregulation of RIG-I expression. This suggests that RIG-I plays an important role in CBV5 sensing. Phospho-I $\kappa$ B and IRF3 detection in Huh cells in response to the four different stimulations is similar to that seen in cardiac cells, with the same conclusions drawn.

The IFN- $\beta$  production in Huh 7.5 cells and Huh 7.5.1 cells are the most significant results here. Huh 7.5.1 cells have an inactivating mutation in RIG-I that leads to a defect in IFN production. As less IFN- $\beta$  production is seen in Huh 7.5.1 cells, this indicates that RIG-I plays a role in CBV5 detection. If detection was performed solely by MDA5, it would be expected that IFN- $\beta$  production in both Huh 7.5 cells and Huh 7.5.1 cells would remain the same, as the RIG-I mutation would

have no effect, due to RIG-I not being involved. Because a decrease in IFN- $\beta$  production is detected, RIG-I plays a role alongside MDA5 in sensing CBV5.

Experimenting on Huh cells alongside human cardiac cells, it can be seen that RIG-I does indeed have a role to play within CBV5 infection, together with MDA5.

### **7.3 RLR Dimerisation**

As well as RIG-I and MDA5, the RLR family also contains LGP2. The exact function and mechanism of LGP2 in innate immunity is still undetermined, although it has been proven to be a regulator for RIG-I- and MDA5-dependent signalling, via its repressor domain (RD). The RD of RIG-I has been shown to be important for controlling RLR-mediated IFN responses. Once a viral ligand binds the RD, a conformational change occurs, converting RIG-I from a closed inactive state to an open active state, resulting in the dimerisation of RIG-I and the initiation of downstream signalling via the CARDs [Cui *et al.*, 2008].

Dimerisation of the RLRs is essential for them to function correctly. LGP2 has been suggested as a negative regulator of the RIG-I- and MDA5-mediated antiviral response, as its overexpression inhibits virus-induced IRF3 and NF- $\kappa$ B activation. One possible explanation for this is that LGP2 sequesters dsRNA away from RIG-I and MDA5, thereby preventing activation of the antiviral signal [Rothenfusser *et al.*, 2005]. A second model is that LGP2, via its RD, inhibits dimerisation of RIG-I and its interaction with IPS-1 [Saito *et al.*, 2007], whilst a third possibility is that LGP2 competes with IKK $\epsilon$  for recruitment to IPS-1 [Komuro and Horvath, 2006]. However, *in vivo* data suggests that LGP2 can act as a positive regulator of RIG-I- and MDA5-mediated antiviral responses, via its ATPase domain [Venkataraman *et al.*, 2007; Satoh *et al.*, 2010].

This study aimed to determine whether the RLRs dimerise in response to CBV5 infection, using immunoprecipitation experiments. Immunoprecipitation is a technique used to precipitate a protein out of a lysate using an antibody specific

for that protein coupled with beads specific for the antibody. RIG-I, MDA5, or LGP2 antibodies were used to precipitate out their respective protein, and SDS-PAGE and western blotting were then used to detect a different protein. The results presented here show that RIG-I and MDA5 exist mainly as homodimers, but also as monomers, in human cardiac cells, and in addition, they can heterodimerise with a percentage of LGP2.

However, the puzzling question is that although heterodimers between LGP2 and RIG-I or MDA5 are present in the LGP2 immunoprecipitations, in the MDA5 or RIG-I immunoprecipitations, LGP2 presence is only detected as a monomer. This could be due to the higher affinity of the LGP2 RD with the other RLRs, enabling it to bind and precipitate RIG-I or MDA5, whereas MDA5 or RIG-I have a lower affinity, and may therefore not be able to bind a detectable percentage of higher LGP2 aggregates.

Overall, these immunoprecipitation experiments conclude that LGP2 and RIG-I or MDA5 associate in cardiac cells, and that there is a synergistic mechanism of RLR association for viral detection.



#### **7.4 Imaging of RLR Interactions**

Confocal microscopy was used to visualise the interaction and colocalisation between IPS-1 and MDA5 and between IPS-1 and RIG-I in human cardiac cells in response to CBV5 stimulation, to determine when RIG-I and MDA5 are most active. RIG-I and MDA5 are both present in the cytoplasm only, and IPS-1 is located on mitochondrial membranes within the cytoplasm, and not in the nucleus, and this is clearly seen in all the images.

In order to remove user bias from images and provide a quantitative value of the extent of colocalisation, the ImageJ and JACoP pieces of software were used [Bolte and Cordelieres, 2006]. The Pearson's correlation coefficient,  $r(\text{obs})$ , measures the covariance between the intensities of each channel in each pixel, and is not sensitive to background or colocalised pixel intensity. It has a linear regression range of -1 to 1, with -1 being total negative correlation (whereby no pixels overlap), 0 being a random correlation, and 1 being total positive correlation (where all the pixels overlap). Values of approximately 0.5 and above are considered reasonable Pearson's coefficients.

Results presented here indicate that both MDA5 and RIG-I show extensive colocalisation with IPS-1, especially within the first two hours of infection. MDA5 showed marginally greater colocalisation with IPS-1 earlier on during CBV5 infection, whilst RIG-I appeared to play a greater role later on during infection. Both had very high Pearson's coefficient values after CBV5 stimulation, indicating that once CBV5 has been detected, MDA5 and RIG-I bind, via CARD-CARD interactions, with IPS-I. The interaction between MDA5 and IPS-1 is

marginally greater than that seen between RIG-I and IPS-1, once more confirming that MDA5 is most likely the primary detector of CBV5, with RIG-I playing a role too.

Overall, both MDA5 and RIG-I act synergistically with IPS-1 to initiate downstream signalling in response to CBV5 infection.

## **7.5 Conclusion**

CBV5 can cause a range of diseases, with the most serious being viral myocarditis (which can lead on to DCM), aseptic meningitis, and pancreatitis. DCM is the major reason for cardiac transplantation in Europe and the USA, and thus the study of CBV5, and how it is detected by the immune system, is of great importance.

The RNA helicases RIG-I and MDA5 are both involved in the sensing of a variety of different viruses and viral PAMPs. Previous literature has suggested that MDA5 is the sole detector of Picornaviridae, of which CBV5 is a member. Results presented here suggest that both MDA5 and RIG-I act synergistically to detect CBV5 and initiate a downstream immune response, although MDA5 appears to be the marginally stronger sensor. The expression levels of both are upregulated in response to CBV5 infection in human cardiac cells, with MDA5 expression levels being slightly greater than RIG-I. However, in Huh cells, RIG-I expression levels are greater than those of MDA5, indicating that it plays a role in CBV5 sensing.

The presence of phospho-I $\kappa$ B (corresponding to NF- $\kappa$ B activation) and IRF3 is detected in both cardiac cells and Huh cells in response to CBV5. In response to ssRNA stimulation, RIG-I and MDA5 expression levels remained low, but phospho-I $\kappa$ B and IRF3 were detected, showing that other PRRs, such as TLR7 or TLR8, are playing a role. IFN- $\beta$  production is also greatly upregulated in response to CBV5 infection. In Huh 7.5.1 cells, which contain an inactivating mutation in

RIG-I that leads to a defect in IFN production, IFN- $\beta$  production is reduced, showing that RIG-I plays a role in CBV5 detection, alongside MDA5.

RIG-I and MDA5 have both been shown to colocalise with the adaptor protein IPS-1 in response to CBV5 infection, again indicating the synergistic response by the two RLRs. The third RLR, LGP2, plays a role in the sensing of CBV5 too. Both RIG-I and MDA5 form dimers in the cytoplasm, with LGP2 remaining a monomer. In response to CBV5 stimulation, LGP2 can heterodimerise with RIG-I and MDA5, potentially upregulating or downregulating their activity. These heterodimers between LGP2 and RIG-I or MDA5 are present in the LGP2 immunoprecipitations, but in the MDA5 or RIG-I immunoprecipitations, LGP2 presence is only detected as a monomer. Determining the extent of affinity of the LGP2 RD with the other RLRs, and the MDA5 or RIG-I RD with LGP2, could help solve this puzzle.

This study has proven that RIG-I plays a greater role in CBV5 sensing than previously thought, and that both MDA5 and RIG-I act synergistically to initiate an innate immune response upon recognition of CBV5. The recent discovery that RIG-I signals to the inflammasome in an IPS-1-independent manner [Poeck *et al.*, 2010] also opens up new possibilities for developing therapeutic targets against CBV5. Inflammasomes are caspase-1 activating multiprotein complexes which assemble in the cytoplasm [Martinon *et al.*, 2009]. Activated caspase-1 cleaves the proforms of the interleukin-1 $\beta$  cytokine family members, leading to their activation and secretion, and initiation of the inflammatory response.

In conclusion, the RLRs play a vital role in the innate immune recognition of CBV5. Other PRRs, including the TLRs and the inflammasome, may also contribute to the innate immune response against CBV5, but further experimentation is needed to elucidate this. The true wonder of the human body's immune system is gradually revealing itself to scientists, who must continue to use every tool at their disposal to combat the ultimate predators: viruses.

## REFERENCES

**Adhikari, A., Xu, M., and Chen, Z.J.** (2007), 'Ubiquitin-mediated activation of TAK1 and IKK', *Oncogene*, **26**(22): 3214-3226

**Agaugué, S., Perrin-Cocon, L., André, P., and Lotteau, V.** (2007), 'Hepatitis C lip-Viro-particle from chronically infected patients interferes with TLR4 signaling in dendritic cell', *PLoS One*, **2**(3): e330

**Airaksinen, A.** (2000), 'The VP1 intracapsid hook and uncoating of enteroviruses', University of Helsinki, Academic Dissertation, URL: <http://ethesis.helsinki.fi/julkaisut/mat/bioti/vk/airaksinen/index.html>

**Akira, S., Uematsu, S., and Takeuchi, O.** (2006), 'Pathogen recognition and innate immunity', *Cell*, **124**(4): 783-801

**Alexopoulou, L., Holt, A.C., Medzhitov, R., and Flavell, R.A.** (2001), 'Recognition of double-stranded RNA and activation of NF-kappaB by Toll-like receptor 3', *Nature*, **413**(6857): 732-738

**Andrejeva, J., Childs, K.S., Young, D.F., Carlos, T.S., Stock, N., Goodbourn, S., and Randall, R.E.** (2007), 'The V proteins of paramyxoviruses bind the IFN-inducible RNA helicase , mda5, and inhibit its activation of the IFN-beta promoter', *Proc Natl Acad Sci U S A*, **101**(49): 17264-17269

**Ashkar, A.A., Bauer, S., Mitchell, W.J., Vieira, J., and Rosenthal, K.L.** (2003), 'Local delivery of CpG oligodeoxynucleotides induces rapid changes in the genital mucosa and inhibits replication, but not entry, of herpes simplex virus type 2', *J Virol*, **77**(16): 8948-8956

**Barral, P.M., Morrison, J.M., Drahos, J., Gupta, P., Sarkar, D., Fisher, P.B., and Racaniello, V.R.** (2007), 'MDA-5 is cleaved in poliovirus-infected cells', *J Virol*, **81**(8): 3677-3684

**Barral, P.M., Sarkar, D., Fisher, P.B., and Racaniello, V.R.** (2009), 'RIG-I is cleaved during picornavirus infection', *Virology*, **391**(2): 171-176

**Basavappa, R., Syed, R., Flore, O., Icenogle, J.P., Filman, D.J., and Hogle, J.M.** (1994), 'Role and mechanism of the maturation cleavage of VP0 in poliovirus assembly: structure of the empty capsid assembly intermediate at 2.9 Å resolution', *Protein Sci*, **3**(10): 1651-1669

**Becton Dickinson (BD)**, URL:

<http://www.bdbiosciences.com/eu/instruments/facscalibur/index.jsp>

**Bedard, K.M., and Semler, B.L.** (2004), 'Regulation of picornavirus gene expression', *Microbes Infect*, **6**(7): 702-713

**Bell, Y.C., Semler, B.L., and Ehrenfeld, E.** (1999), 'Requirements for RNA replication of a poliovirus replicon by coxsackievirus B3 RNA polymerase', *J Virol*, **73**(11): 9413-9421

**Belnap, D.M., Filman, D.J., Trus, B.L., Cheng, N., Booy, F.P., Conway, J.F., Curry, S., Hiremath, C.N., Tsang, S.K., Steven, A.C., and Hogle, J.M.** (2000), 'Molecular tectonic model of virus structural transitions: the putative cell entry states of poliovirus', *J Virol*, **74**(3): 1342-1354

**Belvin, M.P., and Anderson, K.V.** (1996), 'A conserved signaling pathway: the Drosophila toll-dorsal pathway', *Annu Rev Cell Dev Biol*, **12**: 393-416

**Bengtsson, E., and Lamberger, B.** (1966), 'Five-year follow-up study of cases suggestive of acute myocarditis', *Am Heart J*, **72**(6): 751-763

**Bergelson, J.M., Mohanyy, J.G., Crowell, R.L., St John, N.F., Lublin, D.M., and Finberg, R.W.** (1995), 'Coxsackievirus B3 adapted to growth in RD cells binds to decay-accelerating factor (CD55)', *J Virol*, **69**(3): 1903-1906

**Bergelson, J.M., Modlin, J.F., Wieland-Alter, W., Cunningham, J.A., Crowell, R.L., and Finberg, R.W.** (1997a), 'Clinical coxsackievirus B isolates differ from laboratory strains in their interactions with two cell surface receptors', *J Infect Dis*, **175**(3): 697-700



**Bergelson, J.M., Cunningham, J.A., Droguett, G., Kurt-Jones E.A., Krithivas, A., Hong, J.S., Horwitz, M.S., Crowell, R.L., and Finberg, R.W. (1997b),** 'Isolation of a common receptor for Cocksackie B viruses and adenoviruses 2 and 5', *Science*, **275**(5304): 1320-1323

**Bieback, K., Lien, E., Klagge, I.M., Avota, E., Schneider-Schaulies, J., Duprex, W. P., Wagner, H., Kirschning, C.J., Ter Meulen, V., and Schneider-Schaulies, S. (2002),** 'Hemagglutinin protein of wild-type measles virus activates toll-like receptor 2 signaling', *J Virol*, **76**(17): 8729-8736

**The Biotechnology Project at MATC, URL:**

[http://biotech.matcmadison.edu/resources/proteins/labManual/chapter\\_5/procedure5\\_2.htm](http://biotech.matcmadison.edu/resources/proteins/labManual/chapter_5/procedure5_2.htm)

**Blyn, L.B., Towner, J.S., Semler, B.L., and Ehrenfeld, E. (1997),** 'Requirement of poly(rC) binding protein 2 for translation of poliovirus RNA', *J Virol*, **71**(8): 6243-6246

**Boehme, K.W., Guerrero, M., and Compton, T. (2006),** 'Human cytomegalovirus envelope glycoproteins B and H are necessary for TLR2 activation in permissive cells', *J Immunol*, **177**(10): 7094-9102

**Bohn, D., and Benson, L. (2002),** 'Diagnosis and management of pediatric myocarditis', *Paediatr Drugs*, **4**(3): 171-181

**Bolte, S., and Cordelieres, F.P.** (2006), 'A guided tour into subcellular colocalization analysis in light microscopy', *J Microsc*, **224**(3): 213-232

**Borman, A.M., Le Mercier, P., Girard, M., and Kean, K.M.** (1997), 'Comparison of picornaviral IRES-driven internal initiation of translation in cultured cells of different origins', *Nucleic Acids Res*, **25**(5): 925-935

**Bossart, W., and Bienz, K.** (1979), 'Virus replication, cytopathology, and lysosomal enzyme response in enucleated HEp-2 cells infected with poliovirus', *Virology*, **92**(2): 331-339

**Boyapalle, S., Wong, T., Garay, J., Teng, M., San Juan-Vergara, H., Mohapatra, S., and Mohapatra, S.** (2012), 'Respiratory syncytial virus NS1 protein colocalizes with mitochondrial antiviral signaling protein MAVS following infection', *PLoS One*, **7**(2): e29386

**Breitbart, M., and Rohwer, F.** (2008), 'Here a virus, there a virus, everywhere the same virus?', *Trends Microbiol*, **13**(6): 278-284

**Brown, D.M., Kauder, S.E., Cornell, C.T., Jang, G.M., Racaniello, V.R., and Semler, B.L.** (2004), 'Cell-dependent role for the poliovirus 3' noncoding region in positive-strand RNA synthesis', *J Virol*, **78**(3): 1344-1351

**Brown, E.H.** (1973), 'Enterovirus infections', *Br Med J*, **2**(5859): 169-171

**Burzyn, D., Rassa, J.C., Kim, D., Nepomnaschy, I., Ross, S.R., and Piazzon, I.** (2004), 'Toll-like receptor 4-dependent activation of dendritic cells by a retrovirus', *J Virol*, **78**(2): 576-584

**Carson, S.D.** (2001), 'Receptor for the group B coxsackieviruses and adenoviruses: CAR.' *Rev Med Virol*, **11**(4): 219-226

**Cell Signaling Technology**, URL:

[http://www.cellsignal.com/reference/pathway/Toll\\_Like.html](http://www.cellsignal.com/reference/pathway/Toll_Like.html)

**Chen, Z., Benureau, Y., Rijnbrand, R., Yi, J., Wang, T., Warter, L., Lanford, R.E., Weinman, S.A., Lemon, S.M., Martin, A., and Li, K.** (2007), 'GB virus B disrupts RIG-I signaling by NS3/4A-mediated cleavage of the adaptor protein MAVS', *J Virol*, **81**(2): 964-976

**Cheng, G., Zhong, J., Chung, J., and Chisari, F.V.** (2007), 'Double-stranded DNA and double-stranded RNA induce a common antiviral signaling pathway in human cells', *Proc Natl Acad Sci U S A*, **104**(21): 9035-9040

**Cho, M.W., Teterina, N., Egger, D., Bienz, K., and Ehrenfeld, E.** (1994), 'Membrane rearrangement and vesicle induction by recombinant poliovirus 2C and 2BC in human cells', *Virology*, **202**(1): 129-145

**Choe, J., Kelker, M.S., and Wilson, I.A.** (2005), 'Crystal structure of human toll-like receptor 3 (TLR3) ectodomain', *Science*, **309**(5734): 581-585

**Chuang, T.H., and Ulevitch, R.J.** (2000), 'Cloning and characterization of a sub-family of human toll-like receptors: hTLR7, hTLR8, and hTLR9', *Eur Cytokine Netw*, **11**(3): 372-378

**Coban, C., Ishii, K.J., Kawai, T., Hemmi, H., Sato, S., Uematsu, S., Yamamoto, M., Takeuchi, O., Itagaki, S., Kumar, N., Horii, T., and Akira, S.** (2005), 'Toll-like receptor 9 mediates innate immune activation by the malaria pigment hemozoin', *J Exp Med*, **201**(1): 19-25

**Compton, T., Kurt-Jones, E.A., Boehme, K.W., Belko, J., Latz, E., Golenbock, D.T., and Finberg, R.W.** (2003), 'Human cytomegalovirus activates inflammatory cytokine responses via CD14 and Toll-like receptor 2', *J Virol*, **77**(8): 4588-4596

**Cook, C.H., Trgovcich, J., Zimmerman, P.D., Zhang, Y., and Sedmak, D.D.** (2006), 'Lipopolysaccharide, tumor necrosis factor alpha, or interleukin-1beta triggers reactivation of latent cytomegalovirus in immunocompetent mice', *J Virol*, **80**(18): 9151-9158

**Coyne, C.B., Kim, K.S., and Bergelson, J.M.** (2007), 'Poliovirus entry into human brain microvascular cells requires receptor-induced activation of SHP-2', *EMBO J*, **26**(17): 4016-4028

**Crowell, R.L., and Philipson, L.** (1971), 'Specific alterations of the coxsackievirus B3 eluted from HeLa cells', *J Virol*, **8**(4): 509-515

**Cui, S., Eisenächer, K., Kirchhofer, A., Brzózka, K., Lammens, A., Lammens, K., Fujita, T., Conzelmann, K.K., Krug, A., and Hopfner, K.P.** (2008), 'The C-terminal regulatory domain is the RNA 5'-triphosphate sensor of RIG-I', *Mol Cell*, **29**(2): 169-179

**Deitz, S.B., Dodd, D.A., Cooper, S., Parham, P., and Kirkegaard, K.** (2000), 'MHC I-dependent antigen presentation is inhibited by poliovirus protein 3A', *Proc Natl Acad U S A*, **97**(25): 13790-13795

**Diebold, S.S., Kaisho, T., Hemmi, H., Akira, S., and Reis e Sousa, C.** (2004), 'Innate antiviral responses by means of TLR7-mediated recognition of single-stranded RNA', *Science*, **303**(5663): 1529-1531

**Doedens, J.R., and Kirkegaard, K.** (1995), 'Inhibition of cellular protein secretion by poliovirus proteins 2B and 3A', *EMBO J*, **14**(5): 894-907

**Doedens, J.R., Giddings, T.H. Jr., and Kirkegaard, K.** (1997), 'Inhibition of endoplasmic reticulum-to-Golgi traffic by poliovirus protein 3A: genetic and ultrastructural analysis', *J Virol*, **71**(12): 9054-9064

**Du, X., Poltorak, A., Wei, Y., and Beutler, B.** (2000), 'Three novel mammalian toll-like receptors: gene structure, expression, and evolution', *Eur Cytokine Netw*, **11**(3): 362-371

**Edelmann, K.H., Richardson-Burns, S., Alexopoulou, L., Tyler, K.L., Flavell, R.A., and Oldstone, M.B.** (2004), 'Does Toll-like receptor 3 play a biological role in virus infections?', *Virology*, **322**(2): 231-238

**English, R.F., Janosky, J.E., Ettedgui, J.A., and Webber, S.A.** (2004), 'Outcomes for children with acute myocarditis', *Cardiol Young*, **14**(5): 488-493

**Esceverri, A.C., and Dasgupta, A.** (1995), 'Amino terminal regions of poliovirus 2C protein mediate membrane binding', *Virology*, **208**(2): 540-553

**Fairweather, D., Yusung, S., Frisancho, S., Barrett, M., Gatewood, S., Steele, R., and Rose, N.R.** (2003), 'IL-12 receptor beta 1 and Toll-like receptor 4 increase IL-1 beta-and IL-18-associated myocarditis and coxsackievirus replication', *J Immunol*, **170**(9): 4731-4737

**Finberg, R.W., Wang, J.P., and Kurt-Jones, E.A.** (2007), 'Toll like receptors and viruses', *Rev Med Virol*, **17**(1): 35-43

**Fitzgerald, K.A., McWhirter, S.M., Faia, K.L., Rowe, D.C., Latz, E., Golenbock, D.T., Coyle, A.J., Liao, S.M., and Maniatis, T.** (2003), 'IKKepsilon and TBK1 are essential components of the IRF3 signaling pathway', *Nat Immunol*, **4**(5): 491-496

**Foy, E., Li, K., Sumpter, R.Jr., Loo, Y.M., Johnson, C.L., Wang, C., Fish, P.M., Yoneyama, M., Fujita, T., Lemon, S.M., and Gale, M. Jr. (2005),** ‘Control of antiviral defenses through hepatitis C virus disruption of retinoic acid-inducible gene-I signaling’, *Proc Natl Acad Sci U S A*, **102**(8): 2986-2991

**Fredericksen, B.L., and Gale, M. Jr. (2006),** ‘West Nile virus evades activation of interferon regulatory factor 3 through RIG-I-dependent and –independent pathways without antagonizing host defense signaling’, *J Virol*, **80**(6): 2913-2923

**Fredericksen, B.L., Keller, B.C., Fornek, J., Katze, M.G., and Gale, M. Jr. (2008),** ‘Establishment and maintenance of the innate antiviral response to West Nile Virus involves both RIG-I and MDA5 signaling through IPS-1’, *J Virol*, **82**(2): 609-616

**Fricks, C.E., and Hogle, J.M. (1990),** ‘Cell-induced conformational change in poliovirus: externalization of the amino terminus of VP1 is responsible for liposome binding’, *J Virol*, **64**(5): 1934-1945

**Gamarnik, A.V., and Andino, R. (2000),** ‘Interactions of viral protein 3CD and poly(rC) binding protein with the 5’ untranslated region of the poliovirus genome’, *J Virol*, **74**(5): 2219-2226

**Gantner, B.N., Simmons, R.M., Canavera, S.J., Akira, S., and Underhill, D.M. (2003),** ‘Collaborative induction of inflammatory responses by dectin-1 and Toll-like receptor 2’, *J Exp Med*, **197**(9): 1107-1117

**Gaudreault, E., Fiola, S., Olivier, M., and Gosselin, J.** (2007), 'Epstein-Barr virus induces MCP-1 secretion by human monocytes via TLR2', *J Virol*, **81**(15): 8016-8024

**Gay, N.J., and Keith, F.J.** (1991), 'Drosophila Toll and IL-1 receptor', *Nature*, **351**(6325): 355-356

**GE Healthcare Life Sciences**, Amersham ECL Western blotting detection reagents and analysis system Product Booklet, URL:  
[http://www.gelifesciences.com/aptrix/upp00919.nsf/Content/4DE67EABFB9A9D25C1257628001CDC12/\\$file/28955347AD.pdf](http://www.gelifesciences.com/aptrix/upp00919.nsf/Content/4DE67EABFB9A9D25C1257628001CDC12/$file/28955347AD.pdf)

**Giachettik C., Hwang, S.S., and Semler, B.L.** (1992), 'cis-acting lesions targeted to the hydrophobic domain of a poliovirus membrane protein involved in RNA replication', *J Virol*, **66**(10): 6045-6057

**Gitlin, L., Barchet, W., Gilfillan, S., Cella, M., Beutler, B., Flavell, R.A., Diamond, M.S., and Colonna, M.** (2006), 'Essential role of mda-5 in type 1 IFN responses to polyriboinosinic: polyribocytidylic acid and encephalomyocarditis picornavirus', *Proc Natl Acad Sci U S A*, **103**(22): 8459-8464

**Gitlin, L., Benoit, L., Song, C., Cella, M., Gilfillan, S., Holtzman, M.J., and Colonna, M.** (2010), 'Melanoma differentiation-associated gene 5 (MDA5) is involved in the innate immune response to Paramyxoviridae infection in vivo', *PLoS Pathog*, **6**(1): e1000734



- Gorbalenya, A.E., Koonin, E.V., Donchenko, A.P., and Blinov, V.M.** (1988), 'A novel superfamily of nucleoside triphosphate-binding motif containing proteins which are probably involved in duplex unwinding in DNA and RNA replication and recombination', *FEBS Lett.* **235**(1-2): 16-24
- Habjan, M., Andersson, I., Klingstrom, J., Schumann, M., Martin, A., Zimmermann, P., Wagner, V., Pichlmair, A., Schneider, U., Muhlberger, E., Mirazimi, A., and Weber, F.** (2008), 'Processing of genome 5' termini as a strategy of negative-strand RNA viruses to avoid RIG-I-dependent interferon induction', *PLoS One*, **3**(4): e2032
- Hayashi, F., Smith, K.D., Ozinsky, A., Hawn, T.R., Yi, E.C., Goodlett, D.R., Eng, J.K., Akira, S., Underhill, D.M., and Aderem, A.** (2001), 'The innate immune response to bacterial flagellin is mediated by Toll-like receptor 5', *Nature*, **410**(6832): 1099-1103
- Haynes, L.M., Moore, D.D., Kurt-Jones, E.A., Finberg, R.W., Anderson, L.J., and Tripp, R.A.** (2001), 'Involvement of toll-like receptor 4 in innate immunity to respiratory syncytial virus', *J Virol*, **75**(22): 10730-10737
- He, Y., Lin, F., Chipman, P.R., Bator, C.M., Baker, T.S., Shoham, M., Kuhn, R.J., Medof, M.E., and Rossmann, M.G.** (2002), 'Structure of decay-accelerating factor bound to echovirus 7: a virus receptor complex', *Proc Natl Acad Sci U S A*, **99**(16): 10325-10329

**Heil, F., Hemmi, H., Hochrein, H., Ampenberger, F., Kirschning, C., Akira, S., Lipford, G., Wagner, H., and Bauer, S.** (2004), 'Species-specific recognition of single-stranded RNA via toll-like receptor 7 and 8', *Science*, **303**(5663): 1526-1529

**Hewson, C.A., Jardine, A., Edwards, M.R., Laza-Stanca, V., and Johnston, S.L.** (2005), 'Toll-like receptor 3 is induced by and mediates antiviral activity against rhinovirus infection of human bronchial epithelial cells', *J Virol*, **79**(19): 12273-12279

**Hiscott, J., Lin, R., Nakhaei, P., and Paz, S.** (2006), 'MasterCARD: a priceless link to innate immunity', *Trends Mol Med*, **12**(2): 53-56

**Hoebe, K., Georgel, P., Rutschmann, S., Du, X., Mudd, S., Crozat, K., Sovath, S., Shamel, L., Hartung, T., Zähringer, U., and Beutler, B.** (2005), 'CD36 is a sensor of diacylglycerides', *Nature*, **433**(7025): 523-527

**Hornung, V., Ellegast, J., Kim, S., Brzozka, K., Jung, A., Kato, H., Poeck, H., Akira, S., Conzelmann, K., Schlee, M., Endres, S., and Hartmann, G.** (2006), '5'-Triphosphate RNA is the ligand for RIG-I', *Science*, **314**(5801): 994-997

**Hoshino, K., Takeuchi, O., Kawai, T., Sanjo, H., Ogawa, T., Takeda, Y., Takeda, K., and Akira, S.** (1999), 'Cutting edge: Toll-like receptor 4 (TLR4)-deficient mice are hyporesponsive to lipopolysaccharide: evidence for TLR4 as the Lps gene product', *J Immunol*, **162**(7): 3749-3752

**Huber, S., and Ramsingh, A.I.** (2004), 'Coxsackievirus-induced pancreatitis', *Viral Immunol*, **17**(3): 358-369

**Hühn, M.H., McCartney, S.A., Lind, K., Svedin, E., Colonna, M., and Flodström-Tullberg, M.** (2010), 'Melanoma differentiation-associated protein-5 (MDA-5) limits early viral replication but is not essential for the induction of type 1 interferons after Coxsackievirus infection', *Virology*, **401**(1): 42-48

**Iacobelli-Martinez, M., and Nemerow, G.R.** (2007), 'Preferential activation of Toll-like receptor nine by CD46-utilizing adenoviruses', *J Virol*, **81**(3): 1305-1312

**Ikegame, S., Takeda, M., Ohno, S., Nakatsu, Y., Nakanishi, Y., and Yanagi, Y.** (2010), 'Both RIG-I and MDA5 RNA helicases contribute to the induction of alpha/beta interferon in measles virus-infected human cells', *J Virol*, **84**(1): 372-379

**ImageJ**, URL:

<http://rsb.info.nih.gov/ij/>

**ImageJ Plugins**, URL:

<http://rsbweb.nih.gov/ij/plugins/track/jacop.html>

**Invivogen**, URL:

<http://www.invivogen.com/rlr-shrna>

**Isogawa, M., Robek, M.D., Furuichi, Y., and Chisari, F.V.** (2005), 'Toll-like receptor signaling inhibits hepatitis B virus replication in vivo', *J Virol*, **79**(11): 7269-7272

**Janeway, C.A. Jr.** (1989), 'Approaching the asymptote? Evolution and revolution in immunology', *Cold Spring Harb Symp Quant Biol*, **54**(1): 1-13

**Jang, S.K., Kräusslich, H.G., Nicklin, M.J., Duke, G.M., Palmenberg, A.C., and Wimmer, E.** (1988), 'A segment of the 5' nontranslated region of encephalomyocarditis virus RNA directs internal entry of ribosomes during in vitro translation', *J Virol*, **62**(8): 2636-2643

**Jin, M.S., Kim, S.E., Heo, J.Y., Lee, M.E., Kim, H.M., Paik, S.G., Lee, H., and Lee, J.O.** (2007), 'Crystal structure of the TLR1-TLR2 heterodimer induced by binding of a tri-acylated lipopeptide', *Cell*, **130**(6): 1071-1082

**Jin, M.S., and Lee, J.O.** (2008), 'Structures of the toll-like receptor family and its ligand complexes', *Immunity*, **29**(2): 182-191

**Johnson, C.L., and Gale, M. Jr.** (2006), 'CARD games between virus and host get a new player', *Trends Immunol*, **27**(1): 1-4

**Jore, J., De Geus, B., Jackson, R.J., Pouwels, P.H., and Enger-Valk, B.E.** (1988), 'Poliovirus protein 3CD is the active protease for processing of the precursor protein P1 in vitro', *J Gen Virol*, **69**(7): 1627-1636

**Ju, Y., Wang, T., Li, Y., Xin, W., Wang, S., and Li, J.** (2007), 'Coxsackievirus B3 affects endothelial tight junctions: possible relationship to ZO-1 and F-actin, as well as p38 MAPK activity', *Cell Biol Int*, **31**(10): 1207-1213

**Kang, D.C., Gopalkrishnan, R.V., Wu, Q., Jankowsky, E., Pyle, A.M., and Fisher, P.B.** (2002), 'mda-5: An interferon-inducible putative RNA helicase with double-stranded RNA-dependent ATPase activity and melanoma growth-suppressive properties', *Proc Natl Acad Sci U S A*, **99**(2): 637-642

**Kang, J.Y., Nan, X., Jin, M.S., Youn, S.J., Ryu, Y.H., Mah, S., Han, S.H., Lee, H., Paik, S.G., and Lee, J.O.** (2009), 'Recognition of lipopeptide patterns by Toll-like receptor 2-Toll-like receptor 6 heterodimer', *Immunity*, **31**(6): 873-884

**Karin, M., and Ben-Neriah, Y.** (2000), 'Phosphorylation meets ubiquitination: the control of NF-[kappa]B activity', *Annu Rev Immunol*, **18**: 621-663

**Kato, H., Takeuchi, O., Mikamo-Satoh, E., Hirai, R., Kawai, T., Matsushita, K., Hiiragi, A., Dermody, T.S., Fujita, T., and Akira, S.** (2008), 'Length-dependent recognition of double-stranded ribonucleic acids by retinoic acid-inducible gene-I and melanoma differentiation-associated gene 5', *J Exp Med*, **205**(7): 1601-1610

**Kato, H., Takeuchi, O., Sato, S., Yoneyama, M., Yamamoto, M., Matsui, K., Uematsu, S., Jung, A., Kawai, T., Ishii, K.J., Yamaguchi, O., Otsu, K., Tsujimura, T., Koh, C.S., Reis e Sousa, C., Matsuura, Y., Fujita, T., and Akira, S.** (2006), 'Differential roles of MDA5 and RIG-I helicases in the recognition of RNA viruses', *Nature*, **441**(7089): 101-105

**Kawai, T. and Akira, S.** (2006), 'Innate immune recognition of viral infection', *Nat Immunol*, **7**(2): 131-137

**Kawai, T., Takahashi, K., Sato, S., Coban, C., Kumar, H., Kato, H., Ishii, K.J., Takeuchi, O., and Akira, S.** (2005), 'IPS-1, an adaptor triggering RIG-I- and Mda5-mediated type 1 interferon induction', *Nat Immunol*, **6**(10): 981-988

**Kerekatte, V., Keiper, B.D., Badorff, C., Knowlton, K.U., and Rhoads, R.E.** (1999), 'Cleavage of Poly(A)-binding protein by coxsackievirus 2A protease in vitro and in vivo: another mechanism for host protein synthesis shutoff?', *J Virol*, **73**(1): 709-717

**Kerkvliet J., Edukulla, R., and Rodriguez, M.** (2010), 'Novel roles of the picornaviral 3D polymerase in viral pathogenesis', *Adv Virol*, **2010**: 368068

**Kim, H.M., Park, B.S., Kim, J.I., Kim, S.E., Lee, J., Oh, S.C., Enkhbayar, P., Matsushima, N., Lee, H., Yoo, O.J., and Lee, J.O.** (2007), 'Crystal structure of the TLR4-MD-2 complex with bound endotoxin antagonist Eritoran', *Cell*, **130**(5): 906-917

**Kitchens, R.L.** (2000), 'Role of CD14 in cellular recognition of bacterial lipopolysaccharides', *Chem Immunol*, **74**: 61-82

**Komabitech**, URL:

<http://www.komabitech.co.kr/www/techniques/immunodection/wbProtocol.html>

**Komuro, A., and Horvath, C.M.** (2006), 'RNA-and virus-independent inhibition of antiviral signaling by RNA helicase LGP2', *J Virol*, **80**(24): 12332-12342

**Kräusslich, H.G., Nicklin, M.J., Toyoda, H., Etchison, D., and Wimmer, E.** (1987), 'Poliovirus proteinase 2A induces cleavage of eucaryotic initiation factor 4F polypeptide p220', *J Virol*, **61**(9): 2711-2718

**Krug, A., Luker, G.D., Barchet, W., Leib, D.A., Akira, S., and Colonna, M.** (2004), 'Herpes simplex virus type 1 activates murine natural interferon-producing cells through toll-like receptor 9', *Blood*, **103**(4): 1433-1437

**Kumar, H., Kawai, T., Kato, H., Sato, S., Takahashi, K., Coban, C., Yamamoto, M., Uematsu, S., Ishii, K.J., Takeuchi, O., and Akira, S.** (2006), 'Essential role of IPS-1 in innate immune responses against RNA viruses', *J Exp Med*, **203**(7): 1795-1803

**Kurt-Jones, E.A., Chan, M., Zhou, S., Wang, J., Reed, G., Bronson, R., Arnold, M.M., Knipe, D.M., and Finberg, R.W.** (2004), 'Herpes simplex virus 1 interaction with Toll-like receptor 2 contributes to lethal encephalitis', *Proc Natl Acad Sci U S A*, **101**(5): 1315-1320

**Kurt-Jones, E.A., Popova, L., Kwinn, L., Haynes, L.M., Jones, L.P., Tripp, R.A., Walsh, E.E., Freeman, M.W., Golenbock, D.T., Anderson, L.J., and Finberg, R.W.** (2000), 'Pattern recognition receptors TLR4 and CD14 mediate response to respiratory syncytial virus', *Nat Immunol*, **1**(5): 398-401

**Lee, B.E., and Davies, H.D.** (2007), 'Aseptic Meningitis', *Curr Opin Infect Dis*, **20**(3): 272-277

**Le Gall, O., Christian, P., Fauquet, C.M., King, A.M., Knowles, N.J., Nakashima, N., Stanway, G., and Gorbalenya, A.E.** (2008), 'Picornavirales, a proposed order of positive-sense single-stranded RNA viruses with a pseudo-T = 3 virion architecture', *Arch Virol*, **153**(4): 715-727

**Le Goffic, R., Pothlichet, J., Vitour, D., Fujita, T., Meurs, E., Chignard, M., and Si-Tahar, M.** (2007), 'Cutting Edge: Influenza A virus activates TLR3-dependent inflammatory and RIG-I-dependent antiviral responses in human lung epithelial cells', *J Immunol*, **178**(6): 3368-3372



**Lei, Y., Moore, C.B., Liesman, R.M., O'Connor, B.P., Bergstralh, D.T., Chen, Z.J., Pickles, R.J., and Ting, J.P.** (2009), 'MAVS-mediated apoptosis and its inhibition by viral proteins', *PLoS One*, **4**(5): e5466

**Lemaitre, B., Nicolas, E., Michaut, L., Reichhart, J.M., and Hoffman, J.A.** (1996), 'The dorsoventral regulatory gene cassette spätzle/Toll/cactus controls the potent antifungal response in *Drosophila* adults', *Cell*, **86**(6): 973-983

**Li, H., Zhang, J., Kumar, A., Zheng, M., Atherton, S.S., and Yu, F.S.** (2006), 'Herpes simplex virus 1 infection induces the expression of proinflammatory cytokines, interferons and TLR7 in human corneal epithelial cells', *Immunology*, **117**(2): 167-176

**Li, K., Foy, E., Ferreon, J.C., Nakamura, M., Ferreon, A.C., Ikeda, M., Ray, S.C., Gale, M. Jr., and Lemon, S.M.** (2005), 'Immune evasion by hepatitis C virus NS3/4A protease-mediated cleavage of the Toll-like receptor 3 adaptor protein TRIF', *Proc Natl Acad Sci U S A*, **102**(8): 2992-2997

**Li, S., Strelow, A., Fontana, E.J., and Wesche, H.** (2002), 'IRAK-4: a novel member of the IRAK family with the properties of an IRAK-kinase', *Proc Natl Acad Sci U S A*, **99**(8): 5567-5572

**Li, X.D., Sun, L., Seth, R.B., Pineda, G., and Chen, Z.J.** (2005), ‘Hepatitis C virus protease NS3/4A cleaves mitochondrial antiviral signaling protein off the mitochondria to evade innate immunity’, *Proc Natl Acad Sci U S A*, **102**(49): 17717-17722

**Li, X., Lu, H.H., Mueller, S., and Wimmer, E.** (2001), ‘The C-terminal residues of polio virus proteinase 2A(pro) are critical for viral RNA replication but not for cis- or trans-proteolytic cleavage’, *J Gen Virol*, **82**(2): 397-408

**Li, X., Ranjith-Kumar, C.T., Brooks, M.T., Dharmaiah, S., Herr, A.B., Kao, C., and Li, P.** (2009), ‘The RIG-I-like receptor LGP2 recognizes the termini of double-stranded RNA’, *J Biol Chem*, **284**(20): 13881-13891

**Lin, L., Su, Z., Lebedeva, I.V., Gupta, P., Boulkerche, H., Rai, T., Barber, G.N., Dent, P., Sarkar, D., and Fisher, P.B.** (2006), ‘Activation of Ras/Raf protects cells from melanoma differentiation-associated gene-5-induced apoptosis’, *Cell Death Differ*, **13**(11): 1982-1993

**Loo, Y.M., Fornek, J., Crochet, N., Bajwa, G., Perwitasari, O., Martinez-Sobrido, L., Akira, S., Gill, M.A., García-Sastre, A., Katze, M.G., and Gale, M. Jr.** (2008), ‘Distinct RIG-I and MDA5 signaling by RNA viruses in innate immunity’, *J Virol*, **82**(1): 335-345

**Loo, Y.M., Owen, D.M., Li, K., Erickson, A.K., Johnson, C.L., Fish, P.M., Carney, D.S., Wang, T., Ishida, H., Yoneyama, M., Fujita, T., Saito, T., Lee, W.M., Hagedorn, C.H., Lau, D.T., Weinman, S.A., Lemon, S.M., and Gale, M. Jr.** (2006), ‘Viral and therapeutic control of IFN-beta promoter stimulator 1 during hepatitis C virus infection’, *Proc Natl Acad Sci U S A*, **103**(15): 6001-6006

**Lund, J.M., Alexopoulou, L., Sato, A., Karow, M., Adams, N.C., Gale, N.W., Iwasaki, A., and Flavell, R.A.** (2004), ‘Recognition of single-stranded RNA viruses by Toll-like receptor 7’, *Proc Natl Acad Sci U S A*, **101**(15): 5598-5603

**Lund, J., Sato, A., Akira, S., Medzhitov, R., and Iwasaki, A.** (2003), ‘Toll-like receptor 9-mediated recognition of Herpes simplex virus-2 by plasmacytoid dendritic cells’, *J Exp Med*, **198**(3): 513-520

**MacBiophotonics**, URL:

<http://www.macbiophotonics.ca/downloads.htm>

**MacPherson, J.I., Sidders, B., Wieland, S., Zhong, J., Targett-Adams, P., Lohmann, V., Backes, P., Delpuech-Adams, O., Chisari, F., Lewis, M., Parkinson, T., and Robertson, D.L.** (2011), ‘An integrated transcriptomic and meta-analysis of hepatoma cells reveals factors that influence susceptibility to HCV infection’, *PLoS One*, **6**(10): e25584

**Malathi K., Dong, B., Gale, M. Jr., and Silverman, R.H.** (2007), ‘Small self-RNA generated by RNase L amplifies antiviral innate immunity’, *Nature*, **448**(7155): 816-819

**Mandl, J.N., Barry, A.P., Vanderford, T.H., Kozyr, N., Chavan, R., Klucking, S., Barrat, F.J., Coffman, R.L., Staprans, S.I., and Feinberg, M.B.** (2008), ‘Divergent TLR7 and TLR9 signaling and type 1 interferon production distinguish pathogenic and non-pathogenic AIDS virus infections’, *Nat Med*, **14**(10): 1077-1087

**Manolio, T.A., Baughman, K.L., Rodeheffer, R., Pearson, T.A., Bristow, J.D., Michels, V.V., Abelmann, W.H., and Harlan W.R.** (1992), ‘Prevalence and etiology of idiopathic dilated cardiomyopathy’, *Am J Cardiol*, **69**(17): 1458–1466.

**Martinez-Salas, E., and Fernandez-Miragall, O.** (2004), ‘Picornavirus IRES: structure function relationship’, *Curr Pharm Des*, **10**(30): 3757-3767

**Martinon, F., Mayor, A., and Tschopp, J.** (2009), ‘The inflammasomes: guardians of the body’, *Annu Rev Immunol*, **27**: 229-265

**McCartney, S.A., Thackray, L.B., Gitlin, L., Gilfillan, S., Virgin, H.W., and Colonna, M.** (2008), ‘MDA-5 recognition of a murine norovirus’, *PLoS Pathog*, **4**(7): e1000108

**Medzhitov, R., Preston-Hurlburt, P., and Janeway, C.A. Jr.** (1997), 'A human homologue of the *Drosophila* Toll protein signals activation of adaptive immunity', *Nature*, **388**(6640): 394-397

**Melchjorsen, J., Jensen, S.B., Malmgaard, L., Rasmussen, S.B., Weber, F., Bowie, A.G., Matikainen, S., and Paludan, S.R.** (2005), 'Activation of innate defense against a paramyxovirus is mediated by RIG-I and TLR7 and TLR8 in a cell-type-specific manner', *J Virol*, **79**(20): 12944-12951

**Meylan, E., Curran, J., Hofmann, K., Moradpour, D., Binder, M., Bartenschlager, R., and Tschopp, J.** (2005), 'Cardif is an adaptor protein in the RIG-I antiviral pathway and is targeted by hepatitis C virus', *Nature*, **437**(7062): 1167-1172

**Mibayashi, M., Martinez-Sobrido, L., Loo, Y.M., Cardenas, W.B., Gale, M. Jr., and Garcia-Sastre, A.** (2007), 'Inhibition of retinoic acid-inducible gene I-mediated induction of beta interferon by the NS1 protein of influenza A virus', *J Virol*, **81**(2): 514-524

**MicrobiologyBytes**, URL:

<http://www.microbiologybytes.com/virology/Picornaviruses.html>

**Molla, A., Harris, K.S., Paul, A.V., Shin, S.H., Mugavero, J., and Wimmer, E.** (1994), 'Stimulation of poliovirus proteinase 3Cpro-related proteolysis by the genome-linked protein VPg and its precursor 3AB', *J Biol Chem*, **269**(43): 27015-27020

**Mosser, A.G., Caliguiri, L.A., and Tamm, I.** (1972), 'Incorporation of lipid precursors into cytoplasmic membranes of poliovirus-infected HeLa cells', *Virology*, **47**(1): 39-47

**Muckelbauer, J.K., Kremer, M., Minor, I., Diana, G., Dutko, F.J., Groarke, J., Pevear, D.C., and Rossmann, M.G.** (1995), 'The structure of coxsackievirus B3 at 3.5 Å resolution', *Structure*, **3**(7): 653-667

**Mukherjee, A., Morosky, S.A., Shen, L., Weber, C.R., Turner, J.R., Kim, K.S., Wang, T., and Coyne, C.B.** (2009), 'Retinoic acid-inducible gene-1 (RIG-I) associates with the actin cytoskeleton via caspase activation and recruitment domain-dependent interactions', *J Biol Chem*, **284**(10): 6488-6494

**Murray, K.E., and Barton, D.J.** (2003), 'Poliovirus CRE-dependent VPg uridylylation is required for positive sense RNA synthesis but not for negative-strand RNA synthesis', *J Virol*, **77**(8): 4739-4750

**Nakabayashi, H., Taketa, K., Miyano, K., Yamane, T., and Sato, J.** (1982), 'Growth of human hepatoma cells lines with differentiated functions in chemically defined medium', *Cancer Res*, **42**(9): 3858-3863

**Nasirudeen, A.M., Wong, H.H., Thien, P., Xu, S., Lam, K.P., and Liu, D.X.** (2011), 'RIG-I, MDA5 and TLR3 synergistically play an important role in restriction of dengue virus infection', *PLoS Negl Trop Dis*, **5**(1): e926

**National Diagnostics, URL:**

[http://www.nationaldiagnostics.com/article\\_info.php/articles\\_id/53](http://www.nationaldiagnostics.com/article_info.php/articles_id/53)

**NCBI Taxonomy Browser, URL:**

<http://www.ncbi.nlm.nih.gov/Taxonomy/Browser/wwwtax.cgi?id=12058>

**Nicholson-Weller, A., and Wang, C.E.** (1994), 'Structure and function of decay accelerating factor CD55', *J Lab Clin Med*, **123**(4): 485-491

**Nicklin, M.J., Kräusslich, H.G., Toyoda, H., Dunn, J.J., and Wimmer, E.** (1987), 'Poliovirus polypeptide precursors: expression in vitro and processing by exogenous 3C and 2A proteinases', *Proc Natl Acad Sci U S A*, **84**(12): 4002-4006

**Nikon MicroscopyU, URL:**

<http://www.microscopyu.com/articles/confocal/confocalintrobasics.html>

**Novak, J.E., and Kirkegaard, K.** (1991), 'Improved method for detecting poliovirus negative strands used to demonstrate specificity of positive-strand encapsidation and the ratio of positive to negative strands in infected cells', *J Virol*, **65**(6): 3384-3387

**Oganesyan, G., Saha, S.K., Guo, B., He, J.Q., Shahangian, A., Zarnegar, B., Perry, A., and Cheng, G.** (2006), 'Critical role of TRAF3 in the Toll-like receptor-dependent and –independent antiviral response', *Nature*, **439**(7073): 208-211

**Ohman, T., Rintahaka, J., Kalkkinen, N., Matikainen, S., and Nymen, T.A.** (2009), 'Actin and RIG-I/MAVS signaling components translocate to mitochondria upon influenza A virus infection of human primary macrophages', *J Immunol*, **182**(9): 5682-5692

**Orthopoulos, G., Triantafilou, K., and Triantafilou, M.** (2004), 'Coxsackie B viruses use multiple receptors to infect human cardiac cells', *J Med Virol*, **74**(2): 291-299

**Palmenberg, A.C.** (1982), 'In vitro synthesis and assembly of picornaviral capsid intermediate structures', *J Virol*, **44**(3): 900-906

**Park, H.H., Lo, Y.C., Lin, S.C., Wang, L., Yang, J.K., and Wu, H.** (2007), 'The death domain superfamily in intracellular signaling of apoptosis and inflammation', *Annu Rev Immunol*, **25**: 561-586

**Pathak, H.B., Oh, H.S., Goodfellow, I.G., Arnold, J.J., and Cameron, C.E.** (2008), 'Picornavirus genome replication: roles of precursor proteins and rate-limiting steps in oril-dependent VPg uridylylation', *J Biol Chem*, **283**(45): 30677-30688



**Paul, A.V., Cao, X., Harris, K.S., Lama, J., and Wimmer, E.** (1994), 'Studies with poliovirus polymerase 3Dpol. Stimulation of poly(U) synthesis in vitro by purified poliovirus protein 3AB', *J Biol Chem*, **269**(46): 29173-29181

**Paul, A.V., van Boom, J.H., Filippov, D., and Wimmer, E.** (1998), 'Protein-primed RNA synthesis by purified poliovirus RNA polymerase', *Nature*, **393**(6682): 280-284

**Pelletier, J., Kaplan, G., Racaniello, V.R., and Sonenberg, N.** (1988), 'Cap-independent translation of poliovirus mRNA is conferred by sequence elements within the 5' noncoding region', *Mol Cell Biol*, **8**(3): 1103-1112

**Pelletier, J., and Sonenberg, N.** (1988), 'Internal initiation of translation of eukaryotic mRNA directed by a sequence derived from poliovirus RNA', *Nature*, **334**(6180): 320-325

**Petrella, J., Cohen, C.J., Gaetz, J., and Bergelson, J.M.** (2002), 'A zebrafish coxsackievirus and adenovirus receptor homologue interacts with coxsackie B virus and adenovirus', *J Virol*, **76**(20): 10503-10506

**Pichlmair, A., Schulz, O., Tan, C.P., Näslund, T.I., Liljeström, P., Weber, F., and Reis e Sousa, C.** (2006), 'RIG-I-mediated antiviral responses to single-stranded RNA bearing 5'-phosphates', *Science*, **314**(5801): 997-1001

**Picornaviridae, Enteroviruses, URL:**

<http://www.picornaviridae.com/enterovirus/enterovirus.htm>

**Pippig, D.A., Hellmuth, J.C., Cui, S., Kirchhofer, A., Lammens, K., Lammens, A., Schmidt, A., Rotherfusser, S., and Hopfner, K.P.** (2009), 'The regulatory domain of the RIG-I family ATPase LGP2 senses double-stranded RNA', *Nucleic Acids Res*, **37**(6): 2014-2025

**Poeck, H., Bscheider, M., Gross, O., Finger, K., Roth, S., Rebsamen, M., Hanneschläger, N., Schlee, M., Rotherfusser, S., Barchet, W., Kato, H., Akira, S., Inoue, S., Endres, S., Peschel, C., Hartmann, G., Hornung, V., and Ruland, J.** (2010), 'Recognition of RNA virus by RIG-I results in activation of CARD9 and inflammasome signaling for interleukin 1 beta production', *Nat Immunol*, **11**(1): 63-69

**Pollack, R., and Goldman, R.** (1973), 'Synthesis of infective poliovirus in BSC-1 monkey cells enucleated with Cytochalasin B', *Science*, **179**(76): 915-916

**Potter, J.A., Randall, R.E., and Taylor, G.L.** (2008), 'Crystal structure of human IPS-1/MAVS/VISA/Cardif caspase activation recruitment domain', *BMC Struct Biol*, **8**:11

**Racaniello, V.R., and Baltimore, D.** (1981), 'Molecular cloning of poliovirus cDNA and determination of the complete nucleotide sequence of the viral genome', *Proc Natl Acad U S A*, **78**(8): 4887-4891

**Rehwinkel, J., and Reis e Sousa, C.** (2010), 'RIGorous detection: exposing virus through RNA sensing', *Science*, **327**(5963): 284-286

**Rehwinkel, J., Tan, C.P., Goubau, D., Schulz, O., Pichlmair, A., Bier, K., Robb, N., Vreede, F., Barclay, W., Fodor, E., and Reis e Sousa, C.** (2010), 'RIG-I detects viral genomic RNA during negative-strand RNA virus infection', *Cell*, **140**(3): 397-408

**Rieder, E., Paul, A.V., Kim, D.W., van Boom, J.H., and Wimmer, E.** (2000), 'Genetic and biochemical studies of poliovirus cis-acting replication element cre in relation to VPg uridylylation', *J Virol*, **74**(22): 10371-10380

**Rock, F.L., Hardiman, G., Timans, J.C., Kastelein, R.A., and Bazan, J.F.** (1998), 'A family of human receptors structurally related to Drosophila Toll', *Proc Natl Acad Sci U S A*, **95**(2): 588-593

**Rohll, J.B., Moon, D.H., Evans, D.J., and Almond, J.W.** (1995), 'The 3' untranslated region of picornavirus RNA: features required for efficient genome replication', *J Virol*, **69**(12): 7835-7844

**Rossman, M.G., Arnold, E., Erickson, J.W., Frankenberger, E.A., Griffith, J.P., Hecht, H.J., Johnson, J.E., Kamer, G., Luo, M., Mosser, A.G., Rueckert, R.R., Sherry, B., and Vriend, G.** (1985), 'Structure of a human common cold virus and functional relationship to other picornaviruses', *Nature*, **317**(6033): 145-153

**Rossmann, M.G., He, Y., and Kuhn, R.J.** (2002), 'Picornavirus-receptor interactions', *Trends Microbiol*, **10**(7): 324-331

**Rothenfusser, S., Goutagny, N., DiPerna, G., Gong, M., Monks, B.G., Schoenemeyer, A., Yamamoto, M., Akira, S., and Fitzgerald, K.A.** (2005), 'The RNA helicase Lgp2 inhibits TLR-independent sensing of viral replication by retinoic acid-inducible gene-I', *J Immunol*, **175**(8): 5260-5268

**Rudd, B.D., Burstein, E., Duckett, C.S., Li, X., and Lukacs, N.W.** (2005), 'Differential role for TLR3 in respiratory syncytial virus-induced chemokine expression', *J Virol*, **79**(6): 3350-3357

**Saha, S.K., Pietras, E.M., He, J.Q., Kang, J.R., Liu, S.Y., Oganessian, G., Shahangian, A., Zarnegar, B., Shiba, T.L., Wang, Y., and Cheng, G.** (2006), 'Regulation of antiviral responses by a direct and specific interaction between TRAF3 and Cardif', *EMBO J*, **25**(14): 3257-3263

**Saito, T., Hirai, R., Loo, Y.M., Owen, D., Johnson, C.L., Sinha, S.C., Akira, S., Fujita, T., and Gale, M. Jr.** (2007), 'Regulation of innate antiviral defenses through a shared repressor domain in RIG-I and LGP2', *Proc Natl Acad Sci U S A*, **104**(2): 582-587

**Saito, T., Owen, D.M., Jiang, F., Marcotrigiano, J., Gale, M. Jr.** (2008), 'Innate immunity induced by composition-dependent RIG-I recognition of hepatitis C virus RNA', *Nature*, **454**(7203): 523-527

**Sato, A., Linehan, M.M., and Iwasaki, A.** (2006), ‘Dual recognition of herpes simplex viruses by TLR2 and TLR9 in dendritic cells’, *Proc Natl Acad Sci U S A*, **103**(46): 17343-17348

**Sato, K., Ishikawa, T., Okumura, A., Yamauchi, T., Sato, S., Avada, M., Matsumoto, E., Hotta, N., Oohashi, T., Fukuzawa, Y., and Kakumu, S.** (2007), ‘Expression of Toll-like receptors in chronic hepatitis C virus infection’, *J Gastroenterol Hepatol*, **22**(10): 1627-1632

**Satoh, T., Kato, H., Kumagai, Y., Yoneyama, M., Sato, S., Matsushita, K., Tsujimura, T., Fujita, T., Akira, S., and Takeuchi, O.** (2010), ‘LGP2 is a positive regulator of RIG-I-and MDA5-mediated antiviral responses’, *Proc Natl Acad Sci U S A*, **107**(4): 1512-1517

**Schlee, M., and Hartmann, G.** (2010), ‘The chase for the RIG-I ligand – recent advances’, *Mol Ther*, **18**(7): 1254-1262

**Schlegel, A., Giddings, T.H. Jr., Ladinsky, M.S., and Kirkegaard, K.** (1996), ‘Cellular origin and ultrastructure of membranes induced during poliovirus infection’, *J Virol*, **70**(10): 6576-6588

**Schmidt, A., Schwerd, T., Hamm, W., Hellmuth, J.C., Cui, S., Wenzel, M., Hoffmann, F.S., Michallet, M.C., Besch, R., Hopfner, K.P., Endres, S., and Rothenfusser, S.** (2009), '5-triphosphate RNA requires base-paired structures to activate antiviral signaling via RIG-I', *Proc Natl Acad Sci U S A*, **106**(29): 12067-12072

**Sean, P., Nguyen, J.H., and Semler, B.L.** (2009), 'Altered interactions between stem-loop IV within the 5' noncoding region of coxsackievirus RNA and poly(rC) binding protein 2: effects on IRES-mediated translation and viral infectivity', *Virology*, **389**(1-2): 45-58

**Seth, R.B., Sun, L., Ea, C.K., and Chen, Z.J.** (2005), 'Identification and characterization of MAVS, a mitochondrial antiviral signaling protein that activates NF-kappaB and IRF 3', *Cell*, **122**(5): 669-682

**Shafren, D.R., Bates, R.C., Agrez, M.V., Herd, R.L., Burns, G.F., and Barry, R.D.** (1995), 'Coxsackieviruses B1, B3, and B5 use decay accelerating factor as a receptor for cell attachment', *J Virol*, **69**(6): 3873-3877

**Sharma, S., tenOever, B.R., Grandvaux, N., Zhou, G.P., Lin, R., and Hiscott, J.** (2003), 'Triggering the interferon antiviral response through an IKK-related pathway', *Science*, **300**(5622): 1148-1151

**Shimazu, R., Akashi, S., Ogata, H., Nagai, Y., Fukudome, K., Miyake, K., and Kimoto, M.** (1999), 'MD-2, a molecule that confers lipopolysaccharide responsiveness on Toll-like receptor 4', *J Exp Med*, **189**(11): 1777-1782

**Slater, L., Bartlett, N.W., Haas, J.J., Zhu, J., Message, S.D., Walton, R.P., Sykes, A., Dahdaleh, S., Clarke, D.L., Belvisi, M.G., Kon, O.M., Fujita, T., Jeffery, P.K., Johnston, S.L., and Edwards, M.R.** (2010), 'Co-ordinated role of TLR3, RIG-I and MDA5 in the innate response to rhinovirus in bronchial epithelium', *PLoS Pathog*, **6**(11): e1001178

**Smith, A.D., and Dawson, H.** (2006), 'Glutathione is required for efficient production of infectious picornavirus virions', *Virology*, **353**(2): 258-267

**Smyth, M.S., and Martin, J.H.** (2002), 'Picornavirus uncoating', *Mol Pathol*, **55**(4): 214-219

**Spector, D.H., and Baltimore, D.** (1974), 'Requirement of 3'-terminal poly(adenylic acid) for the infectivity of poliovirus RNA', *Proc Natl Acad Sci U S A*, **71**(8): 2983-2987

**Stack, J., Haga, I.R., Schroder, M., Bartlett, N.W., Maloney, G., Reading, P.C., Fitzgerald, K.A., Smith, G.L., and Bowie, A.G.** (2005), 'Vaccinia virus protein A46R targets multiple Toll-like-interleukin-1 receptor adaptors and contributes to virulence', *J Exp Med*, **201**(6): 1007-1018

**Strikas, R.A., Anderson, L.J., and Parker, R.A.** (1986), 'Temporal and Geographic Patterns of Isolates of Nonpolio Enterovirus in the United States, 1970 – 1983', *J Infect Dis*, **153**(2): 346-351

**Sumpter, R. Jr. Loo, Y.M., Foy, E., Li, K., Yoneyama, M., Fujita, T., Lemon, S.M., and Gale, M. Jr.** (2005), 'Regulating intracellular antiviral defense and permissiveness to hepatitis C virus RNA replication through a cellular RNA helicase, RIG-I', *J Virol*, **79**(5): 2689-2699

**Sun, Q., Sun, L., Liu, H.H., Chen, X., Seth, R.B., Forman, J., and Chen, Z.J.** (2006), 'The specific and essential role of MAVS in antiviral innate immune responses', *Immunity*, **24**(5): 633-642

**Szomolanyi-Tsuda, E., Liang, X., Welsh, R.M., Kurt-Jones, E.A., and Finberg R.W.** (2006), 'Role for TLR2 in NK cell-mediated control of murine cytomegalovirus in vivo', *J Virol*, **80**(9): 4286-4291

**Tabeta, K., Georgel, P., Janssen, R., Du, X., Hoebe, K., Crozat, K., Mudd, S., Shamel, L., Sovath, S., Goode, J., Alexopoulou, L., Flavell, R.A., and Beutler, B.** (2004), 'Toll-like receptors 9 and 3 as essential components of innate immune defence against mouse cytomegalovirus infection', *Proc Natl Acad Sci U S A*, **101**(10): 3516-3521



**Takahashi, K., Kawai, T., Kumar, H., Sato, S., Yonehara, S., and Akira, S.** (2006), 'Roles of caspase-8 and caspase-10 in innate immune response to double-stranded RNA', *J Immunol*, **176**(8): 4520-4524

**Takahasi, K., Kumeta, H., Tsuduki, N., Narita, R., Shigemoto, T., Hirai, R., Yoneyama, M., Horiuchi, M., Ogura, K., Fujita, T., and Inagaki, F.** (2009), 'Solution structures of cytosolic RNA sensor MDA5 and LGP2 C-terminal domains: identification of the RNA recognition loop in RIG-I-like receptors', *J Biol Chem*, **284**(26): 17465-17474

**Takahasi, K., Yoneyama, M., Nishihori, T., Hirai, R., Kumeta, H., Narita, R., Gale, M. Jr., Inagaki, F., and Fujita, T.** (2008), 'Nonself RNA-sensing mechanism of RIG-I helicase and activation of antiviral immune responses', *Mol Cell*, **29**(4): 428-440

**Takeda, K., and Akira, S.** (2005), 'Toll-like receptors in innate immunity', *Int Immunol*, **17**(1): 1-14

**Takeuchi, O., and Akira, S.** (2007), 'Recognition of viruses by innate immunity', *Immunol Rev*, **220**: 214-224

**Takeuchi, O., Kawai, T., Mühlradt, P.F., Morr, M., Radolf, J.D., Zychlinsky, A., Takeda, K., and Akira, S.** (2001), 'Discrimination of bacterial lipoproteins by Toll-like receptor 6', *Int Immunol*, **13**(7): 933-940

**Takeuchi, O., Kawai, T., Sanjo, H., Copeland, N.G., Gilbert, D.J., Jenkins, N.A., Takeda, K., and Akira, S.** (1999), 'TLR6: A novel member of an expanding toll-like receptor family', *Gene*, **231**(1-2): 59-65

**Takeuchi, O., Sato, S., Horiuchi, T., Hoshino, K., Takeda, K., Dong, Z., Modlin, R.L., and Akira, S.** (2002), 'Cutting edge: role of Toll-like receptor 1 in mediating immune response to microbial lipoproteins', *J Immunol*, **169**(1): 10-14

**Tosteson, M.T., and Chow, M.** (1997), 'Characterization of the ion channels formed by poliovirus in planar lipid membranes', *J Virol*, **71**(1): 507-511

**Towner, J.S., Ho, T.V., and Semler, B.L.** (1996), 'Determinants of membrane association for the poliovirus protein 3AB', *J Biol Chem*, **271**(43): 26810-26818

**Toyoda, H., Nicklin, M.J., Murray, M.G., Anderson, C.W., Dunn, J.J., Studier, F.W., and Wimmer, E.** (1986), 'A second virus-encoded proteinase involved in proteolytic processing of poliovirus polyprotein', *Cell*, **45**(5): 761-770

**Triantafilou, K., and Triantafilou, M.** (2004), 'Coxsackievirus B4-induced cytokine production in pancreatic cells is mediated through toll-like receptor 4', *J Virol*, **78**(20): 11313-11320

**Triantafilou, K., Orthopoulos, G., Vakakis, E., Ahmed, M.A., Golenbock, D.T., Lepper, P.M., and Triantafilou, M. (2005a), 'Human cardiac inflammatory responses triggered by Coxsackie B viruses are mainly Toll-like receptor (TLR) 8-dependent', *Cell Microbiol*, **7**(8): 1117-1126**

**Triantafilou, K., Vakakis, E., Orthopoulos, G., Ahmed, M.A., Schumann, C., Lepper, P.M., and Triantafilou, M. (2005b), 'TLR8 and TLR7 are involved in the host's immune response to human parechovirus 1', *Eur J Immunol*, **35**(8): 2416-2423**

**Trono, D., Andino, R., and Baltimore, D. (1988), 'An RNA sequence of hundreds of nucleotides at the 5' end of poliovirus RNA is involved in allowing viral protein synthesis', *J Virol*, **62**(7): 2291-2299**

**UniProtKB, Q03053, URL:**

<http://www.uniprot.org/uniprot/Q03053>

**Uzri, D., and Gehrke, L. (2009), 'Nucleotide sequences and modifications that determine RIG-I/RNA binding and signaling activities', *J Virol*, **83**(9): 4174-4184**

**van Kuppeveld, F.J., Hoenderop, J.G., Smeets, R.L., Willems, P.H., Dijkman, H.B., Galama, J.M., and Melchers, W.J. (1997), 'Coxsackievirus protein 2B modifies endoplasmic reticulum membrane and plasma membrane permeability and facilitates virus release', *EMBO J*, **16**(12): 3519-3532**

**Venkataraman, T., Valdes, M., Elsby, R., Kakuta, S., Caceres, G., Saijo, S., Iwakura, Y., and Barber, G.N.** (2007), 'Loss of DExD/H box RNA helicase LGP2 manifests disparate antiviral responses', *J Immunol*, **178**(10): 6444-6455

**ViperDB**, URL:

[http://viperdb.scripps.edu/info\\_page.php?VDB=1cov](http://viperdb.scripps.edu/info_page.php?VDB=1cov)

**Viral Zone, Picornaviridae**, URL:

[http://viralzone.expasy.org/all\\_by\\_protein/33.html](http://viralzone.expasy.org/all_by_protein/33.html)

**Viral Zone, Enterovirus**, URL:

[http://viralzone.expasy.org/all\\_by\\_protein/97.html](http://viralzone.expasy.org/all_by_protein/97.html)

**Wagner, E.K., Hewlett, M.J., Bloom, D.C., and Camerini, D.** (2008), 'Replication of positive-sense RNA viruses', Basic Virology 3<sup>rd</sup> Edition, Blackwell Publishing, Oxford

**Wagner, H.** (2002), 'Interactions between bacterial CpG-DNA and TLR9 bridge innate and adaptive immunity', *Curr Opin Microbiol*, **5**(1): 62-69

**Walter, B.L., Nhuyen, J.H., Ehrenfeld, E., and Semler, B.L.** (1999), 'Differential utilization of poly(rC) binding protein 2 in translation directed by picornavirus IRES elements', *RNA*, **5**(12): 1570-1585

**Wang, J.P., Cerny, A., Asher, D.R., Kurt-Jones, E.A., Bronson, R.T., and Finberg, R.W.** (2010), 'MDA5 and MAVS mediate type 1 interferon responses to coxsackie B virus', *J Virol*, **84**(1): 254-260

**Wang, J.P., Kurt-Jones, E.A., Shin, O.S., Manchak, M.D., Levin, M.J., and Finberg, R.W.** (2005), 'Varicella-zoster virus activates inflammatory cytokines in human monocytes and macrophages via Toll-like receptor 2', *J Virol*, **79**(20): 12658-12666

**Wang, T., Town, T., Alexopoulou, L., Anderson, J.F., Fikrig, E., and Flavell, R.A.** (2004), 'Toll-like receptor 3 mediates West Nile virus entry into the brain causing lethal encephalitis', *Nat Med*, **10**(12): 1366-1373

**Wang, Z., Xiang, L., Shao, J., and Yuan, Z.** (2006), 'The 3' CCACCA sequence of tRNA<sup>Ala</sup>(UGC) is the motif that is important in inducing Th1-like immune response, and this motif can be recognized by Toll-like receptor 3', *Clin Vaccine Immunol*, **13**(7): 733-739

**Wilkins, C., and Gale, M. Jr.** (2010), 'Recognition of viruses by cytoplasmic sensors', *Curr Opin Immunol*, **22**(1): 41-47

**Wimmer, E., Hellen, C.U., and Coa, X.** (1993), 'Genetics of poliovirus', *Annu Rev, Genet*, **27**: 353-436

**Xagorari, A., and Chlichlia, K.** (2008), 'Toll-like receptors and viruses: induction of innate antiviral immune responses', *Open Microbiol J*, **2**: 49-59

**Xu, L.G., Wang, Y.Y., Han, K.J., Li, L.Y., Zhai, Z., and Shu, H.B.** (2005), 'VISA is an adaptor protein required for the virus-triggered IFN-beta signaling', *Mol Cell*, **19**(6): 727-740

**Yamamoto, M., Sato, S., Hemmi, H., Hoshino, K., Kaisho, T., Sanjo, H., Takeuchi, O., Sugiyama, M., Okabe, M., Takeda, K., and Akira, S.** (2003a), 'Role of adaptor TRIF in the MyD88-independent toll-like receptor signaling pathway', *Science*, **310**(5633): 640-643

**Yamamoto, M., Sato, S., Hemmi, H., Sanjo, H., Uematsu, S., Kaisho, T., Hoshino, K., Takeuchi, O., Kobayashi, M., Fujita, T., Takeda, K., and Akira, S.** (2002), 'Essential role for TIRAP in activation of the signalling cascade shared by TLR2 and TLR4', *Nature*, **420**(6913): 324-329

**Yamamoto, M., Sato, S., Hemmi, H., Uematsu, S., Hoshino, K., Kaisho, T., Takeuchi, O., Takeda, K., and Akira, S.** (2003b), 'TRAM is specifically involved in the Toll-like receptor 4-mediated MyD88-independent signaling pathway', *Nat Immunol*, **4**(11): 1144-1150

**Yamamoto, M., and Takeda, K.** (2010), 'Current views of toll-like receptor signaling pathways', *Gastroenterol Res Pract*, **2010**: 240365

**Yamamoto, M., Takeda, K., and Akira, S.** (2004), 'TIR domain-containing adaptors define the specificity of TLR signaling', *Mol Immunol*, **40**(12): 861-868

**Yang, Y., Liang, Y., Qu, L., Chen, Z., Yi, M., Li, K., and Lemon, S.M.** (2007), 'Disruption of innate immunity due to mitochondrial targeting of a picornaviral protease precursor', *Proc Natl Acad Sci U S A*, **104**(17): 7253-7258

**Yarovinsky, F., Zhang, D., Andersen, J.F., Bannenberg, G.L., Serhan, C.N., Hayden, M.S., Hieny, S., Sutterwala, F.S., Flavell, R.A., Ghosh, S., and Sher, A.** (2005), 'TLR11 activation of dendritic cells by a protozoan profilin-like protein', *Science*, **308**(5728): 1626-1629

**Yokota, S., Okabayashi, T., and Fujii, N.** (2010), 'The battle between virus and host: modulation of Toll-like receptor signaling pathways by virus infection', *Mediators Inflamm*, **2010**: 184328

**Yoneyama, M., and Fujita, T.** (2009), 'RNA recognition and signal transduction by RIG-I-like receptors', *Immunol Rev*, **227**(1): 54-65

**Yoneyama, M., Kikuchi, M., Matsumoto, K., Imaizumi, T., Miyagishi, M., Taira, K., Foy, E., Loo, Y.M., Gale, M. Jr., Akira, S., Yonehara, S., Kato, A., and Fujita, T.** (2005), 'Shared and unique functions of the DExD/H-box helicases RIG-I, MDA5, and LGP2 in antiviral innate immunity', *J Immunol*, **175**(5): 2851-2858

**Yoneyama, M., Kikuchi, M., Natsukawa, T., Shinobu, N., Imaizumi, T., Miyagishi, M., Taira, K., Akira, S., and Fukita, T.** (2004), 'The RNA helicase RIG-I has an essential function in double-stranded RNA-induced innate antiviral responses', *Nat Immunol*, **5**(7): 730-737

**Zeiss AxioVision LE Software, URL:**

<http://www.zeiss.de/C12567BE0045ACF1/Contents-Frame/4BFA588C935976C4C1256E0000492173>

**Zeiss LSM Image Browser Software, URL:**

<http://www.zeiss.co.uk/c12567be0045acf1/allbysubject/caa2ef638ec5f0d3c1256adf0050e2f1>

**Zell, R., Sidigi, K., Stelzner, A., and Gorlach, M.** (2002), 'Determinants of the recognition of enteroviral cloverleaf RNA by coxsackievirus B3 proteinase 3C', *RNA*, **8**(2): 188-201

**Zhang, D., Zhang, G., Hayden, M.S., Greenblatt, M.B., Bussey, C., Flavell, R.A., and Ghosh, S.** (2004), 'A toll-like receptor that prevents infection by uropathogenic bacteria', *Science*, **303**(5663): 1522-1526

**Zhang, G., Wilsden, G., Knowles, N.J., and McCauley, J.W.** (1993), 'Complete nucleotide sequence of a coxsackie B5 virus and its relationship to swine vesicular disease virus', *J Gen Virol*, **74**(5):845-853



**Zhao, T., Yang, L., Sun, Q., Arguello, M., Ballard, D.W., Hiscott, J., and Lin, R.** (2007), 'The NEMO adaptor bridges the nuclear factor-kappaB and interferon regulatory factor signaling pathways', *Nat Immunol*, **8**(6): 592-600

**Zhu, J., Huang, X., and Yang, Y.** (2007), 'Innate immune response to adenoviral vectors is mediated by both Toll-like receptor-dependent and -independent pathways', *J Virol*, **81**(7): 3170-3180

**Zhu, J., Martinez, J., Huang, X., and Yang, Y.** (2007), 'Innate immunity against vaccinia virus is mediated by TLR2 and requires TLR-independent production of IFN-beta', *Blood*, **109**(2): 619-625

# Appendix

## **X10 PBS (500ml)**

- 50g NaCl
- 1.25g KCl
- 7.2g Na<sub>2</sub>HPO<sub>4</sub>
- 1.25g KH<sub>2</sub>PO<sub>4</sub>
- 400ml distilled water (dH<sub>2</sub>O)
- pH 7.2
- Top up to 500ml with dH<sub>2</sub>O

For PBS-Tween, add 10ml Tween-20 (rinse tip in buffer).

## **X1 PBS (500ml)**

- 50ml x10 PBS
- 450ml dH<sub>2</sub>O

## **X2 PBS (500ml)**

- 100ml x10 PBS
- 400ml dH<sub>2</sub>O

## **X1 PBS / 0.02%<sub>(w/v)</sub> BSA / 0.02%<sub>(w/v)</sub> Saponin / 0.02%<sub>(w/v)</sub> Sodium Azide (NaN<sub>3</sub>) (500ml)**

- 0.02% = 0.02g in 100ml
- In 500ml need 0.1g
- 0.1g of each added to 500ml x1 PBS

## **10% SDS (100ml)**

- 10.0g SDS
- In 100ml dH<sub>2</sub>O
- Mix on a heater / stirrer

**4% Paraformaldehyde (4% PFA) (200ml)**

- Add 8.0g PFA powder to approx. 80ml of dH<sub>2</sub>O in a glass beaker.
- Heat to 60°C in a fume hood on a heater / stirrer
- Add a few drops of 1M NaOH to help dissolve, whilst still on a heater / stirrer
- When the solid has completely dissolved, top up to 100ml with dH<sub>2</sub>O, let the solution cool to room temperature, add 100ml of x2 PBS

**0.5M Tris pH 6.8 (250ml)**

- 60.5g in 1000ml ( $M = \text{Mass} / M.\text{wt}$  therefore  $0.5 = \text{Mass} / 121$  therefore  $\text{Mass} = 60.5$ )
- 15.1g Tris in 250ml dH<sub>2</sub>O
- pH to 6.8 with concentrated HCl

**X2 SDS-PAGE Reducing Sample Buffer (approx. 40ml)**

- 20ml 0.5M Tris pH 6.8
- 16ml 10% SDS
- 10.0g Glycerol
- 4ml 14.3M β-mercaptoethanol
- Small spatula with a bit of Bromophenol Blue
- Stir with spatula till mixed, transfer to bottle

**Phenol / Chloroform / Isoamyl Alcohol**

- In fume hood, in a 500ml sterile glass bottle
- Add 100ml Phenol + 100ml Chloroform / Isoamyl Alcohol + 100ml dH<sub>2</sub>O
- Leave to settle
- Place in fridge

**Stripping Buffer (200ml)**

- 1.4ml β-Mercaptoethanol (100mM)
- 40ml 10% SDS (=2% in 200ml)
- 1.52g Tris HCl pH6.7 (62.5mM)
- Top up to 200ml with PBS-T

## **Immunoprecipitation Solutions**

### **X2 SDS-PAGE Non-Reducing Sample Buffer (approx. 40ml)**

- 10ml 0.5M Tris pH 6.8
- 8ml 10% SDS
- 5.0g Glycerol
- Small spatula with a bit of Bromophenol Blue
- Stir with spatula till mixed, transfer to bottle

### **Net Buffer pH8 (100ml)**

- 6.056g 500mM TrisHCl
- 8.768g 1.5M NaCl
- 1.86g 50mM EDTA
- Make up to 100ml with dH<sub>2</sub>O

### **10mM Iodoacetamide (50ml)**

- 92.5mg (0.0925g)
- In 50ml dH<sub>2</sub>O

### **10% w/v NP-40 (50ml)**

- 5g NP-40
- In 50ml dH<sub>2</sub>O

### **PMSF Stock (100ml)**

- 1.74g PMSF
- In 100ml Ethanol

### **Protein A Sepharose (PAS) Beads (10%<sub>(w/v)</sub>)**

- 0.1g in 1ml Lysis Buffer
- Incubate >1 hour, to allow beads to 'swell'
- Resuspend PAS by gently pipetting before each use

**Lysis Buffer (50ml)**

- 5ml NET Buffer
- 500µl Iodoacetamide
- 5ml NP-40
- 25µl PMSF
- 20µl Protease Tablets (mixture)
- Make up to 50ml with dH<sub>2</sub>O

**DNA Isolation Solutions****STET Buffer (100ml)**

- 8g Sucrose
- 500µl Triton
- 10ml EDTA (500mM) pH 8 (adjust with HCl)
- 1ml Tris pH 8 (1M) (adjust with HCl)
- Make up to 100ml with dH<sub>2</sub>O

**1M Tris (100ml)**

- 12.1g Tris
- In 100ml dH<sub>2</sub>O
- pH to 8 with HCl

**500mM EDTA (=0.5M EDTA) (100ml)**

- 37.22g EDTA
- In 200ml dH<sub>2</sub>O
- pH to 8 with HCl

**Sucrose Gradient Buffers****60% / 30% / 10% in PBS**

- 60g / 30g / 10g Sucrose (powder) into 3 separate conical flasks
- Top each up to 100ml with PBS
- Fridge

## **SDS-PAGE / Western Blot Solutions**

### **1.5M Tris-HCl pH 8.8 (500ml)**

- 90.85g Tris
- In 500ml dH<sub>2</sub>O
- pH to 8.8 with conc. HCl

### **X2 Transfer Buffer (1000ml)**

- 4.88g Tris
- 20ml 10% SDS
- 400ml Isopropanol (= Propan-2-ol)
- Make up to 1000ml with dH<sub>2</sub>O
- pH to 8.3 with Acetic Acid
- To get X1 TB → split into 2 beakers, add 500ml dH<sub>2</sub>O to each

### **Running Buffer (500ml)**

- 50ml x10 Running Buffer
- 450ml dH<sub>2</sub>O
- [Tris-Glycine pH 8.8] → 25mM Tris, 192mM glycine, 0.1% SDS
- For 10x running buffer:
- 288g glycine
- 60.4g tris base
- 20g SDS
- 1800ml dH<sub>2</sub>O

### **PBS-Tween (2000ml)**

- 200ml x10 PBS into a 1000ml bottle
- Top up to 1000ml with dH<sub>2</sub>O
- Add 2ml PBS-Tween20, dropping the tips into the bottle
- Mix (shake)
- Decant 500ml into a new bottle, top both up with 500ml dH<sub>2</sub>O = 2 x 1000ml bottles of PBS-T

**10% Resolving Gel (for 2 gels)**

- 4.02ml dH<sub>2</sub>O
- 2.5ml 1.5M Tris-HCl pH 8.8
- 100µl 10% SDS
- 3.33ml Acrylamide/Bis
- To Polymerise, add:
  - 50µl 10% APS
  - 10µl TEMED

**4% Stacking Gel (for 2 gels)**

- 6.1ml dH<sub>2</sub>O
- 2.5ml 0.5M Tris-HCl pH 6.8
- 100µl 10% SDS
- 1.3ml Acrylamide/Bis
- To Polymerise, add:
  - 50µl 10% APS
  - 20µl TEMED

**Blocking Reagent (40ml)**

- 2g Milk Powder
- 40ml PBS-T

**Agarose Gel Electrophoresis Solutions****50X ELFO (2M Tris, 50mM EDTA) (1000ml)**

- 242g Tris base
- 100ml EDTA (0.5M)
- pH 7.7 with Acetic acid
- Make up to 1000ml with dH<sub>2</sub>O

**1X ELFO (1000ml)**

- 20ml 50X ELFO in 1000ml dH<sub>2</sub>O

**ELFO Loading Buffer (200ml)**

- 100ml Glycerol
- 20ml 50X ELFO
- 80ml dH<sub>2</sub>O
- A few mg of Bromophenol Blue